

# Towards an Enhanced Wide Area Control System for Damping Out Low Frequency Oscillations in Power Grid

A Thesis Submitted to  
Indian Institute of Technology Hyderabad  
In Partial Fulfillment of the Requirements for  
The Degree of Doctor of Philosophy



Department of Electrical Engineering

March 2019

## Declaration

I declare that this written submission represents my ideas in my own words, and where ideas or words of others have been included, I have adequately cited and referenced the original sources. I also declare that I have adhered to all principles of academic honesty and integrity and have not misrepresented or fabricated or falsified any idea/data/fact/source in my submission. I understand that any violation of the above will be a cause for disciplinary action by the Institute and can also evoke penal action from the sources that have thus not been properly cited, or from whom proper permission has not been taken when needed.

Reddy. ay.

(Signature) 04/03/19

\_\_\_\_\_  
(Nagasekhara Reddy Naguru)

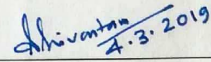
\_\_\_\_\_  
(EE12P1005)



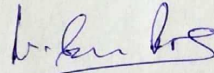
Scanned with  
CamScanner

## Approval Sheet

This thesis entitled Towards an Enhanced Wide Area Control System for Damping Out Low Frequency Oscillations in Power Grid by Nagasekhara Reddy Naguru is approved for the degree of Doctor of Philosophy from IIT Hyderabad.

  
4.3.2019

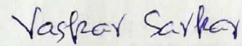
Dr. S.C. Srivastava, Professor  
Dept. of Electrical Eng., IIT Kanpur  
External Examiner 1



Dr. Nilanjan Senroy, Professor  
Dept. of Electrical Eng., IIT Delhi  
External Examiner 2



Dr. Ketan P. Detroja, Associate Professor  
Dept. of Electrical Eng., IIT Hyderabad  
Internal Examiner



Dr. Vaskar Sarkar, Associate Professor  
Dept. of Electrical Eng., IIT Hyderabad  
Adviser/Guide



Dr. Raja Banerjee, Associate Professor  
Dept. of Mechanical & Aerospace Eng., IIT Hyderabad  
Chairman

## Acknowledgements

First of all, I would like to express my sincere gratitude to my supervisor Dr. Vaskar Sarkar for his dedicated guidance, commitment, personal support and encouragement throughout my Ph.D. work. I am very grateful for his valuable time, ideas and advices etc. I could not have achieved this without my supervisor. I also would like to express my thanks to my doctoral committee members for their valuable suggestions and inputs.

I would also like to acknowledge my friend, my co-partner in research, Yatendrababu G V N for his constant support through out all these years. I am truly grateful for spending his valuable time in my research work, thanks for his financial support and assistance in many things. I also wish to thank Kranthi Kumar Reddy M for his valuable support and encouragement.

Next, I would like to express my sincere thanks and acknowledgement to all my fellow labmates (Manjunath.K, Sriram.V, Rishabh Verma) and ex-labmates (Power and Control lab, Power Electronics Lab etc.) who helped me thorough out my Ph.D.

Last but not the least, I would like to thank my family, especially, my beloved sister Rhoda Naguru for her love, care, encouragement and support throughout my Ph.D. work.

**Nagasekhara Reddy Naguru**

# Dedication

Dedicated to my Family

# Abstract

This thesis presents enhanced methodologies in a wide area control system to damp out low frequency oscillations. The primary motivation behind this work is to design a wide area controller to avoid power system blackouts by damping out low frequency oscillations which are existing for longer time duration. The wide area controller can be designed in two ways: state feedback control and output feedback control. From the input point of view, the state feedback controller requires the information about all system states and are not possible to observe all system states in real-time. From the output point of view, the output signals of the controller can be given to the AVR/excitation system of all generators in both control techniques which will increase the cost of the communication network. Moreover, the time delay due to the communication network will affect the wide area controller performance. Therefore, to overcome these problems, in particular, this work addresses the design of a wide area controller with limited measurements to resolve the input side problems. The problems associated with the output side can be overcome by employing a reduced-scale wide area controller design. In addition, the time delay effects can be resolved by using bi-layer wide area control architecture with the incorporation of the practical supplementary controller. The important contributions of this work are as follows.

1. Designing a wide area controller to damp out inter-area oscillations by considering limited measurements with unknown load composition.
2. Designing a reduced-scale architecture of the wide area control system by means of modal sensitivity analysis.
3. Designing a practical supplementary controller design for the bi-layer wide area control architecture through structurally constrained  $H_2$ -norm optimization.

The contribution of the first work is to design a wide area controller with limited measurements without knowing load composition. The primary objective of this

work is to design a state feedback controller to damp out the inter-area oscillations in the power system network with limited wide area measurements. The conventional state feedback controller designed through LQR optimization requires all the state variables as input. However, the dynamics of a power system is governed by a large number of state variables. Therefore, it is, practically, not possible to place sensors everywhere for monitoring the complete system state in real-time. To address the particular issue, an optimized state feedback controller is proposed, which can be implemented with the limited number of state inputs. The structurally constrained  $H_2$ -norm optimization technique is employed to perform the proposed state feedback controller design. The reference frame requirement for defining the rotor angles of generators under the scenario of limited state observability is also investigated. The performance of the wide area controller with limited state inputs is verified through a case study on the New England 39-bus system under different scenarios of state unobservability. Since the WAC design requires a full system description, appropriate load modeling may be critical in the WAC design. Therefore, a mathematical framework is developed to carry out WAC design in the presence of multiple types of load. Both static and dynamic loads are considered. In order to exempt the dynamic load states from the input of WAC, the structurally constrained  $H_2$ -norm optimized WAC design is performed. By recognizing the practical difficulty of obtaining the precise information about actual load composition, this work further investigates the suitability of representing all the loads as constant power loads in the WAC design. Detailed case studies are performed on the IEEE 39-bus system.

The contribution of the second work is to develop an efficient scheme for the proper selection of entities in the wide area control (WAC) loop so as to yield a cost-effective and simplified WAC architecture without compromising with its damping performance. The methodology proposed is based upon a concept of mode-path susceptibility matrix that is obtained by means of the modal sensitivity analysis. In

specific, the significance of a feedback path to change mode shapes is determined by evaluating the sensitivities of different modes to the respective elements of the feedback gain matrix. This is unlike the traditional controllability and observability based approaches. A generalized utility ranking of potential source and sink points of the wide area damping controller is further carried out based upon the mode-path susceptibility matrix. Both the state feedback and the output feedback are taken into account in the methodology proposed for the scale reduction of a WAC architecture. Detailed case studies are performed to verify the effectiveness of the proposed reduced-scale WAC architecture through both off-line simulations and real-time experimentations.

The contribution of the third work is to develop a suitable methodology for the practical realization of the bi-layer wide area control (WAC) architecture. The bi-layer WAC system retains the capability to overcome the communication related problems to a great extent through the deployment of a supplementary wide area damping controller (WADC) along with the conventional WADC. The supplementary WADC was envisaged as a controller that may not have any communication requirements to deliver control signals. It is, therefore, essential to design the supplementary WADC in a way so that the same can be practically implemented without the requirement of any communication network. The precise concern of the present work is to address the proper design of the aforementioned supplementary WADC. The design of the supplementary WADC is carried out through a structurally constrained  $H_2$ -norm optimization calculation. The solution procedure of the particular  $H_2$ -norm optimization problem is established. Detailed simulation studies are performed to evaluate the performance of the proposed supplementary WADC in the standalone mode. The usefulness of the bi-layer WAC architecture to improve the damping of inter-area oscillations under the proposed controller design is thoroughly validated through real-time experimentations.



# Contents

Acknowledgements . . . . .	i
Abstract . . . . .	iii
List of Figures . . . . .	x
List of Tables . . . . .	xiii
List of Symbols . . . . .	xv
List of Acronyms . . . . .	xv
<b>1 Introduction</b>	<b>1</b>
1.1 Power system oscillations . . . . .	1
1.1.1 Intraplant mode oscillations . . . . .	2
1.1.2 Local plant mode oscillations . . . . .	2
1.1.3 Inter-area mode oscillations . . . . .	2
1.1.4 Control mode oscillations . . . . .	2
1.1.5 Torsional mode oscillations . . . . .	2
1.2 Power system stabilizer (PSS) . . . . .	3
1.3 Consequences of inter-area oscillations . . . . .	3
1.4 Wide Area Monitoring Systems (WAMS) . . . . .	4
1.4.1 Phasor measurement units . . . . .	5
1.4.2 WAMS based damping control and communication network . . . . .	6
1.5 Wide Area Control in Power Systems . . . . .	6
1.6 Motivation . . . . .	6

1.7	Organization of the Thesis . . . . .	8
<b>2</b>	<b>Principle of Optimal Feedback Control</b>	<b>10</b>
2.1	Introduction . . . . .	10
2.2	Optimal Control theory . . . . .	10
2.3	Controllability and Observability . . . . .	11
2.4	Stabilizability and Detectability . . . . .	12
2.5	$H_2$ and $H_\infty$ Norms . . . . .	12
2.5.1	Computation of $H_2$ -Norm . . . . .	12
2.5.2	LQR Design through $H_2$ -norm . . . . .	13
2.5.3	Computation of $H_\infty$ -Norm . . . . .	14
2.6	State Feedback Control and Output Feedback Control . . . . .	15
2.7	Structurally Constrained $H_2$ -Norm Optimization . . . . .	16
2.8	Linear and Non-linear Kalman Filtering . . . . .	20
2.8.1	Kalman Filter Algorithm . . . . .	21
2.8.2	Extended Kalman Filter Algorithm . . . . .	21
2.8.3	Unscented Kalman Filter . . . . .	22
2.9	Summary . . . . .	23
<b>3</b>	<b>General WAC Framework for a Power System</b>	<b>24</b>
3.1	Introduction . . . . .	24
3.2	General Architecture of the WAC System . . . . .	24
3.3	Modeling of Power System . . . . .	27
3.3.1	Generator Modeling . . . . .	27
3.3.2	Exciter Model . . . . .	30
3.3.3	Turbine and Speed Governor Model . . . . .	31
3.3.4	Power System Stabilizer Model . . . . .	31
3.3.5	Network Modeling . . . . .	32

3.3.6	Load Modeling . . . . .	32
3.3.7	System Integration . . . . .	37
3.4	Limited Measurement Issue . . . . .	39
3.4.1	Feedback Gain Matrix Structure . . . . .	39
3.4.2	COI Calculation . . . . .	40
3.5	Kalman Filter with unknown inputs in power system applications . . . . .	41
3.6	Case Study . . . . .	42
3.6.1	Optimal wide area control with limited measurements . . . . .	42
3.6.2	Design of wide area controller with unknown load composition . . . . .	47
3.7	Summary . . . . .	50
<b>4</b>	<b>Designing a Reduced-Scale Architecture of the Wide Area Control System</b>	<b>51</b>
4.1	Introduction . . . . .	51
4.2	Principle of wide area controller design and implementation . . . . .	52
4.3	Proposed scheme for the scale reduction of the WAC system . . . . .	58
4.4	Simulation results . . . . .	62
4.5	Experimental Validation . . . . .	68
4.6	Summary . . . . .	72
<b>5</b>	<b>Practical Supplementary Controller Design for the Bi-Level WAC Architecture</b>	<b>73</b>
5.1	Introduction . . . . .	73
5.2	Overview of the conventional WAC system . . . . .	74
5.3	Bi-layer WAC architecture and the proposed design . . . . .	75
5.3.1	Proposed configuration of the supplementary WADC . . . . .	77
5.3.2	Design methodology for the proposed supplementary WADC . . . . .	79
5.4	Simulation study . . . . .	82

5.5	Experimental results . . . . .	85
5.6	Summary . . . . .	90
<b>6</b>	<b>Conclusion and future work</b>	<b>91</b>
6.1	Overall summary . . . . .	92
6.2	WAC Design with limited Measurements and with unknown load com- position . . . . .	92
6.3	Reduced-scale architecture of the wide area control system . . . . .	93
6.4	Practical supplementary controller design . . . . .	93
6.5	Future scopes of work . . . . .	94
6.5.1	Fault tolerant wide area control . . . . .	94
6.5.2	Structurally constrained $H_\infty$ -norm optimized WAC design . . . . .	94
6.5.3	WAC design for a large power system . . . . .	95
	<b>References</b>	<b>96</b>

# List of Figures

1.1	The block diagram of PSS. . . . .	3
1.2	General WAMS structure. . . . .	4
2.1	Control center block diagram. . . . .	15
3.1	General architecture of the traditional WAC system. . . . .	25
3.2	linearized mathematical block diagram representation. . . . .	26
3.3	The structures of feedback gain matrices corresponding to conventional, sparsity promoting [1] and proposed LQR optimizations respectively. . . . .	40
3.4	The New England 39-bus system . . . . .	42
3.5	Eigenvalues of the open loop system. . . . .	43
3.6	Structure of the feedback gain matrix with limited states in Case 1. . . . .	44
3.7	Comparison of closed loop eigenvalues in Case 1 with the closed loop eigenvalues for the feedback controller with all the states. . . . .	44
3.8	Dynamic responses of generator speeds (COI referred) in Case 1 for the outage of Line 14-15. . . . .	45
3.9	Structure of the feedback gain matrix with limited states in Case 2. . . . .	46
3.10	Comparison of closed loop eigenvalues in Case 2 with the closed loop eigenvalues for the feedback controller with all the states. . . . .	46

3.11	Dynamic responses of generator speeds (COI referred) in Case 2 for the outage of Line 14-15. . . . .	46
3.12	Dynamic responses of Generator 1 speed considering static and dynamic loads with load shedding at Bus 7. . . . .	48
3.13	Dynamic response of speeds of Generator 1 and 10 using single design (CP load alone) with load shedding at Bus 7. . . . .	50
4.1	the block diagram of an excitation control system with the WAC signal input. . . . .	53
4.2	The 68-bus test system. . . . .	63
4.3	Eigenvalue comparison between proposed and existing RSWAC schemes. 65	
4.4	Comparison of rotor angle (COI referred) dynamics between proposed and existing RSWAC schemes without time delay. . . . .	66
4.5	Real-time experimentation set up. . . . .	68
4.6	Closed loop eigenvalue comparison between FSWAC and proposed RSWAC systems. . . . .	69
4.7	Comparison of rotor angle (COI referred) dynamics between FSWAC and RSWAC systems with time delay. . . . .	71
5.1	Schematic representation of the bi-layer WAC architecture. . . . .	75
5.2	Comparison of eigenvalue spectra between open loop and closed loop systems in the case of stand-alone presence of supplementary WADC. 82	
5.3	Generator 1 rotor angle dynamics for open loop and closed loop systems in the case of stand-alone presence of supplementary WADC. a) TL_OUT_1, b) TL_OUT_2, c) TL_OUT_3, d) LD_SHD_1. . . . .	83

5.4	Generator 1 rotor angle dynamics for open loop and closed loop systems in the case of stand-alone presence of conventional WADC with no communication delay. a) TL_OUT_1, b) TL_OUT_2, c) TL_OUT_3, d) LD_SHD_1. . . . .	85
5.5	Real-time experimentation set up. . . . .	85
5.6	Comparison of eigenvalue spectra between the traditional mono-layer and proposed bi-layer WAC systems. . . . .	86
5.7	Generator 1 rotor angle dynamics for traditional mono-layer and proposed bi-layer WAC systems. a) TL_OUT_1, b) TL_OUT_2, c) TL_OUT_3, d) LD_SHD_1. . . . .	87

# List of Tables

3.1	Amount of Damping Required for Different Static Load Compositions	48
3.2	Amount of Damping Required for Parameter Variations of Dynamic Load . . . . .	49
4.1	Damping ratios and frequencies of the inter-area modes without WAC	63
4.2	Utility assessment of different generators as source and sink points of the WAC loop . . . . .	64
4.3	List of disturbances considered . . . . .	65
4.4	Comparison of rotor angle settling times between proposed and existing RSWAC schemes . . . . .	67
4.5	Comparison of rotor angle settling times between FSWAC and proposed RSWAC systems . . . . .	70
5.1	Generator angle settling times for the closed loop system with only supplementary WADC . . . . .	84
5.2	Generator angle settling times for the closed loop system with only conventional WADC . . . . .	86
5.3	Generator angle settling times for the bi-layer WAC system . . . . .	89



# List of Symbols

$x$	System state vector
$w$	Disturbance input
$u$	Control input
$y$	Measured output
$A$	System state matrix
$B_w$	Disturbance input matrix
$B_u$	Control input matrix
$C_y$	Measured output matrix
$D_{yw}$	Measurement input-output disturbance matrix
$D_{yu}$	Measurement input-output control matrix
$\Delta$	It is used to represent Perturbed value
$z$	Performance output
$C_z$	Performance output matrix
$D_{zw}$	Performance input-output disturbance matrix
$D_{zu}$	Performance input-output control matrix
$K$	Feedback gain matrix
$u_{wac}$	Wide area control input to the system
$K_{wac}$	State feedback controller gain matrix
$G_{wac}$	Output feedback controller gain matrix
$Q$	LQR state weight matrix
$R$	LQR input weight matrix
$S$	State-input weight matrix

$x_k$	State vector in discrete form at $k$ th instant
$z_k$	Output vector in discrete form at $k$ th instant
$K_k$	Kalman filter gain at $k$ th instant
$\hat{x}_k$	Estimated state vector in discrete form at $k$ th instant
$\chi_{k-1}$	Sigma points at $(k - 1)$ th instant
$\mathbf{X}_{Tot}$	State matrix of generators and its auxiliary devices
$\mathbf{X}_{SYS}$	Total system state matrix
$K_{pss}$	Power system stabilizer gain
$T_w$	Wash out circuit time constant
$T_1, T_2, T_3, T_4$	Time constants of lead-lag blocks of PSS

# List of Acronyms

WAC	Wide Area Control
WADC	Wide Area Damping Controller
PSS	Power System Stabilizer
WAMS	Wide Area Monitoring Systems
COI	Center of Inertia
CP	Constant Power
CC	Constant Current
CZ	Constant Impedance
PDC	Phasor Data Concentrator
PMU	Phasor Measurement Unit
GPS	Global Positioning System
RSWAC	Reduced-scale Wide Area Control
LQR	Linear Quadratic Regulator
EKF	Extended Kalman Filter
UT	Unscented Transformation
RFI	Reference Frame Independent
UKF	Unscented Kalman Filter
AVR	Automatic Voltage Regulator
FSWAC	Full-scale Wide Area Control
ARE	Algebraic Riccati Equation
ADMM	Alternating Direction Method of Multipliers

# Chapter 1

## Introduction

A power system is an interconnection of different components such as generators and its auxiliary devices (exciters, turbines, automatic voltage regulators, power system stabilizers etc.), transmission network, different type of loads, and controllable devices. The stability of a power system refers to the ability of a power system to return back to its steady state when subjected to a disturbance. The primary sources of electrical power energy are the synchronous generators. In power system stability studies, the main challenge is to maintain the synchronism of the interconnected synchronous generators even after a disturbance. As per IEEE/CIGRE Joint Task Force on Stability Terms and Definitions [2], primarily, the power system stability is classified into three categories: rotor angle stability, frequency stability, and voltage stability. In this thesis, the main focus is on to maintain the rotor angle stability even after being subjected to a disturbance.

### 1.1 Power system oscillations

The power system oscillations are mainly concerned with small expeditions of the system conditions about a steady state operating point following a small disturbance. These oscillations are mainly classified into five categories [3]-[4]: Intraplant mode oscillations, Local plant mode oscillations, Inter-area mode oscillations, Control mode oscillations, and Torsional mode oscillations.

### 1.1.1 Intraplant mode oscillations

In this mode, machines on the same power generation site oscillate against each other. The frequency of these oscillations are in the range of 2 to 3 Hz, and the rest of the system is unaffected.

### 1.1.2 Local plant mode oscillations

These oscillations generally involve nearby power plants in which coherent groups of machines within an area swing against each other. The frequency of oscillations is in the range of 1 to 2 Hz.

### 1.1.3 Inter-area mode oscillations

In this mode, two coherent groups of generators swinging against each other. In other words, many synchronous machines on one part of a power system swinging against machines on another part of the system. These are of very low value and are in the range of less than 0.1 to 1 Hz. These oscillations are difficult to control.

### 1.1.4 Control mode oscillations

These oscillations are associated with generators and other controls. Poorly tuned exciters, governors, HVDC converters and SVC controls are the causes of instability of these oscillations.

### 1.1.5 Torsional mode oscillations

In reality, these modes are excited when a multi-stage turbine generator is connected to the grid through a series compensated line [4]. In other words, these oscillations involve relative angular motion between the rotating elements of a unit. These oscillations are in the range of 4 Hz and above. Apart from the excitation systems, other mechanisms can excite torsional oscillations such as dc lines, static converters etc.

Of all these oscillations, as mentioned earlier, inter-area mode oscillations are very difficult to control, and these involve a large part of the system. Therefore, how to damp out these oscillations is one of the biggest problems.

## 1.2 Power system stabilizer (PSS)

The general block diagram of PSS is shown in Fig. 1.1. The primary objective of a PSS is to introduce an electrical torque component in the synchronous machine rotor that is proportional to the deviation of the actual speed from the synchronous speed. Whenever the rotor oscillates, this torque acts as a damping torque to counter the oscillation.

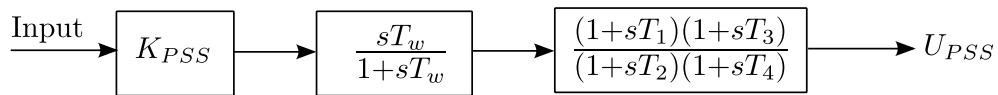


Figure 1.1: The block diagram of PSS.

Intraplant, Local plant, Control, and Torsional oscillations are categorized as local area mode oscillations, which basically take place among the generators within a particular area (i.e., a set of buses that lie in close proximity), can be effectively damped out by using power system stabilizers (PSSs)[3]. The power system stabilizers generate damping signals only based upon the local measurements (i.e., frequencies and power outputs of respective generators) and are locally tuned (i.e., by treating the terminal bus of a generator as an infinite bus). As a result, the low frequency inter-area oscillations that take place among generators from different areas cannot be satisfactorily damped out by the power system stabilizers. The more information and design of PSS can be found in [3], [5].

## 1.3 Consequences of inter-area oscillations

As we have noticed in history, it is observed that power system blackouts are occurred due to inter-area oscillations [5], [6], [7]. Some of the important blackouts are listed below:

1. Italy-Yugoslavia-Austria (1971-1974).
2. Western Electric Coordinating Council (WECC) (1964,1996).
3. South East Australia (1975).
4. Western Australia (1982,1983).
5. Southern Brazil (1975-1980,1984).

Therefore, it can be summarized that inadequate damping of inter-area oscillations is the primary factor leading to system separation. The amount of damping and frequency of oscillations varies with respect to the system operating conditions.

## 1.4 Wide Area Monitoring Systems (WAMS)

The general WAMS structure is shown in Fig. 1.2 [8]. PMUs are located at power system substations to provide voltage and current measurements with time-stamping [9]. From the available measurements, the required quantities can be calculated depending upon the application. The phasor information collected by different PMUs is transferred to the phasor data concentrator (PDC) through the communication network. The PDC collects data from PMUs, reject bad data, align the time stamps, and record the data simultaneously. The output of PDC can be used for monitoring and controlling the power system in real-time.

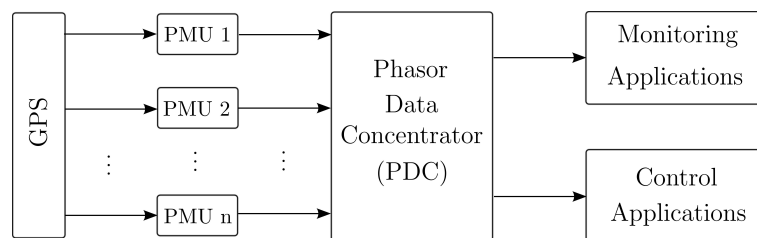


Figure 1.2: General WAMS structure.

WAMS architectures can be classified into three categories: Centralized, Decentralized, and Distributed architectures [10]. In a centralized architecture, PMU data

acquisition, data analysis and initiation of corrective action are performed at a central location. In contrast, the WAMS is split into multiple small areas, and PDCs control the small areas locally using local data in a decentralized architecture. Here, the local controllers are connected to each other if there is an emergency to solve a large problem. Last one, distributed WAMS architecture can be depicted between centralized and decentralized architectures. It includes both local and central controllers. It can be thought of as centralized control with decentralized execution stage.

### 1.4.1 Phasor measurement units

One of the important components in WAMS architecture is PMU. The PMU is a device which samples voltage and current waveforms of a bus with a synchronization signal from the Global Positioning System (GPS) [11]-[12]. In order to estimate phasor and frequency by using PMUs, different algorithms has been reported in literature. With the advent of digital processors, the computational speed has increased significantly. Now, there is a need for digital algorithms which can estimate the phasor and frequency accurately in real-time. Some of the available methods in the literature include zero crossing [13], wavelet transform [14], modified zero crossing, and signal demodulation [15]. In pursuit of higher accuracy for frequency and phasor measurement, the optimization methods such as least mean square methods [16], Kalman filter [17], and Newtons method [18] are being used. A comparative study on different phasor and frequency estimation algorithms that are available in a power system are performed in [19]. The algorithms that are available for frequency estimation include Prony method [20], Polynomial Fitting (PF) [15], Complex Valued Least Square (CLS) [21], and Phase Locked Loop (PLL). For phasor estimation, Discrete Fourier Transform (DFT) [9], PLL, and Smart Discrete Fourier Transform (SDFT) [22] algorithms are used.



### 1.4.2 WAMS based damping control and communication network

As mentioned earlier, inter-area oscillations are the primary cause for power system blackouts. By using WAMS, the controller can be implemented to damp out these oscillations. Depending upon WAMS architectures, the controller design is classified into three categories: centralized, quasi-decentralized, and hierarchical [23]. While transmitting signals from PMUs to the wide-area controller, through the PDC, and then back to generators involve some time delays. These transmission delays depend primarily on the communication network speed. These time delays can deteriorate the wide area controller performance. Therefore, it is necessary to design the controller by considering time delays also.

## 1.5 Wide Area Control in Power Systems

As mentioned earlier, local area mode oscillations can be damped out by means of PSSs. It uses local signals as inputs. These local input signal based controllers are designed based upon single operating condition. However, in reality, power systems constantly experience changes in operating conditions. In addition, local input signals cannot be effective to damp out inter-area oscillations. Under certain operating conditions, an inter-area mode may be controllable from one area and be observable from another. In such cases, local controllers are not effective to damp out that particular inter-area mode oscillation [24]. In order to damp out inter-area oscillations, the wide area control (WAC) system is required. A wide-area control loop is inherently more effective than local loop to damp inter-area modes of oscillations [25]. In [26], the comparison of local control against wide-area control is reported and observed that wide-area control has many advantages over local control.

## 1.6 Motivation

The motivation behind this work to address the following targets.

- In reality, a power system consists of a large number of states, and it is difficult to monitor all the states in real-time with a limited number of sensors. In order to deal with the particular issue, an optimal state feedback controller design is proposed in this work with only observable system states. The methodology proposed is based upon the concept of structurally constrained  $H_2$ -norm optimization.
- Only the source and sink points that can dominantly influence the inter-area modes are considered for the implementation of the WAC loop. This work contributes towards developing an improved scheme for the utility ranking of the source and sink points in the WAC loop so as to design an efficient reduced-scale WAC (RSWAC) system. The specific novelty of this work is as follows.
  1. The utility metrics of source and sink points in the WAC loop are defined based upon modal sensitivities instead of the geometric controllability/observability.
  2. Unlike existing works, no specific restriction is imposed on the number of signals per source/sink point to perform its utility ranking.
- The fundamental concept (i.e., one layer with a communication network and another layer without communication network) of the bi-layer WAC system has already been reported in the literature, and no work could be found till date as to the practical realization of the supplementary controller. In specific, the way by which the supplementary WAC loop can be implemented without the intervention of a communication network is still not addressed in the literature. With this observation, the present work contributes towards prescribing a design of the supplementary wide area damping controller that can practically fit into the architecture of the bi-layer WAC system.

## 1.7 Organization of the Thesis

**Chapter 1** addresses different types of oscillations in the power system and what are the consequences of inter-area oscillations. The role of PSS and the need for a wide area controller is explained. Moreover, the overview of WAMS and WAMS based control techniques are explained. The motivation behind the work is addressed.

**Chapter 2** presents the theory of optimal feedback control. In this chapter, the difference between optimal control and classical control is explained. In optimal control, state feedback and output feedback control methods are demonstrated. In addition, how to represent output feedback control in terms of state feedback control is explained. To estimate the different states in the power system, non-linear Kalman filtering techniques are addressed. The general procedure of structurally constrained  $H_2$ -norm optimization method is explained which is used to design the wide area controller in this work.

**Chapter 3** discusses a general WAC framework for a power system. In this chapter, the modeling of the total power system which is used for designing the wide area controller in the frequency domain and in the time domain. The wide area controller with limited measurements without knowing load composition is presented, and the simulation results are produced by considering the IEEE-39 bus system. In order to estimate the states, extended and unscented Kalman filter techniques related to power system applications are presented.

**Chapter 4** addresses about designing a reduced-scale architecture of the wide area control system. This chapter presents the proposed reduced-scale WAC design by using modal sensitivity analysis. Simulation results show the effectiveness of proposed reduced-scale WAC over existing reduced-scale WAC. Moreover, the proposed technique is compared with full-scale WAC in real-time. It reveals the satisfactory performance of the proposed reduced-scale WAC system even in the practical situation of having limitations in data communication.

**Chapter 5** presents the practical supplementary controller design for the bi-level WAC architecture. In this chapter, the issue of having a practical realization of the

---

supplementary controller for the bi-layer WAC architecture is explained. It is designed by using structurally constrained  $H_2$ -norm optimization technique.

**Chapter 6** presents the main conclusions of the research work presented in the thesis. Proposals for future work are presented.

# Chapter 2

## Principle of Optimal Feedback Control

### 2.1 Introduction

This chapter presents the principle of optimal feedback control that is used for the design. The  $H_2$  and  $H_\infty$ -norms of a state space representation are defined, and further, the  $H_2$ -norm design is extended to the linear quadratic regulator (LQR) problem. In addition, the design of the structurally constrained  $H_2$ -norm optimization technique is explained. Finally, the estimation of states by using both linear (Kalman type) and non-linear (extended and unscented) estimators are illustrated with known and unknown inputs.

### 2.2 Optimal Control theory

In classical control design, we need to design a control signal  $u(t)$  such that  $y(t)$  reaches its steady state as fast as possible. The most common type of controller used is the PID controller. This controller design is based upon the trial and error method to select or tune the controller parameters. On the other hand, the objective of optimal control theory is to determine the control signals that will cause a process to satisfy the physical constraints and at the same time minimize or maximize some

performance criterion [27]. Consider the linear dynamical system described by the following equations:

$$\dot{x}(t) = \mathbf{A}x(t) + \mathbf{B}_w w(t) + \mathbf{B}_u u(t) \quad (2.1)$$

$$y(t) = \mathbf{C}_y x(t) + \mathbf{D}_{yw} w(t) + \mathbf{D}_{yu} u(t), \quad (2.2)$$

where  $x$  is a state vector,  $w$  is a disturbance input,  $u$  is a control input, and  $y$  is the measured output. The above equations (2.1)-(2.2) can be represented in the form of perturbed linearized equations as follows.

$$\Delta \dot{x} = \mathbf{A} \Delta x + \mathbf{B}_w \Delta w + \mathbf{B}_u \Delta u \quad (2.3)$$

$$\Delta y = \mathbf{C}_y \Delta x + \mathbf{D}_{yw} \Delta w + \mathbf{D}_{yu} \Delta u. \quad (2.4)$$

The small-signal stability analysis can be performed based upon the equations (2.3)-(2.4) and transient analysis can be performed based upon the equations (2.1)-(2.2).

## 2.3 Controllability and Observability

An LTI system is controllable if for any initial state  $x(t_0)$  there exists a control input  $u(t)$ , such that an arbitrary final state  $x(t_f)$  can be reached in finite time. The controllability of the system is referred to as the controllability of the pair  $(A, B)$ . Let  $A$  be a stable matrix then the matrix  $P = \int_0^\infty e^{At} B B^T e^{A^T t} dt$  is called the controllability Grammian and it has to satisfy the Lyapunov equation  $AP + PA^T + BB^T = 0$ .

An LTI system is said to be observable if any initial state  $x(t_0)$  can be estimated from the control input  $u(t)$  and the measurements  $y(t)$ . The observability of the system is referred to as the observability of the pair  $(A, C)$ . Let  $A$  be a stable matrix then the matrix  $Q = \int_0^\infty e^{At} C^T C e^{A^T t} dt$  is called the observability Grammian and it has to satisfy the Lyapunov equation  $QA + A^T Q + C^T C = 0$ .

The duality means that  $(A, C)$  is observable if  $(A^T, C^T)$  is controllable. Due to the

duality of observability and controllability, observability has similar characterizations as controllability.

## 2.4 Stabilizability and Detectability

An LTI system is stabilizable if all its uncontrollable modes are stable. In other words, all unstable modes are controllable. A system is said to be stabilizable if there exists a matrix  $M$  such that that given the matrix pair  $(A, B)$ ,  $(ABM)$  is stable.

An LTI system is detectable if all its unobservable modes are stable. In other words, all unstable modes are observable. A system is said to be detectable if there exists a matrix  $L$  such that that given the matrix pair  $(A, C)$ ,  $(ALC)$  is stable.

## 2.5 $H_2$ and $H_\infty$ Norms

Consider the following system:

$$\dot{x}(t) = Ax(t) + B_w w(t) + B_u u(t) \quad (2.5)$$

$$z(t) = C_z x(t) + D_{zw} w(t) + D_{zu} u(t) \quad (2.6)$$

$$y(t) = C_y x(t) + D_{yw} w(t) + D_{yu} u(t), \quad (2.7)$$

where  $w$  is a disturbance input,  $u$  is a control input (computed by the controller  $\mathbf{K}$ ),  $z$  is the performance output, and  $y$  is the measured output. Now, our goal is to synthesize a controller  $\mathbf{K}$  by using either  $H_2$ -norm or  $H_\infty$ -norm, with input  $y$  and output  $u$ , such that the closed loop is stabilized, and the performance output is minimized, given a class of disturbance inputs.

### 2.5.1 Computation of $H_2$ -Norm

Consider a stable linear time-invariant system with the state-space model  $(A, B, C, D)$ , the transfer function  $G(s)$ , and impulse response  $G(t)$ . The  $H_2$ -norm of  $G$  measures

as

$$\begin{aligned}
\|G\|_{L_2}^2 &= \sum_i \sum_j \int_0^\infty \|g_{ij}(t)\|_2^2 dt \\
&= \int_0^\infty \|G(t)\|_F^2 dt \\
&= \text{Tr} \left[ \int_0^\infty G(t)^T G(t) dt \right] \\
&= \frac{1}{2\pi} \text{Tr} \left[ \int_{-\infty}^{+\infty} G(j\omega)^T G(j\omega) d\omega \right] \\
&= \|G\|_{H_2}^2.
\end{aligned} \tag{2.8}$$

Whereas the computation of  $H_2$ -norm through the state space model is defined as follows.

$$\begin{aligned}
\|G\|_{H_2}^2 &= \text{Tr} \left[ \int_0^\infty G(t)^T G(t) dt \right] \\
&= \text{Tr} \left[ \int_0^\infty G(t)^T G(t) dt \right].
\end{aligned} \tag{2.9}$$

We know that  $G(t) = Ce^{At}B$  ( $D = 0$ ), we get

$$\|G\|_{H_2}^2 = \text{Tr} \left[ \int_0^\infty B^T e^{A^T t} C^T C e^{At} B dt \right] \tag{2.10}$$

$$= \text{Tr} [B^T Q B] \tag{2.11}$$

$$= \text{Tr} \left[ \int_0^\infty C e^{At} B B^T e^{A^T t} C^T dt \right] \tag{2.12}$$

$$= \text{Tr} [C P C^T]. \tag{2.13}$$

Where  $Q$  is the observability Grammian, satisfying  $AQ + AQ^T + CC^T = 0$  and  $P$  is the controllability Grammian, satisfying  $A^T P + AP + B^T B = 0$ .

### 2.5.2 LQR Design through $H_2$ -norm

The LQR problem is a special case of  $H_2$ -norm in which we assume full state feedback ( $C_y = I$ ), no disturbance input ( $w = 0$ ), and  $D_{yu} = 0$  (since  $u$  is known). Now, our



objective is to find  $u(t, x) \in L_2$  that minimizes the following expression with initial condition  $x(0)$ .

$$\|z\|_2^2 = \int_0^\infty \|C_z x + D_{zu} u\|_2^2 dt. \quad (2.14)$$

From the above equation (2.14), note that if  $C_z = [\sqrt{Q} \ 0]^T$  and  $D_{zu} = [0 \ \sqrt{R}]^T$  then we get

$$\|z\|_2^2 = \int_0^\infty (x^T Q x + u^T R u) dt. \quad (2.15)$$

The above equation (2.15) represents the standard LQR optimization problem.

### 2.5.3 Computation of $H_\infty$ -Norm

In principle, we would like to find a controller  $\mathbf{K}$  such that minimizes the energy ( $L_2$ ) gain of the closed-loop system, i.e., that minimizes

$$\|T_{zw}\|_{H_\infty} = \sup_{w \neq 0} \frac{\|z\|_{L_2}}{\|w\|_{L_2}} \quad (2.16)$$

A better approach in practice is to pursue a sub-optimal design, i.e., given  $\gamma > 0$ , find a controller  $\mathbf{K}$  such that  $\|T_{zw}\|_{H_\infty} < \gamma$ , if one exists. In other words, assume that the controller  $\mathbf{K}$  and the disturbance  $w$  are playing a zero-sum game, in which the cost is

$$\|z\|_{L_2}^2 - \gamma^2 \|w\|_{L_2}^2. \quad (2.17)$$

Now, our goal is to find out what is the smallest  $\gamma$  such that the controller can win the game. More details can be found in [28].

## 2.6 State Feedback Control and Output Feedback Control

Consider the linearized state-space model of the plant is defined as follows.

$$\Delta \dot{\mathbf{x}} = \mathbf{A}\Delta \mathbf{x} + \mathbf{B}_u\Delta \mathbf{u}_{wac} + \mathbf{B}_w\Delta \mathbf{w} \quad (2.18)$$

$$\Delta \mathbf{y} = \mathbf{C}_y\Delta \mathbf{x} \quad (2.19)$$

$$\Delta \mathbf{z} = \mathbf{C}_z\Delta \mathbf{x} + \mathbf{D}_z\Delta \mathbf{u}_{wac} \quad (2.20)$$

where  $x$  is the state vector,  $u_{wac}$  is the wide area control signal,  $w$  is the disturbance input vector,  $z$  is the performance output vector, and  $y$  is the measurement vector. Fig. 2.1 represents the control center block diagram which can be implemented by using either state feedback or output feedback control. The inputs to the control center are remote measurements with time stamping alignments. The state estimator is optional, and it is present in the case of state feedback control. The feedback gain matrix can be calculated using any one of the methods depending upon the control technique.

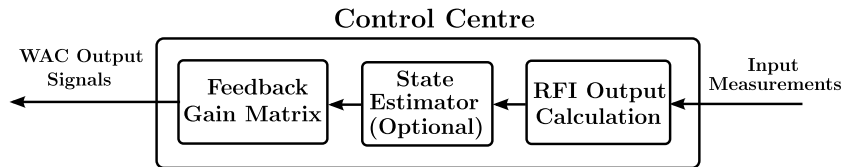


Figure 2.1: Control center block diagram.

For a linearized system, the output feedback can equivalently be represented in the form of state feedback. In the case of the state feedback, the WAC signals are derived through the following equation.

$$\Delta \mathbf{u}_{wac} = \mathbf{K}_{wac}\Delta \mathbf{x}_{wac}. \quad (2.21)$$

Here,  $\mathbf{K}_{wac}$  indicates the state feedback gain matrix. The equivalent state feed-

back matrix corresponding to a physically output feedback control system is obtained through the following equation.

$$\mathbf{K}_{wac} = \mathbf{G}_{wac} \mathbf{C}_y. \quad (2.22)$$

Equation (2.22) effectively imposes some structural constraints on the equivalent state feedback matrix. The structural constraints on the above equivalent state feedback matrix can be explicitly derived as follows [29].

$$\mathbf{K}_{wac} = \mathbf{K}_{wac} \mathbf{C}_y^T (\mathbf{C}_y \mathbf{C}_y^T)^{-1} \mathbf{C}_y. \quad (2.23)$$

## 2.7 Structurally Constrained $H_2$ -Norm Optimization

Consider a general linear dynamical system of the form shown in Equations (2.18)-(2.20). It is required to design an output feedback controller or state feedback controller for the particular system. The Matrix  $\mathbf{C}_y$  is assumed to have full row rank. It is further assumed that some elements of the matrix  $\mathbf{G}_{wac}$  can be zeros because of practical constraints. The structural constraints thus imposed on  $\mathbf{G}_{wac}$  can be written down as follows.

$$\mathbf{G}_{wac} \circ \Theta = \mathbf{0}. \quad (2.24)$$

Here, symbol  $\circ$  indicates the Hadamard product. The entries of the matrix  $\Theta$  are only zeros and ones, and it has the same row and column dimensions as that of  $\mathbf{G}_{wac}$ . The zero entries in  $\mathbf{G}_{wac}$  are determined by the unity entries in  $\Theta$ .

The above output feedback controller design problem is to be transformed into an equivalent state feedback controller design problem with the same form of structural constraints as in (2.24). For that, the original state vector  $\Delta \mathbf{x}$  needs to be transformed

to a new state vector  $\Delta\tilde{\mathbf{x}}$  as follows.

$$\Delta\tilde{\mathbf{x}} = \hat{\mathbf{C}}_y \Delta\mathbf{x}. \quad (2.25)$$

where  $\hat{\mathbf{C}}_y = [\mathbf{C}_y^T \quad \mathbf{C}_r^T]^T$  and matrix  $\mathbf{C}_r$  should be chosen in a way so that  $\hat{\mathbf{C}}_y$  can be invertible. With the new state vector, the input signal vector can be derived as follows.

$$\begin{aligned} \Delta\mathbf{u}_{wac} &= \mathbf{G}_{wac} \Delta\mathbf{y} \\ &= \mathbf{G}_{wac} \mathbf{C}_y \Delta\mathbf{x} \\ &= \begin{bmatrix} \mathbf{G}_{wac} & \mathbf{0} \end{bmatrix} \hat{\mathbf{C}}_y \Delta\mathbf{x} \\ &= \underbrace{\begin{bmatrix} \mathbf{G}_{wac} & \mathbf{0} \end{bmatrix}}_{\tilde{\mathbf{K}}_{wac}} \Delta\tilde{\mathbf{x}}. \end{aligned} \quad (2.26)$$

The equivalent state feedback controller is indicated by  $\tilde{\mathbf{K}}_{wac}$ , which is structurally constrained by the following relationship.

$$\tilde{\mathbf{K}}_{wac} \circ \tilde{\Theta} = \mathbf{0} \quad (2.27)$$

where,

$$\tilde{\Theta} = \begin{bmatrix} \Theta & \mathbf{U} \end{bmatrix}. \quad (2.28)$$

Here,  $\mathbf{U}$  is a matrix (of appropriate dimensions) of all ones.

In the next step, the state and performance output equations are to be expressed

in terms of the new state vector. Those are derived below.

$$\Delta \dot{\tilde{\mathbf{x}}} = \underbrace{\hat{C}_y A \hat{C}_y^{-1}}_{\tilde{A}} \Delta \tilde{\mathbf{x}} + \underbrace{\hat{C}_y B_u}_{\tilde{B}_u} \Delta \mathbf{u}_{wac} + \underbrace{\hat{C}_y B_w}_{\tilde{B}_w} \Delta \mathbf{w} \quad (2.29)$$

$$\Delta \mathbf{z} = \underbrace{C_z \hat{C}_y^{-1}}_{\tilde{C}_z} \Delta \tilde{\mathbf{x}} + D_z \Delta \mathbf{w}. \quad (2.30)$$

Based upon (2.29) and (2.30), the squared  $L_2$ -norm of  $\mathbf{z}(t)$  can be expressed as follows.

$$\begin{aligned} \|\Delta \mathbf{z}\|_2^2 &= \int_0^\infty \Delta \mathbf{z}(t)^T \Delta \mathbf{z}(t) dt \\ &= \int_0^\infty \left\{ \Delta \tilde{\mathbf{x}}(t)^T \tilde{Q} \Delta \tilde{\mathbf{x}}(t) + \Delta \mathbf{u}_{wac}(t)^T \mathbf{R} \Delta \mathbf{u}_{wac}(t) + 2 \Delta \mathbf{u}_{wac}(t)^T \tilde{S} \Delta \tilde{\mathbf{x}}(t) \right\} dt \end{aligned} \quad (2.31)$$

where,

$$\tilde{Q} = \left\{ \hat{C}_y^{-1T} \right\} Q \hat{C}_y^{-1} \quad (2.32)$$

$$\tilde{S} = S \hat{C}_y^{-1} \quad (2.33)$$

$$Q = C_z^T C_z \quad (2.34)$$

$$\mathbf{R} = D_z^T D_z \quad (2.35)$$

$$S = D_z^T C_z. \quad (2.36)$$

The  $H_2$ -norm of the system is defined through the following equation.

$$\|H\|_2 = \sum_{k=1}^{n_w} \|\Delta \mathbf{z}\|_2 : \Delta \mathbf{w}(t) = \phi(t) \mathbf{e}_k. \quad (2.37)$$

Here,  $\mathbf{e}_k$  is the  $k$  th column of the identity matrix. The number of disturbance inputs (i.e. the row size of  $\Delta \mathbf{w}$ ) is indicated by  $n_w$ . Symbol  $\phi(t)$  stands for the unit impulse

function.

The third term in (2.31), which defines the coupling between state and input vectors in the  $L_2$ -norm, is problematic for carrying out the  $H_2$ -norm optimization. In order to eliminate the particular term, further modifications to system equations are required. In specific, the input vector is to be redefined. By recognizing that  $\Delta \mathbf{u}_{wac} = \tilde{\mathbf{K}}_{wac} \Delta \tilde{\mathbf{x}}$ , the  $L_2$ -norm of  $\Delta \mathbf{z}(t)$  can be simplified as follows.

$$\|\Delta \mathbf{z}\|_2^2 = \int_0^\infty \left\{ \Delta \tilde{\mathbf{x}}(t)^T \tilde{\mathbf{Q}}' \Delta \tilde{\mathbf{x}}(t) + \Delta \mathbf{u}'_{wac}(t)^T \mathbf{R} \Delta \mathbf{u}'_{wac}(t) \right\} dt \quad (2.38)$$

where,

$$\tilde{\mathbf{Q}}' = \tilde{\mathbf{Q}} - \tilde{\mathbf{S}}^T \mathbf{R}^{-1} \tilde{\mathbf{S}} \quad (2.39)$$

$$\Delta \mathbf{u}'_{wac} = \tilde{\mathbf{K}}'_{wac} \Delta \tilde{\mathbf{x}}_{wac} \quad (2.40)$$

$$\tilde{\mathbf{K}}'_{wac} = \tilde{\mathbf{K}}_{wac} + \mathbf{R}^{-1} \tilde{\mathbf{S}}. \quad (2.41)$$

Replacements of  $\Delta \mathbf{u}_{wac} = \tilde{\mathbf{K}}_{wac} \Delta \tilde{\mathbf{x}}$  in Equation (2.31) and  $\Delta \mathbf{u}'_{wac} = \tilde{\mathbf{K}}'_{wac} \Delta \tilde{\mathbf{x}}$  in (2.38) yield the same final expression. The state and performance output equations can as well be modified in the following forms.

$$\Delta \dot{\tilde{\mathbf{x}}} = \tilde{\mathbf{A}}' \Delta \tilde{\mathbf{x}} + \tilde{\mathbf{B}}_u \Delta \mathbf{u}'_{wac} + \tilde{\mathbf{B}}_w \Delta \mathbf{w} \quad (2.42)$$

$$\Delta \mathbf{z} = \tilde{\mathbf{C}}'_z \Delta \tilde{\mathbf{x}} + \tilde{\mathbf{D}}'_z \Delta \mathbf{u}'_{wac} \quad (2.43)$$

where,

$$\tilde{\mathbf{A}}' = \tilde{\mathbf{A}} - \tilde{\mathbf{B}}_u \mathbf{R}^{-1} \tilde{\mathbf{S}} \quad (2.44)$$

$$\tilde{\mathbf{C}}'_z = \left[ \tilde{\mathbf{Q}}'^{\frac{1}{2}} \quad \mathbf{0} \right]^T \quad (2.45)$$

$$\tilde{\mathbf{D}}'_z = \left[ \mathbf{0} \quad \mathbf{R}^{\frac{1}{2}} \right]^T. \quad (2.46)$$

The modified state equation is obtained by simple algebraic manipulations, whereas

the modified equation of the performance output results in the same  $L_2$ -norm expression as in (2.38).

By using the latest forms of the state equation, performance output equation and  $L_2$ -norm, the structurally constrained  $H_2$ -norm optimization problem can be formulated as follows [30].

$$\text{Minimize } \left\{ \text{trace} \left( \tilde{\mathbf{B}}_w^T \mathbf{F} \tilde{\mathbf{B}}_w \right) \right\} \quad (2.47)$$

s.t.

$$\begin{aligned} \mathbf{F} \left( \tilde{\mathbf{A}}' + \tilde{\mathbf{B}}_u \tilde{\mathbf{K}}'_{wac} \right) + \left( \tilde{\mathbf{A}}' + \tilde{\mathbf{B}}_u \tilde{\mathbf{K}}'_{wac} \right)^T \mathbf{F} + \\ \left( \tilde{\mathbf{C}}'_z + \tilde{\mathbf{D}}'_z \tilde{\mathbf{K}}'_{wac} \right)^T \left( \tilde{\mathbf{C}}'_z + \tilde{\mathbf{D}}'_z \tilde{\mathbf{K}}'_{wac} \right) = \mathbf{0} \end{aligned} \quad (2.48)$$

$$\left( \tilde{\mathbf{K}}'_{wac} - \mathbf{R}^{-1} \tilde{\mathbf{S}} \right) \circ \tilde{\mathbf{\Theta}} = \mathbf{0}. \quad (2.49)$$

The objective function effectively indicates the squared  $H_2$ -norm of the closed-loop system. The variables in the above optimization problem are  $\mathbf{F}$  and  $\tilde{\mathbf{K}}'_{wac}$ . Matrix  $\mathbf{F}$  is the observability Grammian matrix (of the closed-loop system), which is obtained by solving the Lyapunov Equation (2.48). The structural constraints on  $\tilde{\mathbf{K}}'_{wac}$  is enforced through (2.49). Here also,  $\tilde{\mathbf{K}}'_{wac}$  is structurally constrained to have fixed values at certain locations. However, those fixed values may not necessarily be zeros.

## 2.8 Linear and Non-linear Kalman Filtering

In order to estimate the system states, the most used algorithms are Kalman, extended, and unscented Kalman filter methods. The Kalman filter method can be used to estimate the system states if the system is linear. On the other hand, in order to estimate the non-linear system states, the extended or unscented transformation can be used.

### 2.8.1 Kalman Filter Algorithm

Consider the linear dynamical system in discrete form described by the following equations:

$$x_k = \mathbf{A}x_{k-1} + \mathbf{B}_k u_k \quad (2.50)$$

$$z_k = \mathbf{C}x_k. \quad (2.51)$$

The Kalman filter algorithm for above linear system is as follows:

$$\text{Step 1} \quad \rightarrow \quad \bar{x}_k = A_k x_{k-1} + B_k u_k \quad (2.52)$$

$$\text{Step 2} \quad \rightarrow \quad \bar{P}_k = A_k P_{k-1} A_k^T + R_k \quad (2.53)$$

$$\text{Step 3} \quad \rightarrow \quad K_k = \bar{P}_k C_k^T (C_k P_k C_k^T + Q_k)^{-1} \quad (2.54)$$

$$\text{Step 4} \quad \rightarrow \quad \hat{x}_k = \bar{x}_k + K_k (z_k - C_k \bar{x}_k) \quad (2.55)$$

$$\text{Step 5} \quad \rightarrow \quad \hat{P}_k = (I - K_k C_k) \bar{P}_k \quad (2.56)$$

$$\text{Step 6} \quad \rightarrow \quad \text{return } \hat{x}_k, \hat{P}_k. \quad (2.57)$$

The notations and variables are standard as defined in [31].

### 2.8.2 Extended Kalman Filter Algorithm

For non-linear systems, the extended Kalman filter (EKF) algorithm is probably the most widely used estimation algorithm. However, this method has its own advantages and disadvantages. The EKF algorithm implementation for non-linear systems is described as follows. First, let us consider the generalized non-linear system in discrete form as follows.

$$x_k = f(u_k, x_{k-1}) \quad (2.58)$$

$$z_k = h(x_k). \quad (2.59)$$



The extended Kalman filter algorithm for above non-linear system is as follows:

$$\text{Step 1} \quad \rightarrow \quad \bar{x}_k = f(u_k, x_{k-1}) \quad (2.60)$$

$$\text{Step 2} \quad \rightarrow \quad \bar{P}_k = G_k P_{k-1} G_k^T + R_k \quad (2.61)$$

$$\text{Step 3} \quad \rightarrow \quad K_k = \bar{P}_k C_k^T (C_k \bar{P}_k C_k^T + Q_k)^{-1} \quad (2.62)$$

$$\text{Step 4} \quad \rightarrow \quad \hat{x}_k = \bar{x}_k + K_k (z_k - h(\bar{x}_k)) \quad (2.63)$$

$$\text{Step 5} \quad \rightarrow \quad \hat{P}_k = (I - K_k C_k) \bar{P}_k \quad (2.64)$$

$$\text{Step 6} \quad \rightarrow \quad \text{return } \hat{x}_k, \hat{P}_k. \quad (2.65)$$

The notations and variables are standard as defined in [31].

### 2.8.3 Unscented Kalman Filter

EKF method is difficult to implement, difficult to tune, and reliable only for systems that are close to the linear on the updates. Many of the difficulties of the EKF method arise from its linearization. To overcome the limitations of the EKF method, unscented transformation (UT) was applied in [32] to propagate mean and covariance information by nonlinear transformation. J. K. Uhlmann introduced the concept of unscented transformation [33]. Unscented transformation method is easier to approximate a probability distribution than to approximate a non-linear function. The unscented Kalman filter algorithm for the non-linear system described in (2.58)-(2.59) is as follows:

$$\text{Step 1} \quad \rightarrow \quad \chi_{k-1} = \begin{bmatrix} x_{k-1} & x_{k-1} + \gamma\sqrt{P_{k-1}} & x_{k-1} - \gamma\sqrt{P_{k-1}} \end{bmatrix} \quad (2.66)$$

$$\text{Step 2} \quad \rightarrow \quad \bar{\chi}_k^* = f(u_k, \chi_{k-1}) \quad (2.67)$$

$$\text{Step 3} \quad \rightarrow \quad \bar{x}_k = \sum_{i=0}^{2n} w_m^{[i]} \bar{\chi}_k^{*[i]} \quad (2.68)$$

$$\text{Step 4} \quad \rightarrow \quad \bar{P}_k = \sum_{i=0}^{2n} w_c^{[i]} \left( \bar{\chi}_k^{*[i]} - \bar{x}_k \right) \left( \bar{\chi}_k^{*[i]} - \bar{x}_k \right)^T + R_k \quad (2.69)$$

$$\text{Step 5} \quad \rightarrow \quad \bar{\chi}_k = \begin{bmatrix} \bar{x}_k & \bar{x}_k + \gamma\sqrt{\bar{P}_k} & \bar{x}_k - \gamma\sqrt{\bar{P}_k} \end{bmatrix} \quad (2.70)$$

$$\text{Step 6} \quad \rightarrow \quad \bar{z}_k = h(\bar{\chi}_k) \quad (2.71)$$

$$\text{Step 7} \quad \rightarrow \quad \hat{z}_k = \sum_{i=0}^{2n} w_m^{[i]} \bar{z}_k^{[i]} \quad (2.72)$$

$$\text{Step 8} \quad \rightarrow \quad \mathcal{S}_k = \sum_{i=0}^{2n} w_c^{[i]} \left( \bar{z}_k^{[i]} - \hat{z}_k \right) \left( \bar{z}_k^{[i]} - \hat{z}_k \right)^T + Q_k \quad (2.73)$$

$$\text{Step 9} \quad \rightarrow \quad \bar{P}_k^{x,z} = \sum_{i=0}^{2n} w_c^{[i]} \left( \bar{\chi}_k^{[i]} - \bar{x}_k \right) \left( \bar{z}_k^{[i]} - \hat{z}_k \right)^T \quad (2.74)$$

$$\text{Step 10} \quad \rightarrow \quad K_k = \bar{P}_k^{x,z} \mathcal{S}_k^{-1} \quad (2.75)$$

$$\text{Step 11} \quad \rightarrow \quad \hat{x}_k = \bar{x}_k + K_k(z_k - \hat{z}_k) \quad (2.76)$$

$$\text{Step 12} \quad \rightarrow \quad \hat{P}_k = \bar{P}_k - K_k \mathcal{S}_k K_k^T \quad (2.77)$$

$$\text{Step 13} \quad \rightarrow \quad \text{return } \hat{x}_k, \hat{P}_k. \quad (2.78)$$

The notations and variables are standard as defined in [34].

## 2.9 Summary

In this chapter, the structurally constrained  $H_2$ -norm optimization technique is derived for the wide area controller design. The implementation of the state feedback controller by means of the output feedback controller is presented. In addition, in order to estimate the states, extended and unscented Kalman filter algorithms are presented.

# Chapter 3

## General WAC Framework for a Power System

### 3.1 Introduction

This chapter presents the general wide area controller design for a power system network. It includes the modeling of the total power system, issue of limited measurements, and implementation of non-linear Kalman filter with unknown inputs. The wide area controller is designed by using structurally constrained  $H_2$ -norm optimization to address the limited measurement issue with unknown load composition. Results show that the wide area controller gives good performance even under the situation of a few measurements. This concept is extended to further applications that are explained in the next chapters.

### 3.2 General Architecture of the WAC System

The general architecture of the conventional WAC system is shown in Fig. 3.1. The voltage and current phasors measured by PMUs are transmitted to the control center by means of a wide area monitoring (WAM) communication network [35]. The phasor measurements are received at the control center in the form of time-stamp aligned sets. The time-stamp alignment of phasors is carried out by means of phasor

data concentrators that can be treated as integral parts of the WAM network. At the control center, the phasor data is first converted into the reference frame independent (RFI) output quantities (such as active power, reactive power, and voltage magnitude). In the case of output feedback control [29], [36] [37] [38] [39], the RFI output quantities measured are directly processed through a gain matrix to generate the WAC signals. On the other hand, an intermediate level of state estimation is required in the case of state feedback control [40], [41]. The state feedback controller generates WAC signals based upon the observable dynamic states of the system. The dynamic states of the system are determined by means of an extended Kalman filter (EKF) [42] or unscented Kalman filter (UKF) [43], [44]. Typically, the dynamic state estimation is carried by using subsystem models; therefore, the EKF/UKF algorithm employed should also have the capacity to dynamically determine the inputs to each subsystem [45]. After generating the WAC signals, those are transmitted to power system components (such as generators' excitation systems [24] or FACTS devices [46]) via a WAC network. The implementation of the output feedback control is simpler than the implementation of the state feedback control since the former does not require any state estimator. However, the controller performance may be superior in the case of the state feedback control. This is because the system condition is more precisely addressed while designing and implementing the state feedback controller.

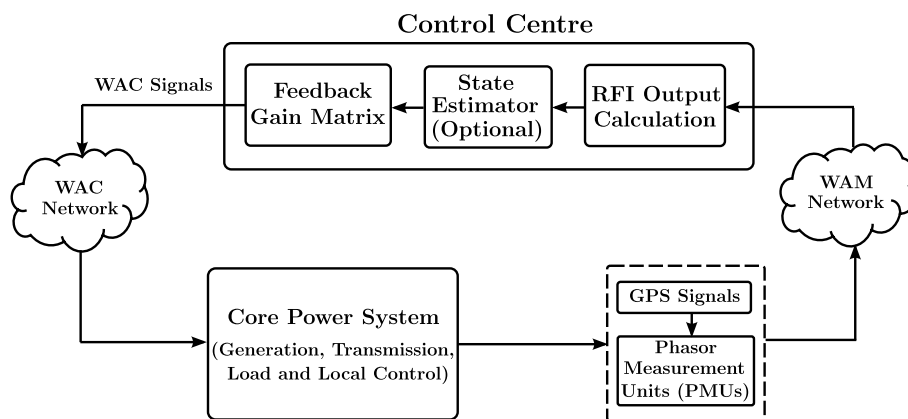


Figure 3.1: General architecture of the traditional WAC system.

The state or output feedback controller is designed based upon the linearized (i.e., small-signal) model of the system. The linearized mathematical block diagram rep-

representation of the traditional WAC system with the output feedback is shown in Fig. 3.2. Here, the block diagram is shown in the state-space form. The plant is basically the power network (i.e., the interconnection of generating units, loads and transmission lines) with local controls. The transportation delay block is introduced to take into account the effect of time delays that take place between phasor measurements and the receipt of corresponding WAC signals at the plant. The time delays are caused because of the latencies of WAM and WAC networks as well as because of the computations involved in generating the WAC signals. In [47], the time delays in WAM and WAC networks are separately shown on the input and output sides, respectively, of the WADC. However, the time delays that happen in the input signals to the WADC should be uniform because of the time-stamp alignment. Therefore, the net time delay effect can be lumped on the output side of the WADC.

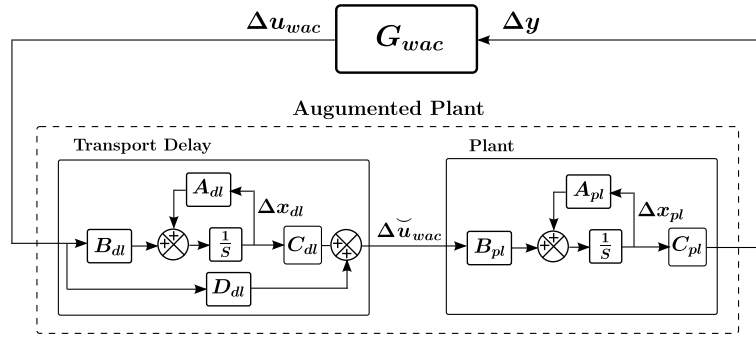


Figure 3.2: linearized mathematical block diagram representation.

In Fig. 3.2, the WAC signal vector generated by the WADC and the delayed WAC signal vector received at the plant are indicated by  $\mathbf{u}_w$  and  $\tilde{\mathbf{u}}_w$ , respectively. It may not be possible to perform the time-stamp alignment of WAC signals transmitted to different components. This may, ultimately, result in different time delays for different WAC signals. The feedback gain matrix deployed is represented by  $\mathbf{G}_w$ . The state vectors associated with the plant and the transportation delay blocks are represented by  $\mathbf{x}_{pl}$  and  $\mathbf{x}_{dl}$ , respectively. The transportation delay block is typically modeled by means of Pade approximation [48] with the finite number of states. In this work, the first order Pade approximation is employed, which is in the line of [49]. The RFI output vector is indicated by  $\mathbf{y}$ . The Vector  $\mathbf{y}$  is usually a function of only

the plant states. Prefix  $\Delta$  is used to indicate the perturbed value of a quantity from the equilibrium.

### 3.3 Modeling of Power System

In this section, the modeling of a power system that includes generator group (generators, exciters, turbines, and PSSs), transmission network and different types of load are explained in detail. The modeling of a generator group can be represented by using differential equations. On the other hand, the network equations are represented in the form of algebraic equations. Loads representation is either differential or algebraic or differential algebraic. It can be varied depending upon the type of load. Thus, a set of differential algebraic equations is used to describe the behavior of the total power system. The modeling of the total power system presented in this section is well defined in [3], [4], and [50].

#### 3.3.1 Generator Modeling

The synchronous generator models used in this study are the two-axis model (4<sup>th</sup> order) and the sub-transient model (6<sup>th</sup> order) [50]. The two-axis model can be obtained from the sub-transient model by eliminating damper winding dynamics ( $\psi_{1d}$  and  $\psi_{2q}$ ). The differential equations describing the sub-transient dynamic behavior

of each generating unit in a power system are given as follows [50].

$$\frac{d\delta_i}{dt} = \omega_i - \omega_s \quad (3.1)$$

$$\frac{d\omega_i}{dt} = \frac{\omega_s}{2H} \left[ T_{Mi} - (\psi_{qi}I_{di} - \psi_{di}I_{qi}) - D(\omega_i - \omega_s) \right] \quad (3.2)$$

$$\frac{dE'_{qi}}{dt} = \frac{1}{T'_{doi}} \left[ -E'_{qi} - (X_{di} - X'_{di}) \left\{ -I_{di} - \frac{X'_{di} - X''_{di}}{(X'_{di} - X_{lsi})^2} \right. \right. \\ \left. \left. \left( \psi_{1di} - (X'_{di} - X_{lsi})I_{di} - E'_{qi} \right) \right\} + E_{fdi} \right] \quad (3.3)$$

$$\frac{dE'_{di}}{dt} = \frac{1}{T'_{qoi}} \left[ -E'_{di} + (X_{qi} - X'_{qi}) \left\{ -I_{qi} - \frac{X'_{qi} - X''_{qi}}{(X'_{qi} - X_{lsi})^2} \right. \right. \\ \left. \left. \left( \psi_{2qi} - (X'_{qi} - X_{lsi})I_{qi} + E'_{di} \right) \right\} \right] \quad (3.4)$$

$$\frac{d\psi_{1di}}{dt} = \frac{1}{T''_{doi}} \left[ -\psi_{1di} + E'_{qi} + (X'_{di} - X_{lsi})I_{di} \right] \quad (3.5)$$

$$\frac{d\psi_{2qi}}{dt} = \frac{1}{T''_{qoi}} \left[ -\psi_{2qi} - E'_{di} + (X'_{qi} - X_{lsi})I_{qi} \right]. \quad (3.6)$$

Where  $i = 1, 2, \dots, m$ ;  $m$  represents total number of generators. The small-signal modeling of above equations (3.1)-(3.6) can be written in matrix form as follows.

$$\Delta \dot{\mathbf{x}}_{gi} = \mathbf{A}_{gi} \Delta \mathbf{x}_{gi} + \mathbf{B}_{1gi} \Delta \mathbf{I}_{dqi} + \mathbf{B}_{2gi} \Delta \mathbf{V}_{gi}. \quad (3.7)$$

For  $m$ -machine system, (3.7) can be expressed in matrix form as

$$\Delta \dot{\mathbf{X}}_G = \mathbf{A}_G \Delta \mathbf{X}_G + \mathbf{B}_{1G} \Delta \mathbf{I}_{DQ} + \mathbf{B}_{2G} \Delta \mathbf{V}_G. \quad (3.8)$$

As we know that at any  $i^{th}$  bus

$$V_{Di} + jV_{Qi} = V_i \cos \theta_i + jV_i \sin \theta_i. \quad (3.9)$$

The small-signal modeling of above equation (3.9) can be written as

$$\underbrace{\begin{bmatrix} \Delta V_{Di} \\ \Delta V_{Qi} \end{bmatrix}}_{\Delta \mathbf{V}_{DQi}} = \underbrace{\begin{bmatrix} -V_i \sin \theta_i & \cos \theta_i \\ V_i \cos \theta_i & \sin \theta_i \end{bmatrix}}_{\mathbf{R}} \underbrace{\begin{bmatrix} \Delta \theta_i \\ \Delta V_i \end{bmatrix}}_{\Delta \mathbf{V}_{gi}}. \quad (3.10)$$

Therefore,  $\Delta \mathbf{V}_{gi}$  can be expressed in terms of  $\Delta \mathbf{V}_{DQi}$  by using the relation  $\Delta \mathbf{V}_{gi} = \mathbf{R}^{-1} \Delta \mathbf{V}_{DQi}$ .

### Generator algebraic equations:

The generator output currents at generator buses can be calculated as follows:

$$\begin{bmatrix} R_{si} & -X'_{qi} \\ X'_{di} & R_{si} \end{bmatrix} \begin{bmatrix} I_{dgi} \\ I_{qgi} \end{bmatrix} = \begin{bmatrix} E'_{di} - V_i \sin(\delta_i - \theta_i) \\ E'_{qi} - V_i \cos(\delta_i - \theta_i) \end{bmatrix}. \quad (3.11)$$

The generator currents in  $d - q$  form can be transformed into  $D - Q$  form by using the following transformation matrix

$$\begin{bmatrix} I_{Dgi} \\ I_{Qgi} \end{bmatrix} = \begin{bmatrix} \sin \delta_i & \cos \delta_i \\ -\cos \delta_i & \sin \delta_i \end{bmatrix} \begin{bmatrix} I_{dgi} \\ I_{qgi} \end{bmatrix}. \quad (3.12)$$

By combining the equations (3.11) and (3.12), the generator currents in  $D - Q$  form can be written as

$$\begin{bmatrix} I_{Dgi} \\ I_{Qgi} \end{bmatrix} = \begin{bmatrix} \sin \delta_i & \cos \delta_i \\ -\cos \delta_i & \sin \delta_i \end{bmatrix} \begin{bmatrix} R_{si} & -X'_{qi} \\ X'_{di} & R_{si} \end{bmatrix}^{-1} \begin{bmatrix} E'_{di} - V_i \sin(\delta_i - \theta_i) \\ E'_{qi} - V_i \cos(\delta_i - \theta_i) \end{bmatrix}. \quad (3.13)$$

The small-signal modeling of above equation (3.13) can be written in matrix form as

$$\Delta \mathbf{I}_{gi} = \mathbf{C}_{gi} \Delta \mathbf{x}_{gi} + \mathbf{D}_{gi} \Delta \mathbf{V}_{gi}. \quad (3.14)$$



For  $m$ -machine system, the above equation (3.14) is modified into

$$\Delta \mathbf{I}_G = \mathbf{C}_G \Delta \mathbf{X}_G + \mathbf{D}_G \Delta \mathbf{V}_{DQG} \quad (3.15)$$

### 3.3.2 Exciter Model

Each generation unit is excited by using an automatic voltage regulator (AVR). Two types of AVRs are used in this work. Differential algebraic equations of IEEE-DC1A type of AVR are given by (3.16)-(3.18) and for IEEE-ST1A type of AVR are given by (3.19)-(3.20) [50].

$$\frac{dE_{fdi}}{dt} = \frac{1}{T_{Ei}} \left[ -K_{Ei} E_{fdi} - E_{fdi} A_{ex} e^{B_{ex} E_{fdi}} + V_{Ri} \right] \quad (3.16)$$

$$\frac{dR_{fi}}{dt} = \frac{1}{T_{Fi}} \left[ -R_{fi} + \frac{K_{Fi}}{T_{Fi}} E_{fdi} \right] \quad (3.17)$$

$$\begin{aligned} \frac{dV_{Ri}}{dt} = \frac{1}{T_{Ai}} \left[ -V_{Ri} + K_{Ai} R_{fi} - \frac{K_{Ai} K_{Fi}}{T_{Fi}} E_{fdi} \right. \\ \left. + K_{Ai} (V_{refi} - V_{ti} + U_{PSSi} + U_{WACi}) \right]. \end{aligned} \quad (3.18)$$

$$\frac{dV_{ti}}{dt} = \frac{1}{T_{ri}} [V_i - V_{ti}] \quad (3.19)$$

$$E_{fdi} = K_{Ai} (V_{refi} - V_{ti} + U_{PSSi} + U_{WACi}) \quad (3.20)$$

Where,  $U_{PSS}$  is the PSS output signal and  $U_{WAC}$  is the wide area controller output signal. The small-signal modeling of each exciter can be written as in (3.21).

$$\Delta \dot{\mathbf{x}}_{exi} = \mathbf{A}_{exi} \Delta \mathbf{x}_{exi} + \mathbf{B}_{1exi} \Delta \mathbf{I}_{dqi} + \mathbf{B}_{2exi} \Delta \mathbf{V}_{gi} + \mathbf{E}_{exi} \Delta \mathbf{U}_{WACi} \quad (3.21)$$

For  $m$ -machine system, (3.21) can be expressed in matrix form as

$$\Delta \dot{\mathbf{X}}_{ex} = \mathbf{A}_{ex} \Delta \mathbf{X}_{ex} + \mathbf{B}_{1ex} \Delta \mathbf{I}_{DQ} + \mathbf{B}_{2ex} \Delta \mathbf{V}_G + \mathbf{E}_{ex} \Delta \mathbf{U}_{WAC}. \quad (3.22)$$

### 3.3.3 Turbine and Speed Governor Model

The turbines are represented using the non-reheat type, and the governors are represented with incremental type [50]. The differential equations describing their behavior are given by

$$\frac{dT_{mi}}{dt} = \frac{1}{T_{CHi}} \left[ -T_{mi} + P_{SVi} \right] \quad (3.23)$$

$$\frac{dP_{SVi}}{dt} = \frac{1}{T_{SVi}} \left[ -P_{SVi} + P_{Ci} - \frac{1}{R_{Di}} \left( \frac{\omega_i}{\omega_s} - 1 \right) \right]. \quad (3.24)$$

The small-signal modeling of each turbine and speed governor can be written as in (3.25).

$$\Delta \dot{\mathbf{x}}_{tui} = \mathbf{A}_{tui} \Delta \mathbf{x}_{tui} + \mathbf{B}_{1tui} \Delta \mathbf{I}_{dqi} + \mathbf{B}_{2tui} \Delta \mathbf{V}_{gi} \quad (3.25)$$

For  $m$ -machine system, (3.25) can be expressed in matrix form as

$$\Delta \dot{\mathbf{X}}_{tu} = \mathbf{A}_{tu} \Delta \mathbf{X}_{tu} + \mathbf{B}_{1tu} \Delta \mathbf{I}_{DQ} + \mathbf{B}_{2tu} \Delta \mathbf{V}_G. \quad (3.26)$$

### 3.3.4 Power System Stabilizer Model

The general block diagram of the power system stabilizer (PSS) is defined in Chapter 1. It consists of one washout filter, two lead-lag blocks, and PSS gain. The PSS can be designed by using either speed or power input. The speed input based PSS design is used in this work. The differential equations governing the behavior of PSS are as follows.

$$\frac{dU_{1i}}{dt} = K_{PSSi} \frac{d\omega_i}{dt} - \frac{1}{T_{wi}} U_{1i} \quad (3.27)$$

$$\frac{dU_{2i}}{dt} = \frac{1}{T_{2i}} \left[ U_{1i} - U_{2i} + T_{1i} \frac{dU_{1i}}{dt} \right] \quad (3.28)$$

$$\frac{dU_{PSSi}}{dt} = \frac{1}{T_{4i}} \left[ U_{2i} - U_{PSSi} + T_{3i} \frac{dU_{2i}}{dt} \right]. \quad (3.29)$$

Where  $i = 1, 2, \dots, m$ ;  $m$  represents total number of generators in the system. The notations are standard, and those can be found detail in [50]. The small-signal modeling

of each PSS can be written as in (3.30).

$$\Delta \dot{\mathbf{x}}_{pssi} = \mathbf{A}_{pssi} \Delta \mathbf{x}_{pssi} + \mathbf{B}_{1pssi} \Delta \mathbf{I}_{dqi} + \mathbf{B}_{2pssi} \Delta \mathbf{V}_{gi} \quad (3.30)$$

For  $m$ -machine system, (3.30) can be expressed in matrix form as

$$\Delta \dot{\mathbf{X}}_{pss} = \mathbf{A}_{pss} \Delta \mathbf{X}_{pss} + \mathbf{B}_{1pss} \Delta \mathbf{I}_{DQ} + \mathbf{B}_{2pss} \Delta \mathbf{V}_G. \quad (3.31)$$

### 3.3.5 Network Modeling

The power system network can be represented in either power balance or current balance form. Here, the linearized network equations are expressed in the current balance form. The network model equations in the current balance form at particular bus are given by

$$\underbrace{\begin{bmatrix} \Delta I_{Di} \\ \Delta I_{Qi} \end{bmatrix}}_{\Delta \mathbf{I}_{DQi}} = \underbrace{\begin{bmatrix} G_{ij} & -B_{ij} \\ B_{ij} & G_{ij} \end{bmatrix}}_{\mathbf{Y}_{DQij}} \underbrace{\begin{bmatrix} \Delta V_{Di} \\ \Delta V_{Qi} \end{bmatrix}}_{\Delta \mathbf{V}_{DQi}} \quad (3.32)$$

for  $i = j = 1, 2, \dots, n$ , where  $n$  represents the total number of buses. For an  $n$ -bus system, the equation (3.32) is modified into

$$\Delta \mathbf{I}_{DQ} = \mathbf{Y}_{DQ} \Delta \mathbf{V}_{DQ}. \quad (3.33)$$

where,  $\mathbf{I}_{DQ}$  represents the bus injection currents,  $\mathbf{V}_{DQ}$  represents the bus voltages and  $\mathbf{Y}_{DQ}$  represents the bus admittance matrix.

### 3.3.6 Load Modeling

The loads are mainly divided into two types, and those are static and dynamic loads. The load at particular load bus may be either static or dynamic or mixed type. The different load types which are used in this work are explained below. Initially, the

current drawn by each load at  $i^{th}$  load bus can be calculated as follows:

$$\begin{aligned} I_{li} &= \left[ \frac{P_{Li} + jQ_{Li}}{\bar{V}_{li}} \right]^* \\ I_{Dli} + jI_{Qli} &= \left[ \frac{P_{Li} - jQ_{Li}}{V_{li}^2} \right] (V_{Dli} + jV_{Qli}). \end{aligned} \quad (3.34)$$

The small-signal modeling of equation (3.34) can be written as

$$\begin{aligned} \begin{bmatrix} \Delta I_{Dli} \\ \Delta I_{Qli} \end{bmatrix} &= \frac{1}{V_{0li}^2} \begin{bmatrix} V_{D0li} & V_{Q0li} \\ V_{Q0li} & -V_{D0li} \end{bmatrix} \underbrace{\begin{bmatrix} \Delta P_{Li} \\ \Delta Q_{Li} \end{bmatrix}}_{\Delta S_{li}} + \\ &\quad \begin{bmatrix} Y_{L1i} & Y_{L2i} \\ Y_{L3i} & Y_{L4i} \end{bmatrix} \underbrace{\begin{bmatrix} \Delta V_{Dli} \\ \Delta V_{Qli} \end{bmatrix}}_{\Delta V_{DQli}} \end{aligned} \quad (3.35)$$

where,  $V_{0li}$  is the initial voltage magnitude at  $i^{th}$  bus and

$$\begin{aligned} Y_{L1i} &= \frac{P_{L0i}}{V_{0li}^2} \left( 1 - \frac{2V_{D0li}^2}{V_{0li}^2} \right) - \frac{2Q_{L0i}}{V_{0li}^4} V_{D0li} V_{Q0li} \\ Y_{L2i} &= \frac{Q_{L0i}}{V_{0li}^2} \left( 1 - \frac{2V_{Q0li}^2}{V_{0li}^2} \right) - \frac{2P_{L0i}}{V_{0li}^4} V_{D0li} V_{Q0li} \\ Y_{L3i} &= \frac{Q_{L0i}}{V_{0li}^2} \left( -1 + \frac{2V_{D0li}^2}{V_{0li}^2} \right) - \frac{2P_{L0i}}{V_{0li}^4} V_{D0li} V_{Q0li} \\ Y_{L4i} &= \frac{P_{L0i}}{V_{0li}^2} \left( 1 - \frac{2V_{Q0li}^2}{V_{0li}^2} \right) + \frac{2Q_{L0i}}{V_{0li}^4} V_{D0li} V_{Q0li} \end{aligned}$$

where  $P_{L0i}$  is the initial actual active power magnitude of  $i^{th}$  load. Equation (3.35) can be written in compact form as

$$\Delta I_{li} = C_{li} \Delta S_{li} + D_{li} \Delta V_{DQli}. \quad (3.36)$$

For  $i = m + 1$  to  $n$ -buses in the system, the equation (3.36) is modified into

$$\Delta I_L = C_L \Delta S_L + D_L \Delta V_{DQL} \quad (3.37)$$

where  $\mathbf{C}_L$ , and  $\mathbf{D}_L$  are block diagonal matrices.

### Static Loads

Two types of static load models which are generally used in the power system studies and those are exponential and polynomial loads. Based on the exponents used in the exponential loads, the load characteristics will be varied. Whereas, the polynomial load is a combination of different exponential loads. The general form of exponential load model at  $i^{th}$  load bus can be written as in the following form:

$$P_{Li} = z_i P_{L0i}^{nom} \left( \frac{V_{Li}}{V_{0Li}} \right)^{\alpha_i} \quad (3.38)$$

$$Q_{Li} = z_i Q_{L0i}^{nom} \left( \frac{V_{Li}}{V_{0Li}} \right)^{\beta_i} \quad (3.39)$$

where, the exponents  $\alpha_i$  and  $\beta_i$  values will be varied according to the type of load. In general three particular load exponents are used in the power system and those are constant impedance (CZ) load ( $\alpha_i = \beta_i = 2$ ), constant current (CC) load ( $\alpha_i = \beta_i = 1$ ) and constant power (CP) load ( $\alpha_i = \beta_i = 0$ ).  $P_{L0i}^{nom}$  and  $Q_{L0i}^{nom}$  represents the initial nominal values of active power and reactive power respectively.

The polynomial load model consists of different exponential load models. The polynomial load model which is used in this work is a combination of CP, CC, and CZ loads. Therefore, the generalized small-signal modeling of exponential and polynomial load models in terms of  $\Delta V_{Dli}$  and  $\Delta V_{Qli}$  can be written as

$$\begin{bmatrix} \Delta P_{Li} \\ \Delta Q_{Li} \end{bmatrix} = \mathbf{K}_{sta} \begin{bmatrix} V_{D0li} & V_{Q0li} \\ V_{D0li} & V_{Q0li} \end{bmatrix} \begin{bmatrix} \Delta V_{Dli} \\ \Delta V_{Qli} \end{bmatrix}. \quad (3.40)$$

where  $\mathbf{K}_{sta}$  is static load constant matrix and its values will be varied according to the type of load. Equation (3.40) can be written in compact form as

$$\Delta \mathbf{S}_{li} = \mathbf{D}_{li} \Delta \mathbf{V}_{DQli}. \quad (3.41)$$

If all the loads are expressed in the form of either exponential or polynomial load

model then the equation (3.41) will be modified into

$$\Delta \mathbf{S}_L = \mathbf{D}_L \Delta \mathbf{V}_{DQL} \quad (3.42)$$

where  $\mathbf{D}_L$  is a block diagonal matrix.

### Dynamic Loads

Two types of dynamic loads are presented in this work. Those are multiplicative and additive generic load models, and these can be found detail in [51]. The dynamic variable ( $z$ ) is multiplied in multiplicative type and added in additive type.

#### a) *Multiplicative generic load model*

The power consumed by the multiplicative generic load model is given by:

$$P_{Li} = z_{Pi} P_{L0i}^{nom} \left( \frac{V_{li}}{V_{0li}} \right)^{\alpha_{ti}} \quad (3.43)$$

$$Q_{Li} = z_{Qi} Q_{L0i}^{nom} \left( \frac{V_{li}}{V_{0li}} \right)^{\beta_{ti}}. \quad (3.44)$$

In steady state ( $z_{Pi} = z_{Qi} = 1$ ), hence the multiplicative generic load model equations (3.43) and (3.44) becomes:

$$P_{Si} = P_{L0i}^{nom} \left( \frac{V_{li}}{V_{0li}} \right)^{\alpha_{si}} \quad (3.45)$$

$$Q_{Si} = Q_{L0i}^{nom} \left( \frac{V_{li}}{V_{0li}} \right)^{\beta_{si}}. \quad (3.46)$$

Usually the transient load exponents ( $\alpha_{ti}, \beta_{ti}$ ) will have larger values than the steady state load exponents ( $\alpha_{si}, \beta_{si}$ ). The load dynamics of the multiplicative model are given by the following differential equations:

$$\frac{dz_{Pi}}{dt} = \frac{1}{T_{Pi}} \left[ \left( \frac{V_{li}}{V_{0li}} \right)^{\alpha_{si}} - z_{Pi} \left( \frac{V_{li}}{V_{0li}} \right)^{\alpha_{ti}} \right] \quad (3.47)$$

$$\frac{dz_{Qi}}{dt} = \frac{1}{T_{Qi}} \left[ \left( \frac{V_{li}}{V_{0li}} \right)^{\beta_{si}} - z_{Qi} \left( \frac{V_{li}}{V_{0li}} \right)^{\beta_{ti}} \right] \quad (3.48)$$

where  $T_{P_i}$  and  $T_{Q_i}$  are the time constants of load dynamic variables  $z_{P_i}$  and  $z_{Q_i}$  respectively.

b) *Additive generic load model*

The power consumed by the additive generic load model is given by:

$$P_{Li} = P_{L0i}^{nom} \left[ \left( \frac{V_{li}}{V_{0li}} \right)^{\alpha_{ti}} + z_{P_i} \right] \quad (3.49)$$

$$Q_{Li} = Q_{L0i}^{nom} \left[ \left( \frac{V_{li}}{V_{0li}} \right)^{\beta_{ti}} + z_{Q_i} \right]. \quad (3.50)$$

In steady state  $z_{P_i} = z_{Q_i} = 0$ , hence the additive generic load model equations (3.49) and (3.50) becomes same as the multiplicative generic model in steady state which are defined in equations (3.45) and (3.46). The load dynamics of the additive model are given by the following differential equations:

$$\frac{dz_{P_i}}{dt} = \frac{1}{T_{P_i}} \left[ -z_{P_i} + \left( \frac{V_{li}}{V_{0li}} \right)^{\alpha_s} - \left( \frac{V_{li}}{V_{0li}} \right)^{\alpha_t} \right] \quad (3.51)$$

$$\frac{dz_{Q_i}}{dt} = \frac{1}{T_{Q_i}} \left[ -z_{Q_i} + \left( \frac{V_{li}}{V_{0li}} \right)^{\beta_s} - \left( \frac{V_{li}}{V_{0li}} \right)^{\beta_t} \right]. \quad (3.52)$$

The generalized small-signal modeling of dynamic states defined in multiplicative and additive dynamic loads in terms of  $\Delta V_{Dli}$  and  $\Delta V_{Qli}$  can be written as

$$\begin{bmatrix} T_{P_i} \Delta \dot{z}_{P_i} \\ T_{Q_i} \Delta \dot{z}_{Q_i} \end{bmatrix} = \begin{bmatrix} -1 & 0 \\ 0 & -1 \end{bmatrix} \begin{bmatrix} \Delta z_{P_i} \\ \Delta z_{Q_i} \end{bmatrix} + \mathbf{K}_{dyn1} \begin{bmatrix} \Delta V_{Dli} \\ \Delta V_{Qli} \end{bmatrix}. \quad (3.53)$$

The equation (3.53) can be rewritten in compact form as follows:

$$\Delta \dot{\mathbf{x}}_{li} = \mathbf{A}_{li_{dyn}} \Delta \mathbf{x}_{li} + \mathbf{B}_{li_{dyn}} \Delta \mathbf{V}_{DQli}. \quad (3.54)$$

The generalized small-signal modeling of power consumed by multiplicative and additive dynamic loads in terms of  $\Delta V_{Dli}$  and  $\Delta V_{Qli}$  can be written as

$$\begin{bmatrix} \Delta P_{Li} \\ \Delta Q_{Li} \end{bmatrix} = \begin{bmatrix} P_{L0i}^{nom} & 0 \\ 0 & Q_{L0i}^{nom} \end{bmatrix} \begin{bmatrix} \Delta z_{Pi} \\ \Delta z_{Qi} \end{bmatrix} + \mathbf{K}_{dyn2} \begin{bmatrix} \Delta V_{Dli} \\ \Delta V_{Qli} \end{bmatrix}. \quad (3.55)$$

The matrices  $\mathbf{K}_{dyn1}$  and  $\mathbf{K}_{dyn2}$  will be varied according to the dynamic changes in load. The equation (3.55) can be rewritten in compact form as follows:

$$\Delta S_{li} = \mathbf{H}_{li_{dyn}} \Delta \mathbf{x}_{li} + \mathbf{D}_{li_{dyn}} \Delta \mathbf{V}_{DQli}. \quad (3.56)$$

If all the loads are expressed in the form of either multiplicative or additive dynamic load model, then the equations (3.54) and (3.56) will be modified into

$$\Delta \dot{\mathbf{X}}_L = \mathbf{A}_{L_{dyn}} \Delta \mathbf{X}_L + \mathbf{B}_{L_{dyn}} \Delta \mathbf{V}_{DQL} \quad (3.57)$$

$$\Delta \mathbf{S}_L = \mathbf{H}_{L_{dyn}} \Delta \mathbf{X}_L + \mathbf{D}_{L_{dyn}} \Delta \mathbf{V}_{DQL} \quad (3.58)$$

where  $\mathbf{A}_{L_{dyn}}$ ,  $\mathbf{B}_{L_{dyn}}$ ,  $\mathbf{H}_{L_{dyn}}$ ,  $\mathbf{H}_{L_{dyn}}$ , and  $\mathbf{D}_{L_{dyn}}$  are block diagonal matrices.

### 3.3.7 System Integration

The integration of the entire power system contains generator group, network and different loads. The generator and load terminal voltages need to be converted into bus voltages for the integration of the total system. Therefore, the relation between generator terminal voltages, load terminal voltages and bus voltages are defined as follows:

$$\mathbf{V}_{DQG} = \mathbf{M}_G^T \mathbf{V}_{DQ} \quad (3.59)$$

$$\mathbf{V}_{DQL} = \mathbf{M}_L^T \mathbf{V}_{DQ}. \quad (3.60)$$



where,  $M_G$  and  $M_L$  are incidence matrices corresponding to generator and load buses respectively. In order to calculate the small-signal bus voltages ( $\Delta V_{DQ}$ ), the equation (3.33) can be rewritten in terms of generator and load currents as follows:

$$M_G \Delta I_G - M_L \Delta I_L = Y_{DQ} \Delta V_{DQ} \quad (3.61)$$

where,  $\Delta I_G$  and  $\Delta I_L$  equations are already defined in (3.15) and (3.37) respectively. The value of  $\Delta S_L$  in  $\Delta I_L$  equation can be obtained from either equation (3.42) or (3.58) based on the type of load. If all the loads are expressed in the form of either dynamic or different composition loads then the system integration is defined as follows:

$$\begin{bmatrix} \Delta \dot{X}_{Tot} \\ \Delta \dot{X}_L \end{bmatrix} = \begin{bmatrix} A_{Tot} & \mathbf{0} \\ \mathbf{0} & A_{L_{dyn}} \end{bmatrix} \begin{bmatrix} \Delta X_{Tot} \\ \Delta X_L \end{bmatrix} + \begin{bmatrix} B_{Tot} M_G^T \\ B_{L_{dyn}} M_L^T \end{bmatrix} \Delta V_{DQ} + \begin{bmatrix} E_{ex} \\ \mathbf{0} \end{bmatrix} \Delta U_{WAC}. \quad (3.62)$$

If all the loads are only static type, then substitute  $\Delta X_L = \mathbf{0}$  in equation (3.62) to get the total integrated system. Equation (3.62) can be rewritten in compact form as follows:

$$\Delta \dot{X}_{SYS} = A_{SYS} \Delta X_{SYS} + E_G \Delta U_{WAC} \quad (3.63)$$

where,  $\Delta X_{Tot} = [\Delta X_G \ \Delta X_{ex} \ \Delta X_{tu} \ \Delta X_{pss}]^T$ ,  $\Delta X_{SYS} = [\Delta X_G \ \Delta X_L]^T$  and  $A_{SYS}$  is the entire system state matrix. It is used to find out the local and inter-area modes of oscillations occurred in a power system network by using eigenvalue analysis.

## 3.4 Limited Measurement Issue

The different states involved in a power system are the generator states, exciter states, turbine states, speed governor states, and PSSs states. It is, however, not possible to obtain the information of all the states in real time based upon only PMU measurements. The typical states that can be directly determined from the PMU measurements are the rotor angles (w.r.t a synchronously rotating reference frame) and rotor speeds of generators at the corresponding buses. In [26], an unscented Kalman filtering methodology is proposed to determine four states of a generator based upon the PMU measurements. All the other states may remain unobservable. Moreover, PMUs may also not be placed at all the generator locations. In that case, it will not be possible to get the state information from all the generators. This, in turn, makes the conventional LQR control inapplicable.

### 3.4.1 Feedback Gain Matrix Structure

The wide area controller with limited state inputs can be designed by means of the structurally constrained  $H_2$ -norm optimization technique. The number of columns in the state feedback gain matrix that is obtained from the conventional LQR optimization is still equal to the total number of states in the system. However, the entries in the columns corresponding to the unobservable states are to be set to zero by means of the structurally constrained  $H_2$ -norm optimization. On the other hand, the entries in the columns corresponding to the observable states are left to be free. Therefore, the outputs of the wide area controller become independent of the states that are not observable. This is equivalent to implementing a wide area controller with inputs drawn from only the observable states. It is to be emphasized again that the concept of sparsity promoting LQR design proposed in [1] is different from the limited state input based structurally constrained  $H_2$ -norm optimization proposed in this work. The structural difference between the conventional, sparsity-promoting [1] and the proposed limited state input based feedback gain matrices are shown in Fig. 3.3.

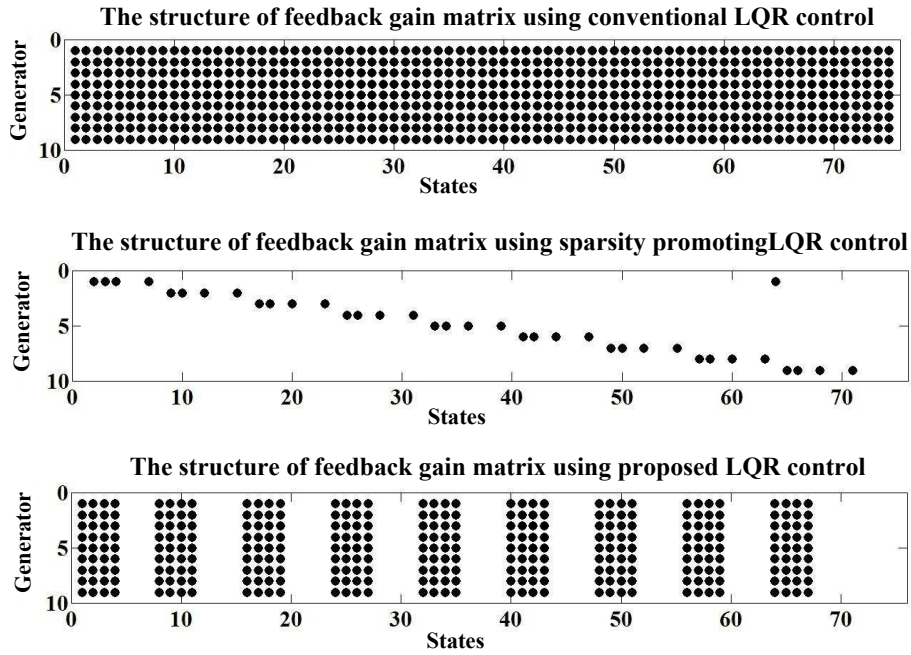


Figure 3.3: The structures of feedback gain matrices corresponding to conventional, sparsity promoting [1] and proposed LQR optimizations respectively.

### 3.4.2 COI Calculation

As mentioned previously, PMUs provide rotor angle information of generators with respect to the synchronously rotating reference frame. In order to perform wide area control (design and implementation), all the rotor angles must be specified with respect to a reference frame whose speed converges to system frequency in steady state. The speed of the particular reference frame is taken as the weighted average of the individual rotor speeds. Let,  $\omega_{r,i}$  and  $\theta_{r,i}$  be actual rotor speed and angle of the  $i$ th generator. The rotor angle information of the  $i$ th generator, as is obtained from the PMU, is symbolized as  $\delta_{r,i}$ . The speeds of the synchronously rotating reference frame and the state feedback reference frame are indicated by  $\omega_s$  and  $\omega_{ref}$ , respectively. The rotor angle with respect to the state feedback reference frame is symbolized as  $\hat{\delta}_{r,i}$ . Therefore,

$$\delta_{r,i} = \theta_{r,i} - \omega_s t = \int (\omega_{r,i} - \omega_s) dt \quad (3.64)$$

$$\hat{\delta}_{r,i} = \theta_{r,i} - \int \omega_{ref} dt = \delta_{r,i} - \int (\omega_{ref} - \omega_s) dt \quad (3.65)$$

$$\omega_{ref} = \frac{\sum_{i=1}^{N_G} w_i \omega_{r,i}}{\sum_{i=1}^{N_G} w_i} \quad (3.66)$$

$$\hat{\delta}_{r,i} = \delta_{r,i} - \frac{\sum_{i=1}^{N_G} w_i \delta_{r,i}}{\sum_{i=1}^{N_G} w_i}. \quad (3.67)$$

Here,  $N_G$  indicates the number of generators in the system and  $w_i$  indicates the weight assigned to the rotor speed of the  $i$ th generator in the state feedback reference frame. The rotor angles with respect to the state feedback reference frame can be derived from the PMU measurements by employing (3.67). Typically, the rotor angles are referred to the center of inertia (COI) reference frame. For the COI reference frame, the weights are defined according to the inertia constants of the generators. It is, however, not possible to include the rotor angle of generator in defining the state feedback reference frame unless the rotor angle state of the particular generator is observable. Otherwise, as is obvious from (3.67), none of the rotor angle states with respect to the state feedback reference frame will be observable. In that case, the state feedback reference frame can be chosen according to the COI of the generators of observable rotor angle states, whereas, the weight factors corresponding to the other generators can simply be set to zero.

### 3.5 Kalman Filter with unknown inputs in power system applications

In general, a Kalman filter can be used to estimate the states when the system is linear. However, the power system is a set of non-linear differential algebraic equations. Therefore, in order to estimate the non-linear system states either EKF or UKF can be used. The traditional extended Kalman filter requires both the inputs and measurements to be known to estimate the required synchronous machine states. However, in reality, sometimes it is not possible to have the information about inputs such as mechanical torque ( $T_m$ ) and excitation voltage ( $E_{fd}$ ). The EKF-UI method has solved this problem even in having no prior information about unknown inputs. The more details about the EKF-UI algorithm can be found in [42]. The major

restriction of EKF-UI is that the number of output measurements should be larger than the number of unknown inputs [52].

### 3.6 Case Study

In this section, the case study is performed and produced results for two situations: limited measurements and unknown load composition. In both cases, as mentioned earlier, the wide area controller is designed by means of structurally constrained  $H_2$ -norm optimization.

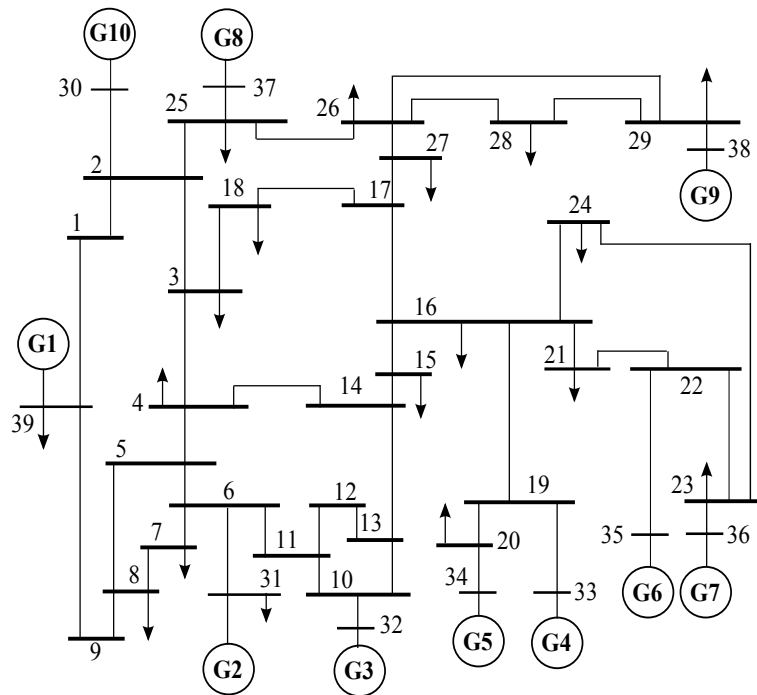


Figure 3.4: The New England 39-bus system

#### 3.6.1 Optimal wide area control with limited measurements

The wide area controller performance with limited states is demonstrated by considering the New England 39-bus system. The New England 39-bus system is shown in Fig. 3.4. The system consists of 10 generators. Each generator is equipped with PSS. The exciters are of the IEEE-ST1A type. The generators are represented by

means of the two-axis model and the network is represented by means of the phasor model. Loads are represented by means of a constant impedance model. The detailed dynamic and small signal modelings of system components are explained in [50]. The information about the line, generator data and PSS parameters of the New England 39-bus system are provided in [53]. The base case power flow result is obtained from the bus data provided in [53]. The eigenvalues of the open loop system are shown in Fig. 3.5. It can be observed that some of the open loop system eigenvalues are lying behind the 10% damping line.

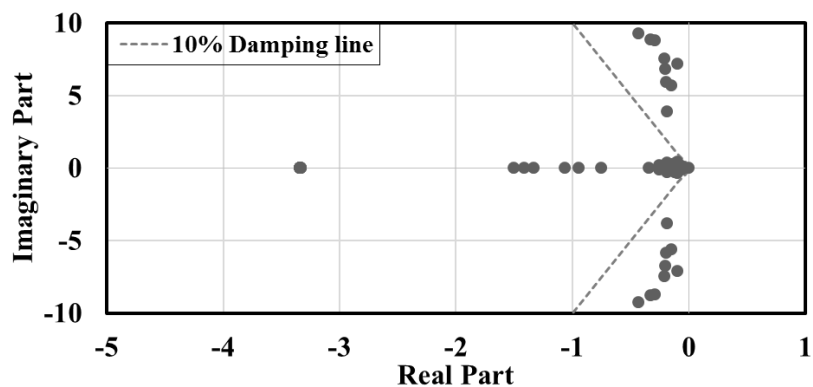


Figure 3.5: Eigenvalues of the open loop system.

In this particular study, the wide area controller with limited states is designed for two different cases. For the first case, it is assumed that PMUs are installed at all the generator buses. However, none of the PMU is equipped with non-linear state estimator. For the second case, each PMU is assumed to be equipped with non-linear state estimator. However, there are only limited number of generator buses where PMUs are placed. For both the cases, same number of states are considered. In the conventional LQR control design, the values of  $Q$  matrix are assigned based upon the participating states of inter-area modes of the system. High values are assigned to the most participating states and low values are assigned to the less participating states. The  $R$  matrix is chosen as identity matrix to share the control cost burden equally to all the generators.

### Case 1: PMUs are Placed at All the Generator Buses without Non-linear State Estimator

For this particular case, state information is available for all the generators. However, for each generator, only the frequency and rotor angle states are observable. Therefore, in the structurally constrained  $H_2$ -norm optimization proposed, large penalty is applied for the entries in the columns (of state feedback gain matrix) corresponding to the states other than the frequency and rotor angles states of the generators. For the entries in the columns corresponding to the frequency and rotor angles states of the generators no penalty is applied (i.e., penalty factor is set to zero). The structure of the corresponding Case 1 state feedback gain matrix is shown in Fig. 3.6.

The closed loop eigenvalues of system for the ideal case and Case 1 are plotted in Fig. 3.7. Here, the “ideal case” refers to the scenario in which all the system states are observable. For the ideal case, the state feedback controller is designed by means of conventional LQR optimization. Compared to the ideal case, the eigenvalues of the closed loop system in Case 1 slightly move towards to the imaginary axis. However, all the eigenvalues are lying inside the 10% damping line.

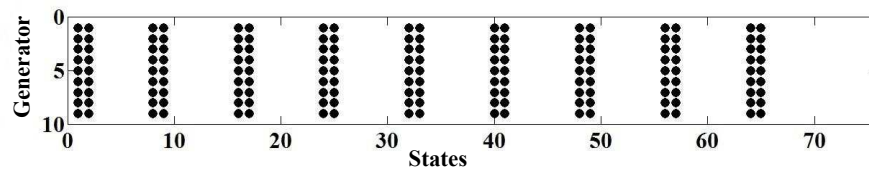


Figure 3.6: Structure of the feedback gain matrix with limited states in Case 1.

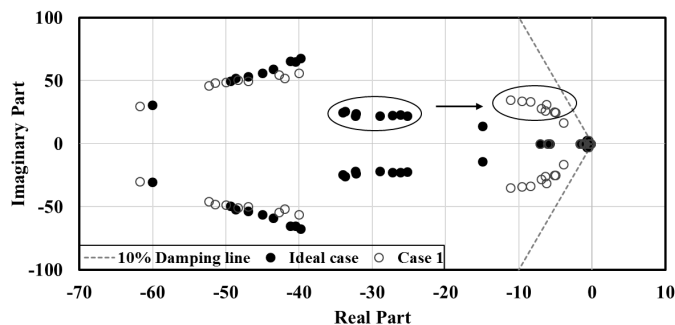


Figure 3.7: Comparison of closed loop eigenvalues in Case 1 with the closed loop eigenvalues for the feedback controller with all the states.

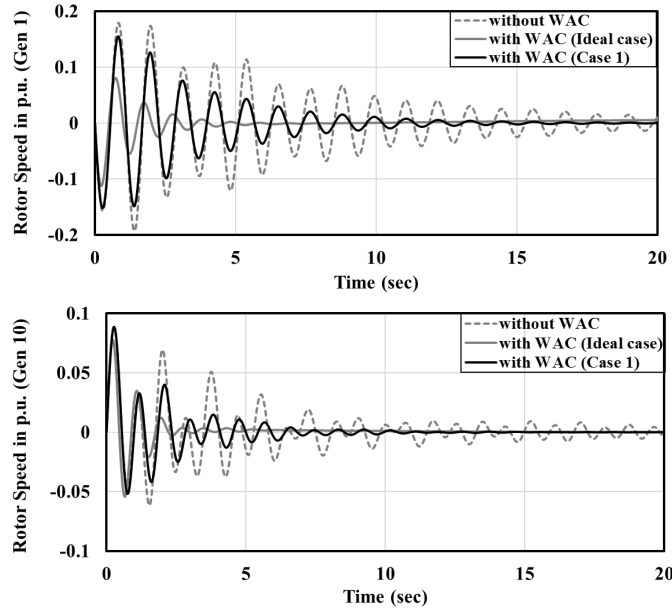


Figure 3.8: Dynamic responses of generator speeds (COI referred) in Case 1 for the outage of Line 14-15.

The effectiveness of the controller based upon only frequency and rotor angle states of all generators is further verified in time domain. The time domain simulation of system is carried out by considering the outage of Line 14-15. The time variations of the rotor speeds (w.r.t COI) of Generators 1 and 10 with and without state feedback controllers are plotted in Fig. 3.8. The performance of the state feedback controller designed for Case 1 is to some extent inferior to the performance of the ideal state feedback controller. However, significant improvement over the open loop system is still observed.

### Case 2: PMUs are Placed at Limited Number of Generator Buses with Non-linear State Estimator

For this particular case, state information is available only for limited number of generators. However, all the states of a generator (for which state information is available) are observable. The proposed structurally constrained  $H_2$ -norm optimization technique is used to obtain the required feedback gain matrix structure. Here, PMUs are assumed to be placed near Generators 2, 5, 7, 8, and 9. The structure of



the corresponding Case 2 state feedback gain matrix is shown in Fig. 3.9.

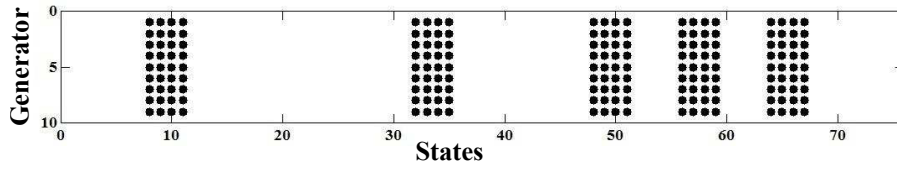


Figure 3.9: Structure of the feedback gain matrix with limited states in Case 2.

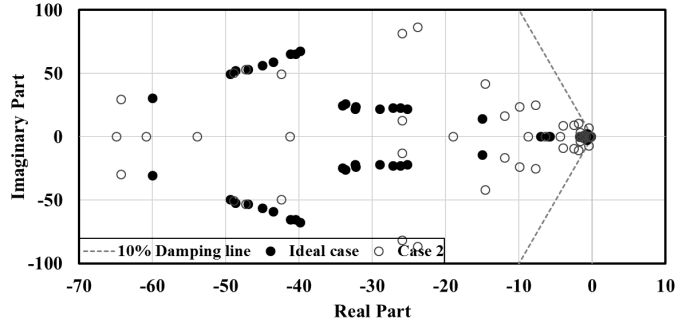


Figure 3.10: Comparison of closed loop eigenvalues in Case 2 with the closed loop eigenvalues for the feedback controller with all the states.

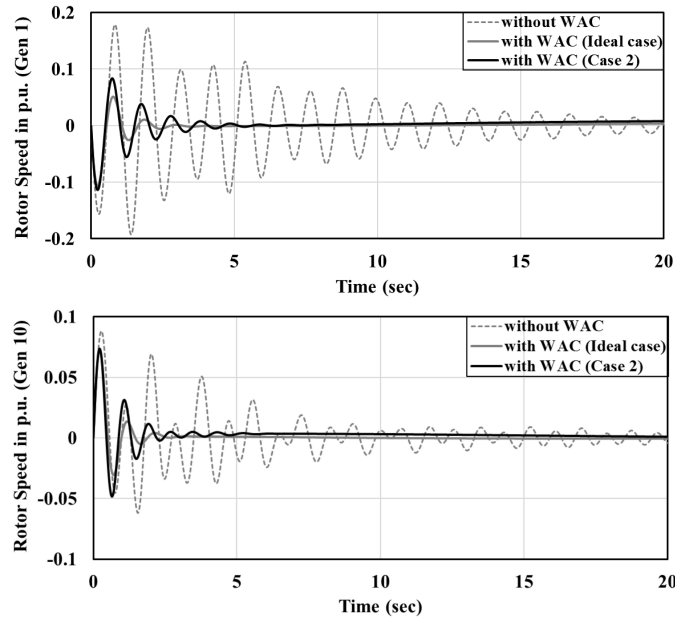


Figure 3.11: Dynamic responses of generator speeds (COI referred) in Case 2 for the outage of Line 14-15.

The closed loop eigenvalues of system for the ideal case and Case 2 are plotted in Fig. 3.10. The time variations of the rotor speeds (w.r.t COI) of Generators 1 and

10 with and without state feedback controllers are plotted in Fig. 3.8 (for the outage of the same line). It can be easily observed that the performance of the wide area controller designed for Case 2 is far superior compared to the performance of the wide area controller designed for Case 1.

### 3.6.2 Design of wide area controller with unknown load composition

The WAC performance with unknown load composition is demonstrated by considering the New England 39-bus system. The New England 39-bus system is shown in Fig. 3.4. In this particular study, the WAC is designed for two cases. For the first case, the WAC design is performed precisely by dealing with the loading scenario. The controller design is different for different load compositions (for the same nominal power level). For the second case, irrespective of actual load compositions, the WAC is designed by assuming all the loads are static and are of CP type. The PMUs are assumed to be placed only a Generators 2, 5, 7, 8 and 9. There is a state estimator associated with each PMU. The structure of the corresponding feedback gain matrix is shown in Fig. 3.9.

#### Case 1: Individual WAC Design for Each Load Composition in the Presence of Static and Dynamic Loads

In this case, the WAC is designed by considering multiple load types (static and dynamic). An individual WAC is designed for each load composition. The different load compositions which are considered in this work are shown in Table 3.1 and Table 3.2. The last column in both tables represents the amount of damping required to damp out the inter-area oscillations occurred in the system. Fig. 3.12 represents, the rotor speed of generator 1 in p.u. corresponding different load types (static and dynamic) following load shedding at Bus 7. At time  $t=2$  sec, the load is switched off at Bus 7. Fig. 3.12(a) represents the static load waveforms without and with WAC.

The unknown parameters in dynamic load models are transient and steady state

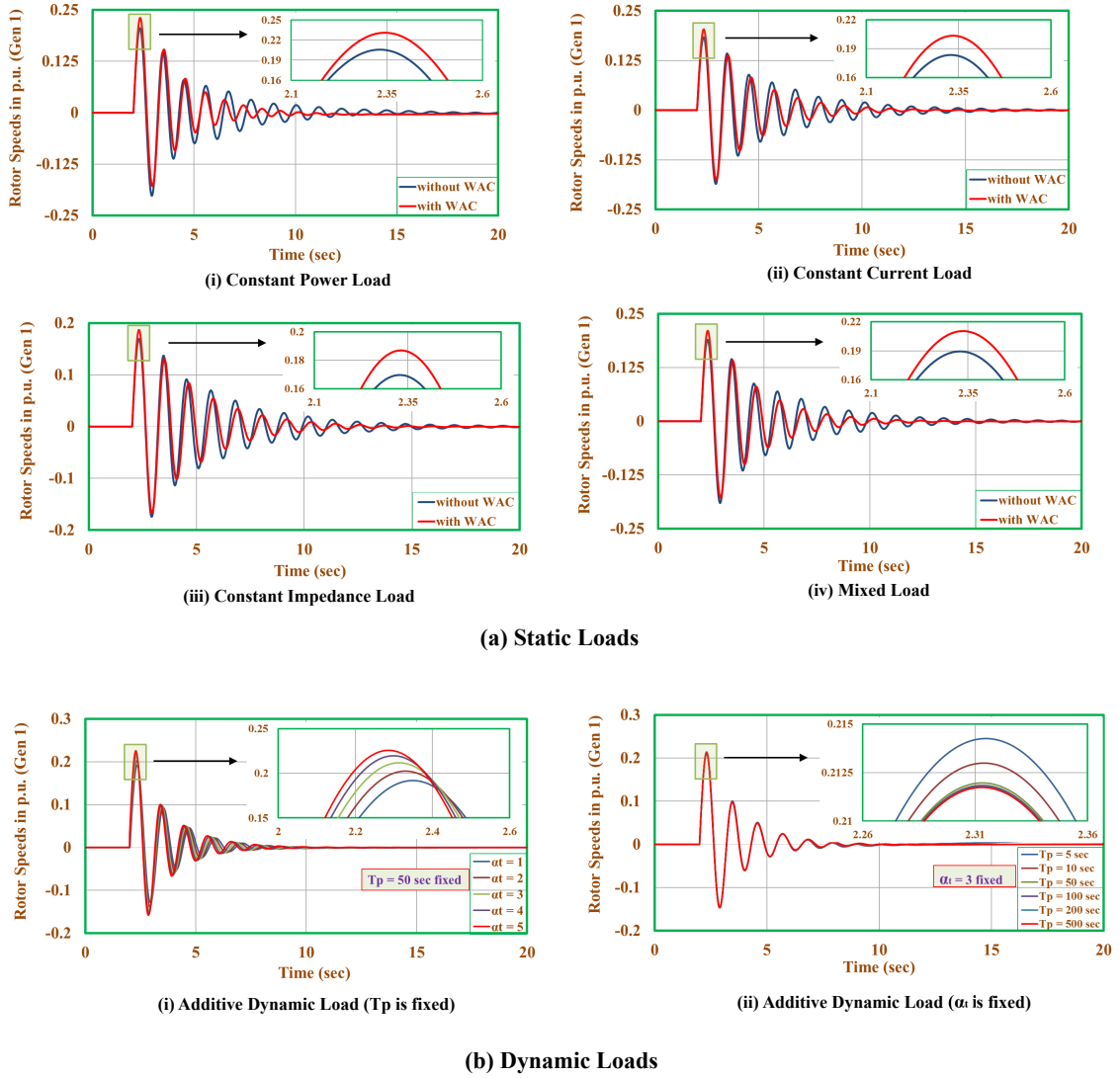


Figure 3.12: Dynamic responses of Generator 1 speed considering static and dynamic loads with load shedding at Bus 7.

Table 3.1: Amount of Damping Required for Different Static Load Compositions

Load composition	Static loads			Amount of damping required for WAC
	CP	CC	CZ	
Composition 1	100%	–	–	<b>0.236 p.u.</b>
Composition 2	–	100%	–	<b>0.206 p.u.</b>
Composition 3	–	–	100%	<b>0.188 p.u.</b>
Composition 4	50%	30%	20%	<b>0.215 p.u.</b>

load exponents ( $\alpha_t, \beta_t$  and  $\alpha_s, \beta_s$ ) and the time constants ( $T_P$  and  $T_Q$ ). These can be determined by performing field tests at the main substations [51]. The  $\alpha_s$  and

Table 3.2: Amount of Damping Required for Parameter Variations of Dynamic Load

Load composition	Dynamic load		Amount of damping required for WAC
	$T_P$	$\alpha_t$	
Composition 5	50 sec	1	<b>0.19 p.u.</b>
		2	<b>0.20 p.u.</b>
		3	<b>0.21 p.u.</b>
		4	<b>0.22 p.u.</b>
		5	<b>0.23 p.u.</b>
Composition 6	5 sec	3	<b>0.2140 p.u.</b>
	10 sec		<b>0.2127 p.u.</b>
	50 sec		<b>0.2123 p.u.</b>
	100 sec		<b>0.2122 p.u.</b>
	200 sec		<b>0.2121 p.u.</b>
	500 sec		<b>0.2120 p.u.</b>

$\beta_s$  values are taken as 0.6. The values of  $\alpha_t$  and  $\beta_t$  are considered to be equal. The values of  $T_P$  and  $T_Q$  are considered to be equal. Fig. 3.12(b) represents the dynamic load waveforms with WAC by varying time constant ( $T_P$ ) and transient exponent ( $\alpha_t$ ). Amount of damping required for both parameter variations are tabulated in Table 3.2. From Table 3.1 and Table 3.2, it is observed that the amount of damping required for CP load is more than remaining loads.

### Case 2: Applicability of WAC Design by Assuming CP Load Alone to the Remaining All Loads

In practice, the load composition at each bus will be varied from time to time. Therefore, the WAC has to be redesigned for every time based on the load composition. However, in reality, it is difficult to redesign the WAC each and every time according to the load composition. Based upon the previous observation of the damping performances of load specific wide area controllers in Case 1, the controller is designed by treating all the loads as CP loads irrespective of actual load composition. Fig. 3.13 represents the dynamic responses of generator speeds of generator 1 and 10 for load shedding at Bus 7 with the same (i.e., CP based) WAC for all the loading scenarios. Fig. 3.13 reveals that the WAC with CP load requires more amount of damping compared to other loads.

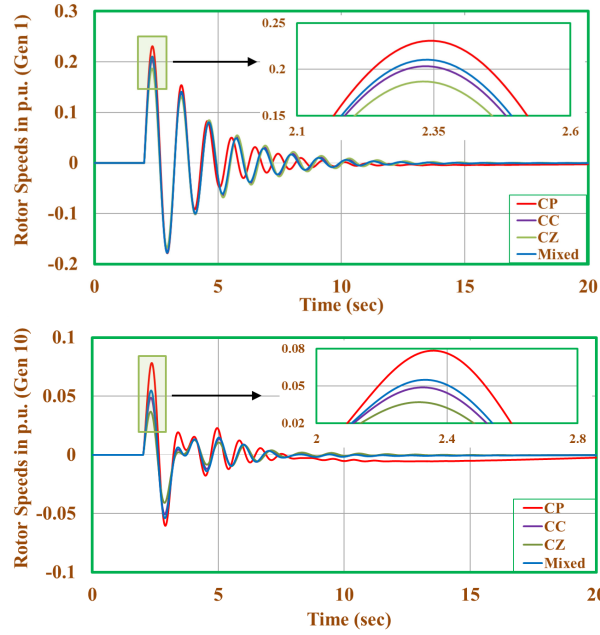


Figure 3.13: Dynamic response of speeds of Generator 1 and 10 using single design (CP load alone) with load shedding at Bus 7.

### 3.7 Summary

In this chapter, total power system modeling is presented to find out different types of oscillations that are existing in the system. After that, to damp out these oscillations, in particular, inter-area oscillations, the wide area controller is designed. EKF-UI algorithm is used to estimate the different states of a synchronous generator. By taking these states as inputs to the wide area controller, the feedback gain matrix is calculated by using structurally constrained  $H_2$ -norm optimization method. Results display the effectiveness of the controller under different situations.

# Chapter 4

## Designing a Reduced-Scale Architecture of the Wide Area Control System

### 4.1 Introduction

This chapter presents a design of the reduced-scale architecture of the wide area control system by means of modal sensitivity analysis. The primary objective is to rank all the potential source and sink points of the WAC loop according to an estimation of their utility to mitigate inter-area oscillations. Only the top ranked source and sink points are to be selected in the final WAC loop. The utility rankings of the source and sink points are conventionally carried out based upon the concepts of geometric observability and geometric controllability [24], [54]. The present chapter contributes towards developing an improved scheme for the utility ranking of the source and sink points in the WAC loop. The specific novelty of this work is as follows.

1. The utility metrics of source and sink points in the WAC loop are defined based upon modal sensitivities instead of the geometric controllability/observability.
2. Unlike existing works, no specific restriction is imposed on the number of signals

per source/sink point to perform its utility ranking.

## 4.2 Principle of wide area controller design and implementation

The general architecture of the WAC system is shown in Fig. 3.1 (Chapter 3). The phasors and frequencies measured by phasor measurement units (PMUs) are transmitted to the control center by means of a wide area monitoring (WAM) communication network. The WAM system is, in essence, a multifunctional infrastructure that is used for both the purposes of obtaining the dynamic WAC action as well as to monitor the system condition (i.e., loading and stability statuses) in real-time for the possible corrective actions [55]. The wide area control system can be realized by means of either the state feedback [41] or the output feedback [29]. In the case of the state-feedback control, two sequential processes are carried out at the control center to generate the WAC signals. First of all, the dynamic states of the system are determined by means of an extended Kalman filter (EKF) [42] or an unscented Kalman filter (UKF) [43]. The EKF/UKF generates information about the system states based upon time-stamp aligned measurements. The time-stamp alignment is carried out by means of phasor data concentrators that can be treated as integral parts of the WAM network. It is to be noted that the power measurements are not directly obtained from PMUs. Those are rather calculated from voltage and current phasors. Typically, the dynamic state estimation is carried by using subsystem models; therefore, the EKF/UKF algorithm employed should also have the capacity to dynamically determine the inputs to each subsystem [44]. The WAC signals are generated by multiplying the estimated state vector from the EKF/UKF with a state feedback gain matrix. Unlike the state feedback, no intermediate stage of state estimation is required for the output feedback. The WAC signals for the output feedback are derived by directly processing the measurements through the feedback gain matrix. After generating the WAC signals, those are transmitted to power system

components (such as generators' excitation control systems or FACTS devices) via a WAC communication network. Fig. 4.1 shows the block diagram of an excitation control system with the WAC signal input.

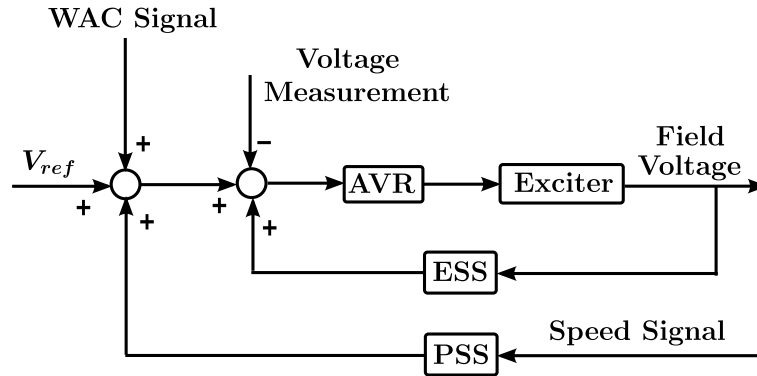


Figure 4.1: the block diagram of an excitation control system with the WAC signal input.

The mathematical block diagram representation of the power system with the WAC loop is shown in Fig. 3.2 (Chapter 3). Here, the block diagram is produced in the state-space form based upon the linearized (small-signal) model of power system dynamics. The WAC loop is shown with output feedback. It is to be noted that the wide area damping controller is usually designed by using the small-signal model of the system [40], [1], [24], [54], [46], [41], [29]. The state, input, output and feed through matrices in a state-space block is represented by  $\mathbf{A}(\cdot)$ ,  $\mathbf{B}(\cdot)$ ,  $\mathbf{C}(\cdot)$ , and  $\mathbf{D}(\cdot)$ , respectively. Determination of linearized state-space model parameters for the power system is explained in [56]. The WAC signal vector generated by the wide area damping controller is indicated by  $\mathbf{u}_{wac}$ . The measurement vector and the feedback gain matrix are represented by  $\mathbf{y}$  and  $\mathbf{G}_{wac}$ , respectively. Prefix  $\Delta$  is used to indicate the perturbed value of a quantity from the equilibrium. The transportation delay block is introduced to take into account the effect of time delays that take place in the WAC loop because of the latencies of WAM and WAC networks as well as because of the computations involved in generating the WAC signals.

Originally the transportation delay of  $\tau_d$  second is represented by means of the transfer function  $e^{-\tau_d s}$ . For the practical treatment of the transportation delay in the controller design, the particular transfer function is to be approximated as a finite or-



der rational transfer function. This can be achieved through the Pade approximation [37]. The transfer function  $e^{-\tau_d s}$  can be expanded as follows.

$$e^{-\tau_d s} = \frac{e^{-\frac{\tau_d}{2}s}}{e^{\frac{\tau_d}{2}s}} = \frac{1 - \frac{\tau_d}{2}s + \frac{\tau_d^2}{8}s^2 - \dots}{1 + \frac{\tau_d}{2}s + \frac{\tau_d^2}{8}s^2 + \dots}. \quad (4.1)$$

The Pade approximation basically refers to truncating the orders of both numerator and denominator in the above expression. Similarly to [49], only the first order Pade approximation is considered in this work. With the first order Pade approximation of the transportation delay, the state-space model parameters of the delay block in Fig. 3.2 appear as follows.

$$\mathbf{A}_{dl} = -\mathbf{B}_{dl} = -2 \begin{bmatrix} \tau_{d,1} & 0 & \cdots & 0 \\ 0 & \tau_{d,2} & \cdots & 0 \\ \vdots & \vdots & \ddots & \vdots \\ 0 & 0 & \cdots & \tau_{d,N_u} \end{bmatrix}^{-1} \quad (4.2)$$

$$\mathbf{C}_{dl} = -2\mathbf{D}_{dl} = \begin{bmatrix} 2 & 0 & \cdots & 0 \\ 0 & 2 & \cdots & 0 \\ \vdots & \vdots & \ddots & \vdots \\ 0 & 0 & \cdots & 2 \end{bmatrix}. \quad (4.3)$$

Here,  $\tau_{d,j}$  indicates the transportation delay associated with the  $j$ th WAC signal. The number of WAC signals generated (i.e., row size of  $\mathbf{u}_{wac}$ ) is indicated by  $N_u$ . In [47], the time delays in WAM and WAC networks are separately shown on the input and output sides, respectively, of the wide area damping controller. However, the time delays that happen in different input signals to the wide area damping controller should be uniform because of the time-stamp alignment of measurements collected. Therefore, the net time delay effect can be lumped on the output side of the wide area damping controller (which can be easily proven by using the original transfer function representation of the transportation delay). The same representation is adopted in

this work.

Typically, the wide area damping controller design is carried out by means  $H_\infty$ -norm [28] or  $H_2$ -norm optimization [1], [57], [30], [58]. The  $H_\infty$ -norm optimization can yield a robust design, whereas, better transient response can be achieved by using a  $H_2$ -norm optimized wide area damping controller [59]. In order to simplify the wide area damping controller design, an augmented plant model should be defined by combing the original plant and the time delay blocks [60]. The state, WAC input and physical output matrices of the augmented plant are represented by  $\mathbf{A}$ ,  $\mathbf{B}_u$  and  $\mathbf{C}_y$ , respectively, where,

$$\mathbf{A} = \begin{bmatrix} \mathbf{A}_{pl} & \mathbf{B}_{pl}\mathbf{C}_{dl} \\ \mathbf{0} & \mathbf{A}_{dl} \end{bmatrix} \quad (4.4)$$

$$\mathbf{B}_u = \begin{bmatrix} \mathbf{D}_{dl}^T \mathbf{B}_{pl}^T & \mathbf{B}_{dl}^T \end{bmatrix}^T \quad (4.5)$$

$$\mathbf{C}_y = \begin{bmatrix} \mathbf{C}_{pl} & \mathbf{0} \end{bmatrix}. \quad (4.6)$$

In Fig. 3.2, no disturbance input is shown. However, in order to define the  $H_2/H_\infty$  norm, a disturbance input and a performance output should be specified [59], [61]. The disturbance input and performance output vectors are symbolized as  $\mathbf{w}$  and  $\mathbf{z}$ , respectively. By considering the disturbance input, the state equation of the augmented plant can be rewritten as,

$$\Delta \dot{\mathbf{x}} = \mathbf{A}\Delta \mathbf{x} + \mathbf{B}_u \Delta \mathbf{u}_{wac} + \mathbf{B}_w \Delta \mathbf{w}. \quad (4.7)$$

The state vector of the augmented plant (which include both the plant and delay states) is indicated by  $\mathbf{x}$ . The equation of the performance output vector appears as follows.

$$\Delta \mathbf{z} = \mathbf{C}_z \Delta \mathbf{x} + \mathbf{D}_z \Delta \mathbf{u}_{wac}. \quad (4.8)$$

Parameters  $\mathbf{B}_w$ ,  $\mathbf{C}_z$  and  $\mathbf{D}_z$  are to be specified by the user depending upon the

specific performance requirement. Typically,  $\mathbf{C}_z$  and  $\mathbf{D}_z$  are chosen as follows.

$$\mathbf{C}_z^T = \begin{bmatrix} \mathbf{Q}^{\frac{1}{2}} & \mathbf{0} \end{bmatrix} \quad (4.9)$$

$$\mathbf{D}_z^T = \begin{bmatrix} \mathbf{0} & \mathbf{R}^{\frac{1}{2}} \end{bmatrix}. \quad (4.10)$$

That is,  $\mathbf{z}$  is chosen as an  $(N_s + N_u) \times 1$  vector with due consideration for both the state disturbance and the control effort. Here,  $N_s$  indicates the number of state variables. As in the LQR control,  $\mathbf{Q}$  and  $\mathbf{R}$  should be symmetric positive semi-definite and symmetric positive definite matrices, respectively.

The WAC signals are generated according to the following equation.

$$\Delta \mathbf{u}_{wac} = \mathbf{G}_{wac} \Delta \mathbf{y}. \quad (4.11)$$

In this work, the wide area damping controller is designed by means of the  $H_2$ -norm optimization. For the dynamic system model (4.7), (4.8) and (4.11), the  $H_2$ -norm optimization can be formulated as follows.

$$\text{Minimize } \left\{ \text{trace} \left( \mathbf{B}_w^T \mathbf{F} \mathbf{B}_w \right) \right\} \quad (4.12)$$

s.t.

$$\mathbf{F} \left( \mathbf{A} + \mathbf{B}_u \mathbf{K}_{wac} \right) + \left( \mathbf{A} + \mathbf{B}_u \mathbf{K}_{wac} \right)^T \mathbf{F} + \left( \mathbf{C}_z + \mathbf{D}_z \mathbf{K}_{wac} \right)^T \left( \mathbf{C}_z + \mathbf{D}_z \mathbf{K}_{wac} \right) = \mathbf{0} \quad (4.13)$$

$$\mathbf{K}_{wac} - \mathbf{G}_{wac} \mathbf{C}_y = \mathbf{0} \quad (4.14)$$

$$\left( \mathbf{A} + \mathbf{B}_u \mathbf{K}_{wac} \right) \prec \mathbf{0}. \quad (4.15)$$

The objective function effectively indicates the squared  $H_2$ -norm of the closed loop system. The derivation of the closed form of expression of the  $H_2$ -norm [that is shown in (4.12)] from its basic definition can be found in [59] and [61]. The variables in the above optimization problem are  $\mathbf{F}$ ,  $\mathbf{K}_{wac}$  and  $\mathbf{G}_{wac}$ . Matrix  $\mathbf{F}$  is the observability Grammian matrix (of the closed loop system), which is obtained by solving the

Lyapunov equation (4.13). The equivalent state feedback gain matrix is indicated by  $\mathbf{K}_{wac}$ . The structural constraints on  $\mathbf{K}_{wac}$  are enforced through (4.14). Finally, Constraint (4.15) is enforced to ensure the negative definiteness (thus, the stability) of the closed loop state matrix.

The analytical framework presented above is also suitable for designing a physical state feedback controller by equivalently treating the observable system states as the system outputs. The corresponding  $\mathbf{C}_y$  matrix can simply be obtained from an  $N_s \times N_s$  identity matrix by eliminating the rows corresponding to unobservable states. In the case of the complete observability of system states (from the measurements collected at the control center), no structural constraint is effectively imposed by (4.14) in the design of the state feedback controller. In the absence of (4.14), the  $H_2$ -norm optimization problem boils down to the simple LQR problem [1]. In that case, the optimal solution of the state feedback controller can be obtained directly by solving the algebraic Riccati equation [62]. However, it is difficult to estimate all the system states in real-time only from the PMU measurements. For example, the states associated with the transportation delay block cannot be estimated. In addition, exclusion of an element from the WAM network (thus, not considering its outputs for the generation of WAC signals) makes its states unobservable. The columns of matrix  $\mathbf{K}_{wac}$  corresponding to the unobservable states should be zero vectors. Therefore, for the state feedback, Equation (4.14) can be simplified as follows.

$$\mathbf{K}_{wac} \circ \Theta = \mathbf{0}. \quad (4.16)$$

Here, symbol  $\circ$  indicates the Hadamard product. The entries of matrix  $\Theta$  are only zeros and ones, and it has the same row and column dimensions as that of  $\mathbf{K}_{wac}$ . In order to enforce a column of  $\mathbf{K}_{wac}$  to become zero, the respective column of the  $\Theta$  matrix should be set to a vector of all ones. The particular optimization problem can be easily solved by employing the alternating direction method of multipliers technique proposed in [30]. The state feedback controller should be implemented in the  $dq$  domain (i.e., with all the input quantities referred to a  $dq$  reference frame) since

it needs to produce constant outputs in the steady state. The angle of particular  $dq$  reference frame should be chosen according to the center-of-inertia (COI) of generators with observable angle states [56].

### 4.3 Proposed scheme for the scale reduction of the WAC system

The WAC loop is, in effect, composed of several feedback paths. There is a feedback line from each input to each output of the wide area damping controller, resulting in  $N_y \times N_u$  feedback paths in the WAC loop. Here,  $N_y$  indicates the number of input signals (i.e., the plant outputs measured) to the wide area damping controller. A mode is differently affected by different feedback paths. The total number of modes is indicated by  $N_{md}$ . The susceptibility of a mode to a particular feedback path can be described by means of a mode-path susceptibility index. The overall mode-path susceptibility information can be presented through an  $(N_u \times N_y \times N_{md})$  matrix  $\Gamma$ .

The mode-path susceptibility effectively indicates the involvement of a particular feedback path in changing the shape of a particular mode. In this chapter, the mode-path susceptibility index values are assessed based upon the sizes by which different paths contribute towards altering a mode shape (from open loop to closed loop) after the full-scale WAC (FSWAC) loop is installed with optimized feedback gain matrix. About the mode shape, the real part of the respective eigenvalues is of prime interest here. This is because the pace at which the amplitude of an oscillatory mode can be damped out is determined solely by the real part of the corresponding eigenvalue. The contributions of different paths in changing a mode shape can be approximately determined by means of mode-path sensitivity factors. According to first order Taylor's series approximation around the open loop condition, an eigenvalue can be expressed as a linear function of the feedback path gain values as follows.

$$\lambda_k \approx \lambda_k^{ol} + \sum_{i,j} \left\{ \left. \frac{\partial \lambda_k}{\partial G_{wac,j,i}} \right|_{G_{wac}=\mathbf{0}} \right\} G_{wac,j,i}. \quad (4.17)$$

Here,  $\lambda_k$  and  $\lambda_k^{ol}$  indicate eigenvalues corresponding to the  $k$ th mode for the closed loop and open loop systems, respectively. Corresponding to an oscillatory mode, there should be two eigenvalues. Any of those two eigenvalues can be considered. The gain of the Feedback Path  $i - j$  (i.e., from the  $i$ th input signal to the  $j$ th output signal) is indicated by  $G_{wac,j,i}$ . Based upon the above linearized expression and the adopted notion of mode-path susceptibility, the expression of the susceptibility of Mode  $k$  to the Feedback Path  $i - j$  appears as,

$$\Gamma_{i,j,k} = \left| \text{Re} \left\{ \frac{\partial \lambda_k}{\partial G_{wac,j,i}} \bigg|_{\mathbf{G}_{wac}=\mathbf{0}} \right\} G_{wac,j,i}^{fsopt} \right|. \quad (4.18)$$

Here, the superscript “fsopt” indicates the full-scale optimal solution. The optimal gain value used in the above equation can be obtained from the  $H_2$ -norm or the  $H_\infty$ -norm optimization of the FSWAC system. It is to be noted that the mode-path susceptibility index defined above is always a unit-less quantity.

The sensitivity of an eigenvalue to the gain of a feedback path can be evaluated through the following equation.

$$\frac{\partial \lambda_k}{\partial G_{wac,j,i}} = \sum_{p=1}^{N_s} \sum_{q=1}^{N_s} \frac{\partial \lambda_k}{\partial \tilde{A}_{p,q}} \frac{\partial \tilde{A}_{p,q}}{\partial G_{wac,j,i}} \quad (4.19)$$

$$= \sum_{p=1}^{N_s} \sum_{q=1}^{N_s} \psi_{k,p} \phi_{q,k} B_{u,p,j} C_{y,i,q}. \quad (4.20)$$

Here,  $\psi_k$  and  $\phi_k$  are the left and right eigenvectors corresponding to the  $k$ th mode. Those are taken as row vector and column vector, respectively. The closed-loop state matrix is indicated by  $\tilde{\mathbf{A}}$ . That is,

$$\tilde{\mathbf{A}} = \mathbf{A} + \mathbf{B}_u \mathbf{G}_{wac} \mathbf{C}_y. \quad (4.21)$$

The derivation of the sensitivity of an eigenvalue with respect to an element of the state matrix can be found in [3].

The usefulness (for damping out inter-area oscillations) of different input and output signals of the wide area damping controller needs to be evaluated from the

mode-path susceptibility matrix. The utility indices for the  $i$ th input signal and  $j$ th output signal are indicated by  $\zeta_{ip,i}$  and  $\zeta_{op,j}$ , respectively. Those can be evaluated through the following equations.

$$\zeta_{ip,i} = \max \{ \Gamma_{i,1}^{\max}, \Gamma_{i,2}^{\max}, \dots, \Gamma_{i,N_u}^{\max} \} \quad (4.22)$$

$$\zeta_{op,j} = \max \{ \Gamma_{1,j}^{\max}, \Gamma_{2,j}^{\max}, \dots, \Gamma_{N_y,j}^{\max} \}. \quad (4.23)$$

where,

$$\Gamma_{i,j}^{\max} = \max \{ \Gamma_{i,j,k} : k \in \mathfrak{S}_{md} \}. \quad (4.24)$$

Here,  $\mathfrak{S}_{md}$  indicates the set of all inter-area modes. The utility indices calculated for the input and output signals of the wide area damping controller are to be converted to source and sink utility indices, respectively. In the case the measurements collected from the output ports of an element (such as a generator) are fed as inputs to the wide area damping controller, the respective element serves as a source point. Similarly, if any WAC signal is sent to the input port of an element, the respective element serves as a sink point. An element may serve both as source and sink points if both its input and output ports are used in the WAC loop. However, every WAC signal is usually derived by combining the outputs of all the elements that are connected to the source side of the wide area damping controller. The source and sink utility indices (symbolized as  $\zeta_{sr}$  and  $\zeta_{sn}$ ) are calculated through the following equations.

$$\zeta_{sr,m} = \max \{ \zeta_{ip,i} : i \in \mathfrak{S}_{sr,m} \} \quad (4.25)$$

$$\zeta_{sn,n} = \max \{ \zeta_{op,j} : j \in \mathfrak{S}_{sr,n} \}. \quad (4.26)$$

The set of the input signals generated by Source  $m$  is indicated by  $\mathfrak{S}_{sr,m}$ , whereas,  $\mathfrak{S}_{sr,n}$  indicates the set of output signals received at Sink  $n$ .

The design of the RSWAC architecture according to the proposed methodology involves the following steps.

1. Identifying all potential source and sink points for the WAC loop.
2. Designing the feedback gain matrix for the full-scale WAC system by including all potential source and sink points.
3. Evaluating the mode-path susceptibility factors for the FSWAC loop.
4. Evaluating the utility indices of all available source and sink points.
5. Eliminating the source and sink points with low utility values.

The  $H_2$ -norm optimized feedback gain matrices for both the FSWAC and RSWAC architectures can be obtained by solving the optimization problem (4.12)-(4.15). However, the linear structural constraint (4.14) needs to be suitably updated (by appropriately forming the constant matrix  $\mathbf{C}_y$ ) after deriving the reduced-scale WAC architecture.

The methodology proposed in [24] and [54] for obtaining a reduced-scale WAC architecture can also be explained by using the concept of mode-path susceptibility matrix. According to [24] and [54], the elements of the mode-path susceptibility matrix should be defined as follows.

$$\Gamma_{i,j,k} = \gamma_{i,k}^{gmo} \times \gamma_{j,k}^{gmc} \quad (4.27)$$

where,

$$\gamma_{j,k}^{gmc} = \frac{\left\{ \sum_{p=1}^{N_s} B_{u,p,j} \psi_{k,p} \right\}}{\sqrt{\left\{ \sum_{p=1}^{N_s} |B_{u,p,j}|^2 \right\} \left\{ \sum_{p=1}^{N_s} |\psi_{k,p}|^2 \right\}}} \quad (4.28)$$

$$\gamma_{i,k}^{gmo} = \frac{\left\{ \sum_{p=1}^{N_s} C_{y,i,q} \phi_{q,k} \right\}}{\sqrt{\left\{ \sum_{q=1}^{N_s} |C_{y,i,q}|^2 \right\} \left\{ \sum_{q=1}^{N_s} |\phi_{q,k}|^2 \right\}}} \quad (4.29)$$



Symbols  $\gamma_{i,k}^{gmo}$  and  $\gamma_{j,k}^{gmc}$  indicate the geometric observability and geometric controllability of Mode  $k$  with respect to the  $i$ th input signal and  $j$ th output signal, respectively, of the wide area damping controller. It is to be noted that the inputs and outputs, here, are specified with respect to the wide area damping controller, not with respect to the plant.

The proposed expression of the mode-path susceptibility index shown in (4.18) is not equivalent to Equation (4.27) that is used in literature. In addition, the earlier RSWAC architecture is obtained by sorting out individual input and output signals rather than the complete source and sink points. Thus, even though a source/sink is selected in the WAC loop, not all its output/input ports may be used as per the existing sorting and selection scheme (unless there is only input/output port per device). It is, however, to be noted that after selecting a particular source or sink point in the RSWAC loop, there is no need to be further selective about choosing its input or output ports. There may not any reduction in the communication infrastructure requirement because of this additional selectiveness. Therefore, a source or sink point is always used in full-fledged fashion in this work.

## 4.4 Simulation results

The performance of the proposed WAC architecture is validated by considering a 68-bus test system. The test system is shown in Fig. 4.2. The particular system consists of 16-generators. Each generator is equipped with a PSS. The exciters are of the IEEE-ST1A type. The generators are represented by means of the sub-transient model and loads are taken to be of the constant impedance type. The mechanical torque input to each generator is assumed to be constant. The detailed information about lines, generators and loads can be found in [63]. The PSS parameters are taken from [64].

Initially, the inter-area modes of oscillation for the open loop system are identified through the small-signal stability analysis around a base case operating point. The base case operating point is obtained by performing power flow analysis with the

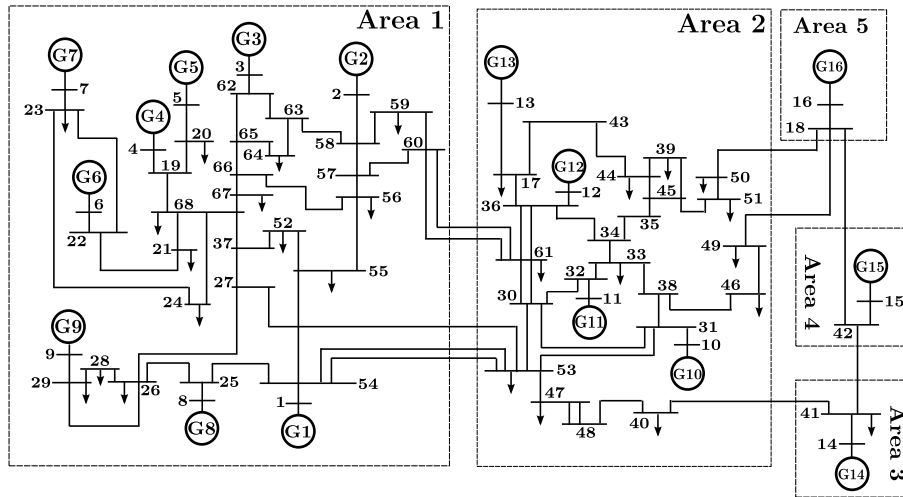


Figure 4.2: The 68-bus test system.

generation and load profiles mentioned in [63]. The frequencies and damping ratios of inter-area modes of oscillation identified are shown in Table 4.1. The typical frequency range of inter-area modes is 0.3 Hz-1 Hz. Although the frequency of Mode 5 is slightly higher than 1 Hz, it has a very low damping ratio. Therefore, in line of [1] and [65], the particular mode is also recognized as an inter-area mode.

Table 4.1: Damping ratios and frequencies of the inter-area modes without WAC

Mode Index	Damping ratio	Frequency (Hz)	Coherent generator groups
1	0.0207	0.3905	(14,15) vs (1,2,3,4,5,6,7,8,9,12,13,16)
2	0.0266	0.5217	16 vs 14
3	0.0193	0.5981	(12,13) vs (9,16)
4	0.0480	0.7931	15 vs (14,16)
5	0.0446	1.3141	10 vs (1,8)

The wide area damping controller is implemented by taking observable generator states as input signals. The outputs of the wide area damping controller are fed to the excitation control systems of generators. Therefore, generators serve as both source points and sink points in the WAC loop. The source-end and sink-end utility values evaluated for generators by using proposed and existing methodologies are produced in Table 4.2. It can be seen that the proposed and existing mode-path susceptibility matrices lead to completely different utility rankings of generators. The RSWAC loop with the proposed utility ranking is derived by eliminating ten bottom ranked

generators from each end. On the other hand, only nine bottom ranked generators are eliminated from each end to build the RSWAC loop according to the existing criterion. The wide area damping controller is designed by considering both  $\mathbf{Q}$  and  $\mathbf{R}$  as diagonal matrices. The  $\mathbf{R}$  matrix is simply chosen as the identity matrix. For  $\mathbf{Q}$ , the diagonal entry corresponding to an angle or frequency state is set to 100. All other diagonal entries are set to zeros. The  $H_2$ -norm of the performance output vector is calculated with respect to disturbances at WAC signal input terminals of the augmented plant. Thus,  $\mathbf{B}_w$  is taken to be the same as  $\mathbf{B}_u$ . The  $H_2$ -norm optimization is carried out by using the full-order system model.

Table 4.2: Utility assessment of different generators as source and sink points of the WAC loop

Generator id.	Source utility index		Sink utility index	
	Proposed scheme	Existing scheme	Proposed scheme	Existing scheme
1	0.2093	$0.8888 \times 10^{-3}$	0.1269	$0.4627 \times 10^{-3}$
2	0.3135	$1.4930 \times 10^{-3}$	0.3135	$1.3317 \times 10^{-3}$
3	0.5274	$1.0910 \times 10^{-3}$	0.5274	$1.4930 \times 10^{-3}$
4	0.5513	$0.5097 \times 10^{-3}$	0.5513	$0.7694 \times 10^{-3}$
5	0.5497	$1.0741 \times 10^{-3}$	0.5497	$0.8697 \times 10^{-3}$
6	0.4212	$0.7356 \times 10^{-3}$	0.4212	$0.6675 \times 10^{-3}$
7	0.5563	$0.4728 \times 10^{-3}$	0.5563	$0.4608 \times 10^{-3}$
8	0.6983	$1.3264 \times 10^{-3}$	0.6983	$1.2433 \times 10^{-3}$
9	1.5011	$3.4266 \times 10^{-3}$	1.5011	$3.4266 \times 10^{-3}$
10	0.3650	$1.5228 \times 10^{-3}$	0.3650	$1.5228 \times 10^{-3}$
11	0.1074	$0.3183 \times 10^{-3}$	0.1074	$0.4290 \times 10^{-3}$
12	0.6253	$1.4632 \times 10^{-3}$	0.6253	$1.4632 \times 10^{-3}$
13	2.0053	$0.4476 \times 10^{-3}$	2.0053	$0.8250 \times 10^{-3}$
14	2.8964	$0.3111 \times 10^{-3}$	2.8964	$0.3707 \times 10^{-3}$
15	1.4953	$0.3707 \times 10^{-3}$	1.4953	$0.3297 \times 10^{-3}$
16	1.0438	$0.3548 \times 10^{-3}$	1.0438	$0.5669 \times 10^{-3}$

The eigenvalue spectra of the small signal models of open loop and closed loop (with different RSWAC loops) systems are shown in Fig. 4.3. The communication delay is presently assumed to be zero. All the eigenvalue spectra are compared with respect to the 10% damping line. The 10% damping line is a useful classifier [5], [66], [67] to differentiate between healthy and unhealthy eigenvalues. Eigenvalues on the

right hand side of the 10% damping line are primarily responsible for unacceptably prolonged inter-area oscillations. From Fig. 4.3, it can be seen that several eigenvalues lie on the right side of the 10% damping line before the deployment of any wide area damping controller. After installing an RSWAC loop based upon the existing utility ranking scheme, some eigenvalues could be shifted to the left side of the 10% damping line. However, a significant number of eigenvalues still lie on its right side. On the other hand, none of the eigenvalues sits on the right side of the 10% damping line after the deployment of the proposed reduced-scale version of the wide area damping controller.

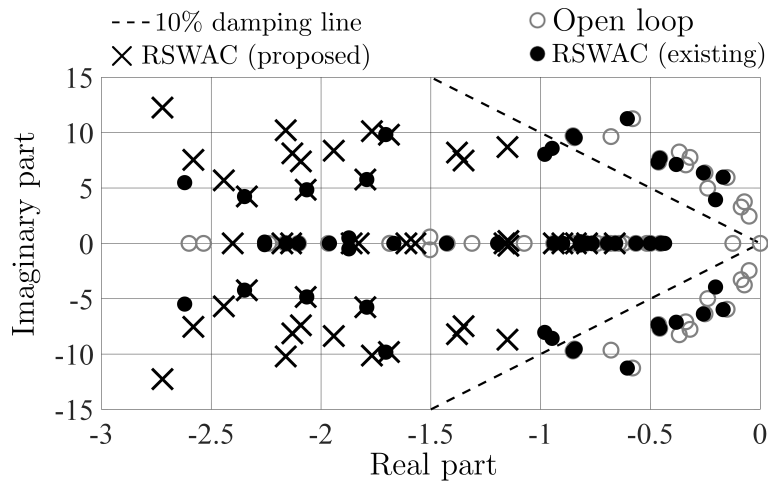


Figure 4.3: Eigenvalue comparison between proposed and existing RSWAC schemes.

Table 4.3: List of disturbances considered

Disturbance id	Type of disturbance	Location	Time
TL_OUT_1	Line outage	Between Buses 60 and 61	At 2.5 sec
TL_OUT_2	Line outage	Between Buses 27 and 53	At 2.5 sec
TL_OUT_3	Line outage	Between Buses 53 and 54	At 2.5 sec
LD_SHD_1	Load shedding	At Bus 23	At 2.5 sec

The time domain simulations are carried out by considering the disturbances described in Table 4.3. The corresponding dynamics responses of the rotor angles of Generators 12, 13 and 14 are plotted in Fig. 4.4. Here, the rotor angles are referred to the system COI (i.e., the COI of all the generators in the system). The dynamic simulations are run for 200 seconds. However, for better portrayal of the relative

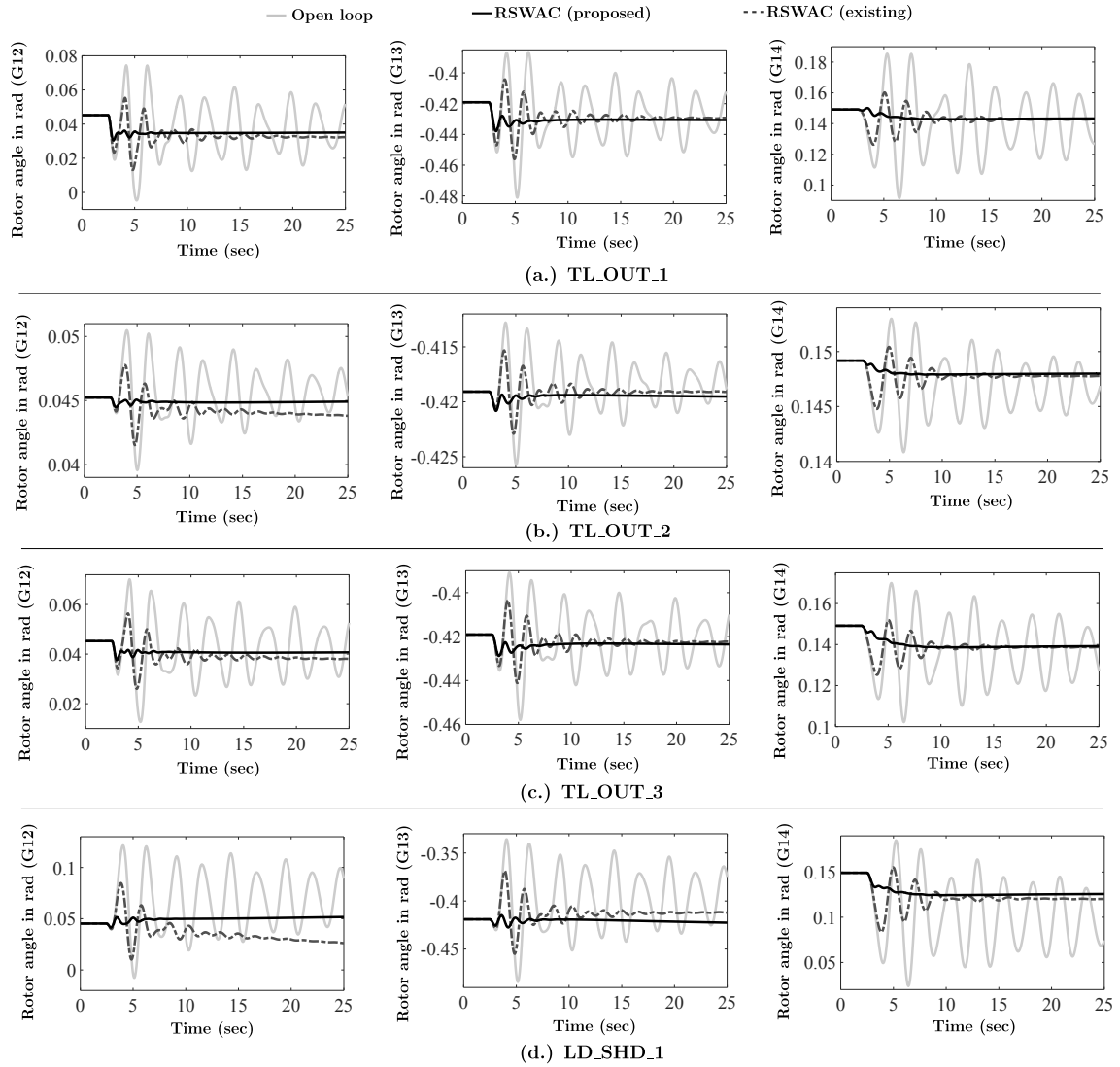


Figure 4.4: Comparison of rotor angle (COI referred) dynamics between proposed and existing RSWAC schemes without time delay.

damping performances of different RSWAC systems, plots are produced only over a window of 25 seconds. Unlike PSSs, the outputs of a wide area damping controller are not zeros in the steady-state. Therefore, the power system converges to different steady-states with different wide area damping controllers. From the plots shown in Fig. 4.4, it can be seen that persistent low frequency oscillations exist in the rotor angles if no wide area damping controller is used. The oscillations in rotor angles could be quickly damped out through the incorporation of the proposed wide area damping controller. The RSWAC loop derived by employing the existing utility rank-

Table 4.4: Comparison of rotor angle settling times between proposed and existing RSWAC schemes

Generator id	Settling time in sec (5% tolerance band)							
	TL_OUT_1		TL_OUT_2		TL_OUT_3		LD_SHD_1	
	RSWAC (proposed)	RSWAC (existing)	RSWAC (proposed)	RSWAC (existing)	RSWAC (proposed)	RSWAC (existing)	RSWAC (proposed)	RSWAC (existing)
G1	5.2892	13.8720	5.0136	22.7083	4.9822	11.9561	6.3923	56.9672
G2	8.6582	13.7539	5.8966	40.2294	9.9643	17.0186	6.3193	95.0761
G3	4.2871	69.4198	5.1106	137.180	5.2902	99.9311	6.5645	97.9636
G4	5.1632	16.9879	4.1445	53.6482	5.3925	16.9918	6.2449	79.9412
G5	5.3030	13.1433	5.2785	17.3292	5.4531	13.1049	6.4101	36.1922
G6	5.2592	13.9530	5.1637	49.7140	5.4153	16.9019	5.7827	54.5298
G7	5.2662	15.3527	5.1880	54.4944	5.4159	16.9509	5.7280	56.0124
G8	5.4050	17.8287	5.1247	45.9554	5.1339	13.0990	8.9142	98.4897
G9	5.8962	13.9954	5.0653	29.1847	5.9027	13.7464	6.9473	75.8495
G10	5.2387	78.9858	6.9673	78.2541	6.2030	71.8875	15.895	75.5680
G11	7.7128	16.4776	17.0391	48.6842	6.2445	16.3638	13.501	77.1092
G12	7.1549	108.9590	21.6828	138.0274	6.6664	115.7931	21.5744	147.7407
G13	7.3942	19.5113	18.0464	50.7848	16.3300	21.0549	23.0883	94.9465
G14	14.9904	18.1650	13.2233	56.7346	12.9878	23.4184	11.5271	97.7782
G15	13.8338	21.2244	6.2360	65.1651	12.6488	21.3422	6.29030	76.7721
G16	13.9422	15.5900	12.7514	21.4875	13.8673	15.5420	11.8530	54.9674

ing scheme can also damp out rotor oscillations; however, the damping performance is much poorer. The comparison of rotor angle settling times between the proposed and existing RSWAC schemes is presented in Table 4.4. The settling time is calculated by using an inbuilt MATLAB function and with respect to a tolerance level of 5%. The differences in settling times clearly justify the superiority of the proposed scheme to identify appropriate generators for constructing the RSWAC loop. It is interesting to observe the rotor angle dynamics of Generator 12. The particular generator is present in the RSWAC loop of the old architecture. However, the respective RSWAC loop still fails to damp out its rotor oscillation within a time frame of seconds. Sometimes, even, the rotor oscillation of Generator 12 persists for nearly three minutes in the above case. On the other hand, Generator 12, along with its five other companions from the RSWAC loop of existing design, is identified as a non-dominant generator by the proposed methodology. Although Generator 12 is not present in the proposed RSWAC loop, its rotor oscillation could be damped out much faster with this new RSWAC system. In all the instances, the rotor angles of generators are found to reach the new steady-state in less than half minute.

## 4.5 Experimental Validation

The performance of the proposed controller is further verified by using a real-time experimental setup. The experimental setup considered is shown in Fig. 4.5. It consists of the eMEGAsim real time simulator (OPAL-RT, Model no-OP5600), one host computer and another computer that performs the control center functionality. The eMEGAsim real time simulator and the desktop PCs communicate with one other via an ethernet switch over a UDP network. The eMEGAsim simulator is used to run the power system dynamics (with core components) in real-time by using the RT-Lab software. The PMUs are also implemented in the real-time simulator by using the recursive discrete Fourier transform formulation [9] with 100 samples per cycle. The power system dynamics and phasor calculations are run in different cores. The time-stamping of a measurement set is made according to the simulation time. The dynamic simulation is run with a step size of  $166.667 \mu\text{s}$ . The role of the host computer is to develop the power system (as well as PMU) model and load it into the eMEGAsim real-time simulator. The state estimator and the state feedback controller are run in the computer designated as the control center.

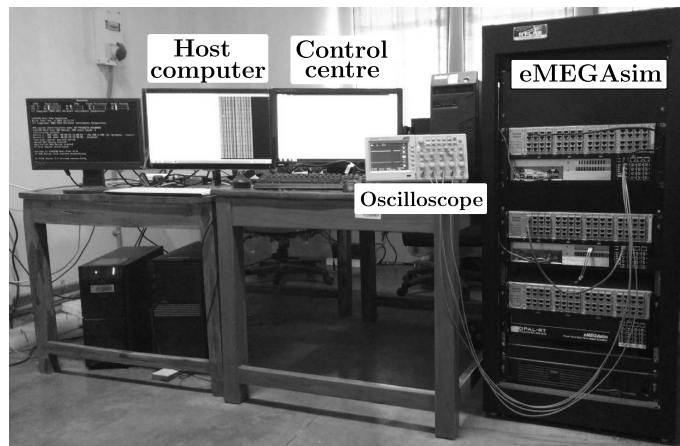


Figure 4.5: Real-time experimentation set up.

In the simulation study, it is assumed that the measurements of system quantities are continuously available. In reality, only discrete measurements are available since PMUs can report data only at a finite rate. The reporting rate that is considered in this work is 60 samples/sec, which is consistent with the standard IEEE C37.118.1-

2011 [68] for the 60 Hz system. The state estimation and WAC signal generation are re-executed only after a new data set (i.e., data set with a new time stamp) arrives. The execution time of the control center functionality is less than 3 ms for both the full-scale and reduced-scale wide area damping controllers. Therefore, it is ensured that all the computations related to state estimation and WAC signal generation get completed before the next data set arrives from PMUs. The WAC signal received by a generator is latched until a new WAC signal arrives. The communication between the real-time simulator and the control center is managed via the Python application program interface.

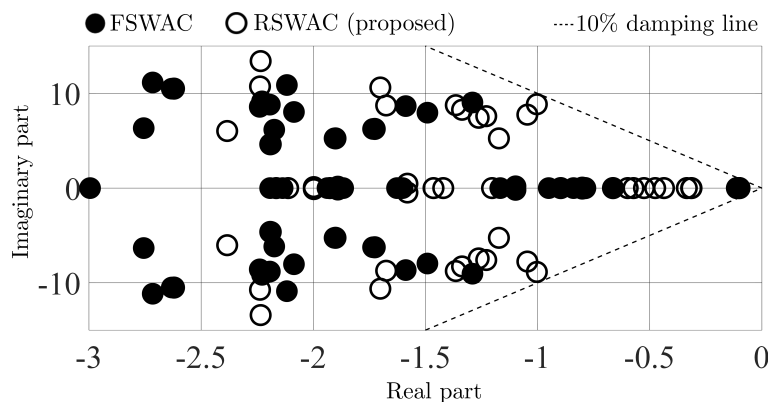


Figure 4.6: Closed loop eigenvalue comparison between FSWAC and proposed RSWAC systems.

The original timed delay in the WAC loop is found to be only 10 ms. In order to further increase the time delay, transportation delay blocks of 190 ms additional delay are placed before the communication network socket in the real-time simulation. It is to be noted that the communication delay in the WAC loop is, in reality, random in nature. However, for the sake of simplicity and not to lose focus on the actual context, the wider area damping controller design is performed in this work by assuming fixed time delay in the WAC loop. The communication delay considered in the wide area damping controller design can be interpreted as the mean time delay to feedback the WAC signal. There is a research scope for designing a robust wide area damping controller by optimizing its performance over all possible time delays. Alternatively, if practically feasible, network delay compensators [47], [69], [70] can be used.



Table 4.5: Comparison of rotor angle settling times between FSWAC and proposed RSWAC systems

Generator id	Settling time in sec (5% tolerance band)							
	TL_OUT_1		TL_OUT_2		TL_OUT_3		LD_SHD_1	
	FSWAC	RSWAC	FSWAC	RSWAC	FSWAC	RSWAC	FSWAC	RSWAC
G1	5.1584	14.1259	4.6043	5.1863	4.8801	11.8632	5.2927	7.3704
G2	9.9649	14.4452	10.9011	12.6937	11.8800	15.1734	5.0470	6.4463
G3	8.5033	14.5613	9.5981	9.9809	11.2125	15.3196	7.3665	7.6755
G4	10.7644	15.3474	9.8331	10.2587	11.1741	15.5587	5.2561	6.5964
G5	10.0249	15.1850	4.9896	5.4064	10.9490	15.4523	5.2893	6.8074
G6	9.7280	14.9213	7.0051	8.2150	10.0344	15.2257	5.2326	6.5976
G7	9.7714	14.9379	4.1525	5.2956	10.1394	15.2607	5.2330	6.5836
G8	10.3158	14.8585	9.7532	11.1617	5.0062	14.6119	5.3105	7.2729
G9	11.6704	15.8583	8.6169	9.6786	11.0156	15.5309	7.8482	8.0073
G10	6.7578	8.2391	8.4337	18.0439	8.2369	9.0149	9.4924	20.8067
G11	6.0693	9.4020	6.7513	21.2418	5.2943	7.8572	7.2323	20.2617
G12	12.0713	17.1496	9.0140	23.7013	8.0717	18.3135	10.1281	23.5630
G13	7.2497	8.2566	7.6325	22.8336	7.2211	20.7348	8.2506	23.8959
G14	13.7339	19.6637	8.8484	17.0030	11.7831	18.0998	9.9178	16.0190
G15	13.3262	18.2664	8.0126	13.6683	12.4108	17.7128	5.8314	9.8089
G16	13.5064	18.6270	11.2302	17.2992	13.4242	18.5755	9.3159	16.5771

The RSWAC loop architecture remains the same as in the case of zero communication delay (please see the previous section). The comparison of eigenvalue spectra between full-scale and reduced-scale WAC systems is produced in Fig. 4.6. The results of the rotor dynamics are collected in an oscilloscope through the analog output ports. Each quantity is scaled up or down within the range from -10 to 10 before sending it to an analog output port. For the purpose of better comparison between different WAC systems, measurements collected in the oscilloscope are reproduced in the form of MATLAB plots. The corresponding results are shown in Fig. 4.7. The comparison of the settling times of rotor oscillations between the FSWAC and the proposed RSWAC systems is presented in Table 4.5.

Compared to the transients in Fig. 4.4, some deterioration can be observed in the transients shown in Fig. 4.7. The particular result is indicative of the fact that the time delay and the unavailability of continuous measurements from PMUs can degrade the WAC performance. However, RSWAC loop proposed is still able to damp out all the rotor oscillations within half minute. As expected, the RSWAC system exhibits somewhat inferior performance compared to the FSWAC system. In certain instances, the extra time required to damp out the rotor oscillation, because of reducing the scale of the WAC system, is nearly 15 seconds. On the other hand, the cost of installing the proposed reduced-scale WAC infrastructure would be much

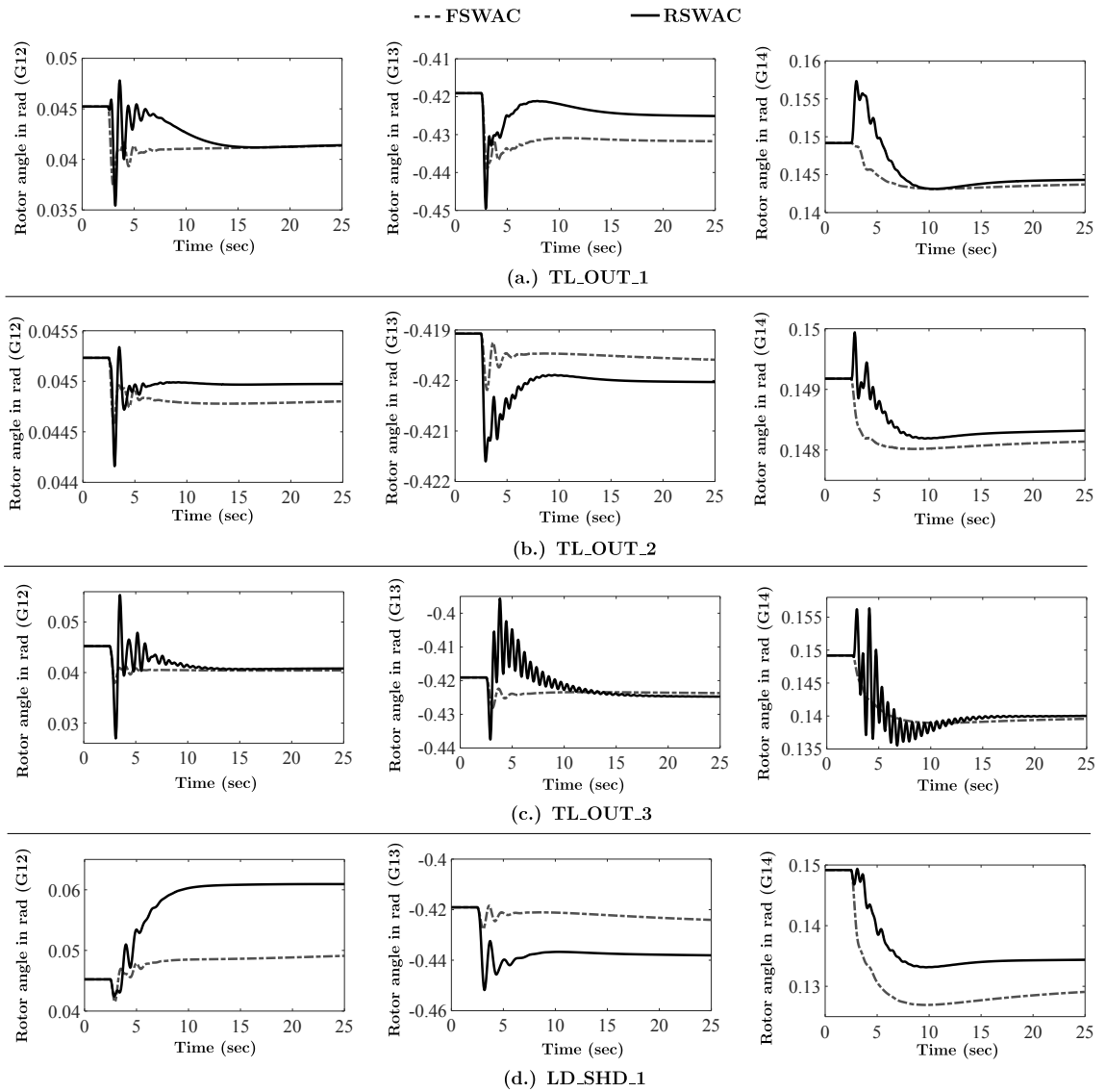


Figure 4.7: Comparison of rotor angle (COI referred) dynamics between FSWAC and RSWAC systems with time delay.

lower than the cost of installing the full-scale WAC infrastructure. For the present system, only 6 generators, out of 16 generators, are used to build the RSWAC loop, which, in turn, significantly reduces the communication requirement. Thus, the cost of implementing the WAC action can be significantly saved by bearing with a slightly prolonged rotor oscillation.

## 4.6 Summary

A novel technique to identify the dominantly effective source and sink points in the WAC loop is proposed in this chapter. A new mode-path susceptibility matrix is proposed to determine the utility levels of different source and sink points to mitigate inter-area oscillations. The modal sensitivities to the feedback gain matrix are used to determine the proposed mode-path susceptibility matrix. Effectively, the contributions of different feedback paths to change a mode shape are evaluated by means of the first order Taylor's series approximation. A reduced-scale WAC loop can be constructed by eliminating all the non-dominant source and sink points of the wide area damping controller. The methodology proposed is further extended to general sources and sinks without any restriction on the number of signals per source/sink point. This, in turn, makes it possible to derive a reduced-scale architecture for both the state feedback and the output feedback. Case studies are performed on obtaining a reduce-scale state feedback controller among the generators. The RSWAC loop obtained by using the proposed mode-path susceptibility matrix exhibits much superior damping performance compared to its existing counterpart. It is also revealed that a higher number of generators can be eliminated from the WAC loop based upon the prescribed utility ranking scheme. In order to take into account practical effects such as communication delay, phasor measurement, finite data reporting rate and independent control center functionalities, an RT experimentation is carried out by employing a real-time simulator. The RT experimentation reveals satisfactory performance of the proposed RSWAC system even in the practical situation of having limitations in data communication.

# Chapter 5

## Practical Supplementary

## Controller Design for the Bi-Level

## WAC Architecture

### 5.1 Introduction

This chapter presents a design of the supplementary wide area damping controller that can practically fit into the architecture of the bi-layer WAC system. In order to overcome the problems associated with data communication, a bi-layer WAC architecture was proposed in [71]. The bi-layer WAC architecture comprises of two WAC loops in parallel. The main WAC loop is implemented in a conventional manner by using a system-wide communication network. On the other hand, no such communication network should be used in the supplementary WAC loop. Although the fundamental concept (i.e., one layer with the communication network and another layer without communication network) of the bi-layer WAC system has already been reported in the literature, no work could be found till date as to the practical realization of the supplementary controller. Therefore, this chapter contributes towards the design of practical supplementary WADC. The proposed design of the supplementary WADC is achieved through the  $H_2$ -norm optimization after imposing necessary constraints on

the structure of the respective feedback gain matrix. The detailed mathematical procedure is derived for solving the above mentioned structurally-constrained  $H_2$ -norm optimization problem.

## 5.2 Overview of the conventional WAC system

The overview of the conventional WAC system is explained detail in Section 3.2 and Section 4.2. In order to simplify the wide area controller design, an augmented plant model should be defined by combing the original plant and the time delay blocks [29], [60]. The boundary of the augment plant is drawn with dotted lines in Fig. 3.1(b). Moreover, in order the assess the controller performance, a disturbance input vector (symbolized as  $\mathbf{d}$ ) and a performance output vector (symbolized as  $\mathbf{z}$ ) are to be defined. Thus, the linearized state-space model of the augmented plant should be written down as follows.

$$\Delta \dot{\mathbf{x}} = \mathbf{A}\Delta \mathbf{x} + \mathbf{B}_u\Delta \mathbf{u}_w + \mathbf{B}_d\Delta \mathbf{d} \quad (5.1)$$

$$\Delta \mathbf{y} = \mathbf{C}_y\Delta \mathbf{x} \quad (5.2)$$

$$\Delta \mathbf{z} = \mathbf{C}_z\Delta \mathbf{x} + \mathbf{D}_z\Delta \mathbf{u}_w \quad (5.3)$$

where,

$$\mathbf{x} = \begin{bmatrix} \mathbf{x}_{pl}^T & \mathbf{x}_{pl}^T \end{bmatrix}^T \quad (5.4)$$

$$\mathbf{A} = \begin{bmatrix} \mathbf{A}_{pl} & \mathbf{B}_{pl}\mathbf{C}_{dl} \\ \mathbf{0} & \mathbf{A}_{dl} \end{bmatrix} \quad (5.5)$$

$$\mathbf{B}_u = \begin{bmatrix} \mathbf{D}_{dl}^T\mathbf{B}_{pl}^T & \mathbf{B}_{dl}^T \end{bmatrix}^T \quad (5.6)$$

$$\mathbf{C}_y = \begin{bmatrix} \mathbf{C}_{pl} & \mathbf{0} \end{bmatrix}. \quad (5.7)$$

Parameters  $\mathbf{B}_d$ ,  $\mathbf{C}_z$  and  $\mathbf{D}_z$  are to be specified by the user depending upon the specific performance requirement. Matrix  $\mathbf{G}_w$  is designed in a way so that the resultant

feedback signal vector (i.e.,  $\mathbf{u}_w$ ) can minimize the  $H_\infty$ -norm or  $H_2$ -norm of performance outputs in response to the given disturbance inputs. In [67], [71], the WADC is designed by minimizing the  $H_\infty$ -norm of the closed loop system. The  $H_2$ -norm optimized WADC design is addressed in [29], [30] and [1]. The  $H_\infty$ -norm optimization can yield a robust design, whereas, better transient response can be achieved through the  $H_2$ -norm optimization [59].

### 5.3 Bi-layer WAC architecture and the proposed design

The schematic block diagram representation (in terms of the linearized state-space model) of the general bi-layer WAC architecture is shown in Fig. 5.1. As mentioned earlier, the bi-layer WAC system is characterized by a supplementary WAC loop (that does not use any communication network) in parallel to the conventional WAC loop. Two sets of information (represented by vectors  $\mathbf{y}_m$  and  $\mathbf{y}_s$  respectively) are received from the plant to generate the WAC signals. The first set of information is used to generate damping signals through the traditional wide area controller. The other set of information is required to generate the supplementary WAC signals.

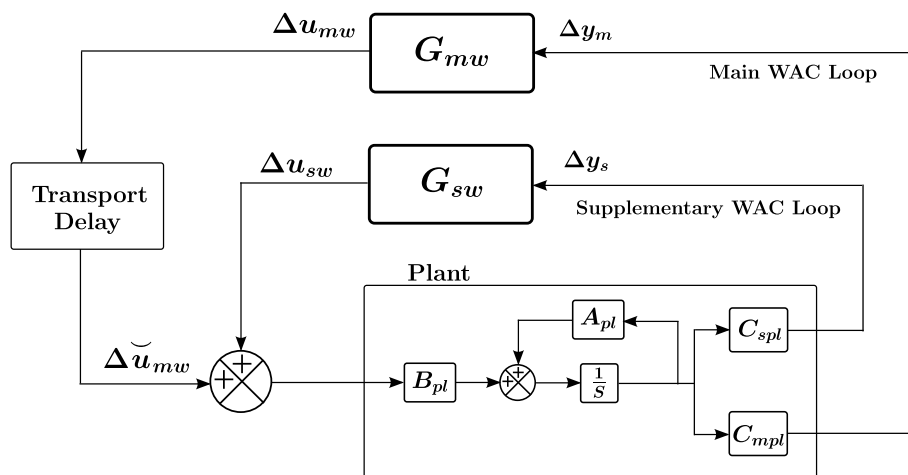


Figure 5.1: Schematic representation of the bi-layer WAC architecture.

The damping controllers in the main and supplementary WAC loops are to be

sequentially designed. It is useful to design the supplementary WADC first so as to make the WAC system resilient to communication failures [71]. Thus, in the first stage, only the supplementary WADC is to be designed by assuming that the main WADC is absent. The state-space model to be considered at this stage is shown below.

$$\Delta \dot{\mathbf{x}} = \mathbf{A}_s \Delta \mathbf{x} + \mathbf{B}_{su} \Delta \mathbf{u}_{sw} + \mathbf{B}_d \Delta \mathbf{d} \quad (5.8)$$

$$\Delta \mathbf{y}_s = \mathbf{C}_{sy} \Delta \mathbf{x} \quad (5.9)$$

$$\Delta \mathbf{z} = \mathbf{C}_{sz} \Delta \mathbf{x} + \mathbf{D}_{sz} \Delta \mathbf{u}_{sw} \quad (5.10)$$

where,

$$\mathbf{B}_{su} = \begin{bmatrix} \mathbf{B}_{pl}^T & \mathbf{0} \end{bmatrix}^T \quad (5.11)$$

$$\mathbf{C}_{sy} = \begin{bmatrix} \mathbf{C}_{spl} & \mathbf{0} \end{bmatrix} \quad (5.12)$$

$$\mathbf{C}_z = \begin{bmatrix} \mathbf{Q}^{\frac{1}{2}} & \mathbf{0} & \mathbf{0} \end{bmatrix}^T \quad (5.13)$$

$$\mathbf{D}_{sz} = \begin{bmatrix} \mathbf{0} & \mathbf{R}_s^{\frac{1}{2}} & \mathbf{0} \end{bmatrix}^T. \quad (5.14)$$

The symmetric square matrices  $\mathbf{Q}$  and  $\mathbf{R}_s$  have the dimensions of  $(N_s \times N_s)$  and  $(N_u \times N_u)$ , respectively. Similarly to the LQR optimization, those are the user-specified parameters. Here,  $N_s$  indicates the number of state variables and  $N_u$  is the number of controlled equipments. There are  $(N_s + 2N_u)$  performance output quantities in  $\mathbf{z}$ . Matrix  $\mathbf{A}_s$  is given by the same expression as that of  $\mathbf{A}$  in (5.5). All other notations used here are defined in the previous section or in Fig. 5.1.

After obtaining the feedback gain matrix for the supplementary WAC loop, the plant model needs to be updated for considering the main WAC signals. The supplementary WAC loop should be included in the updated plant model. Thus, the main WADC design is carried out by employing the following state-space model of

the system.

$$\Delta \dot{\mathbf{x}} = \mathbf{A}_m \Delta \mathbf{x} + \mathbf{B}_{mu} \Delta \mathbf{u}_{mw} + \mathbf{B}_d \Delta \mathbf{d} \quad (5.15)$$

$$\Delta \mathbf{y}_m = \mathbf{C}_{my} \Delta \mathbf{x} \quad (5.16)$$

$$\Delta \mathbf{z} = \mathbf{C}_{mz} \Delta \mathbf{x} + \mathbf{D}_{mz} \Delta \mathbf{u}_{mw} \quad (5.17)$$

where,

$$\mathbf{A}_m = \mathbf{A}_s + \mathbf{B}_{su} \mathbf{G}_{sw}^* \mathbf{C}_{sy} \quad (5.18)$$

$$\mathbf{C}_{mz} = \mathbf{C}_{sz} + \mathbf{D}_{sz} \mathbf{G}_{sw}^* \mathbf{C}_{sy} \quad (5.19)$$

$$\mathbf{C}_{my} = \begin{bmatrix} \mathbf{C}_{mpl} & \mathbf{0} \end{bmatrix} \quad (5.20)$$

$$\mathbf{D}_{mz} = \begin{bmatrix} \mathbf{0} & \mathbf{0} & \mathbf{R}_m^{\frac{1}{2}} \end{bmatrix}^T. \quad (5.21)$$

Similarly to  $\mathbf{R}_s$ ,  $\mathbf{R}_m$  in (5.21) is a user-specified ( $N_u \times N_u$ ) symmetric matrix. Matrix  $\mathbf{B}_{mu}$  in (5.15) and matrix  $\mathbf{B}_u$  in (5.1) are identical. The optimal solution of the supplementary WADC obtained from the first stage of design is indicated by  $\mathbf{G}_{sw}^*$ . The same has to be fed as a parameter to the second stage for designing the main WADC.

### 5.3.1 Proposed configuration of the supplementary WADC

The inputs to and the signal flow in the supplementary WAC loop are to be restricted to make it free from any extensive communication requirement. First of all, the supplementary WAC signals must be generated only based upon the measurements collected near the controlled devices. With this consideration,  $\mathbf{u}_{sw}$ ,  $\mathbf{y}_s$  and  $\mathbf{G}_{sw}$  can be partitioned as follows.

$$\mathbf{u}_{sw} = \begin{bmatrix} u_{sw,1} & u_{sw,2} & \cdots & u_{sw,N_u} \end{bmatrix}^T \quad (5.22)$$

$$\mathbf{y}_s = \begin{bmatrix} \mathbf{y}_{s,1}^T & \mathbf{y}_{s,2}^T & \cdots & \mathbf{y}_{s,N_u}^T \end{bmatrix}^T \quad (5.23)$$



$$\mathbf{G}_{sw} = \begin{bmatrix} \mathbf{G}_{sw,1,1} & \mathbf{G}_{sw,1,2} & \cdots & \mathbf{G}_{sw,1,N_u} \\ \mathbf{G}_{sw,2,1} & \mathbf{G}_{sw,2,2} & \cdots & \mathbf{G}_{sw,2,N_u} \\ \vdots & \vdots & \ddots & \vdots \\ \mathbf{G}_{sw,N_u,1} & \mathbf{G}_{sw,N_u,2} & \cdots & \mathbf{G}_{sw,N_u,N_u} \end{bmatrix}. \quad (5.24)$$

Here, the supplementary WAC signal fed to the  $k$ th controlled equipment is indicated by  $u_{sw,k}$ . Vector  $\mathbf{y}_{s,k}$  indicates the measurements collected from the neighborhood of the  $k$ th controlled equipment to feed into the supplementary WAC loop. The contribution of the  $l$ th equipment in generating the supplementary WAC signal for the  $k$ th equipment is indicated by  $\mathbf{G}_{sw,k,l}$ . It is, however, not possible to establish a signal flow between two remotely located equipments unless a wide area communication network is used. Therefore, in order to make the supplementary WAC loop free from any extensive communication requirement,  $\mathbf{G}_{sw,k,l}$  must be set to zero if the  $k$ th and  $l$ th equipments are not closely located.

It may also be necessary to have a local communication network to manage the signal flow between two closely located equipments. In the case no use of the communication network is intended in the supplementary WAC loop, the corresponding feedback gain matrix must be designed with a block-diagonal structure. This, in turn, indicates that the supplementary WAC signal for a device is to be generated from its own outputs only. In that case, the supplementary WADC can be effectively implemented as a collection of local controllers. However, unlike other local controllers, such as PSSs, the components of the supplementary WADC cannot be tuned individually. The entire supplementary WADC should be designed at a time through a system-level study. Thus, the fundamental idea that is employed here to realize the supplementary WADC is to employ a set of local controllers that have been designed in a coordinated manner by recognizing the system-wide dynamics. In principle, the PSSs can also be designed in the similar manner. However, producing any such design is a very complex task since each PSS gives birth to several new state variables. On the other hand, the supplementary WADC does not add any new state variable to the system.

### 5.3.2 Design methodology for the proposed supplementary WADC

In [71], the supplementary WADC was designed via  $H_\infty$ -norm optimization. However, the available  $H_\infty$ -norm optimization techniques cannot recognize the structural limitations of the feedback gain matrix. That is, no specific structure of the output feedback gain matrix can be specified to the  $H_\infty$ -norm optimizer. On the other hand, the supplementary WADC proposed retains a certain structure with zeros at pre-specified locations. The structural constraint on the feedback gain matrix in the supplementary WAC loop can be compactly written down as follows.

$$\mathbf{G}_{sw} \circ \Theta_{sw} = \mathbf{0}. \quad (5.25)$$

Here, symbol  $\circ$  indicates the Hadamard product. The entries of matrix  $\Theta_{sw}$  are only zeros and ones, and it has the same row and column dimensions as that of  $\mathbf{G}_{sw}$ . The zero entries in  $\mathbf{G}_{sw}$  are determined by the unity entries in  $\Theta_{sw}$ .

It is possible to design a structurally constrained state feedback gain matrix through the  $H_2$ -norm optimization. Therefore, in the case of the  $H_2$ -norm optimization, the output feedback is to be equivalently represented as state feedback as follows.

$$\Delta \mathbf{u}_{sw} = \mathbf{G}_{sw} \mathbf{C}_{sy} \Delta \mathbf{x}. \quad (5.26)$$

This, in turn, enforces the following constraint on the equivalent state feedback gain matrix (symbolized as  $\mathbf{K}_{sw}$ ) to be designed.

$$\mathbf{K}_{sw} = \mathbf{G}_{sw} \mathbf{C}_{sy}. \quad (5.27)$$

Equations (5.25) and (5.27) together define the structural constraints for the  $H_2$ -norm optimization problem. There are two approaches to perform the structurally constrained  $H_2$ -norm optimization for designing the state feedback gain matrix. In

[29], a methodology based upon iteratively updating the algebraic Riccati equation (ARE) was proposed to obtain a suboptimal solution. The particular method may, however, face convergence problem for a complex power system. In addition, Constraint (5.25) cannot be taken into account in the approach of [29]. In the other approach, the  $H_2$ -norm optimization problem is solved by using the alternating direction method of multipliers (ADMM) [30], [1]. However, the methodology proposed in [30], [1] can be directly applied only when  $\mathbf{C}_{sy}$  (i.e., the measurement output matrix) is an identity matrix.

In this work, the supplementary WADC is designed through ADMM-based  $H_2$ -norm optimization only. In order to convert the problem into the form required by the ADMM-based algorithm, a suitable state-variable transformation technique is proposed. The new state vector and the measurement output vector (symbolized as  $\Delta\tilde{\mathbf{x}}$  and  $\Delta\tilde{\mathbf{y}}_s$ , respectively) should be chosen as follows.

$$\Delta\tilde{\mathbf{y}}_s = \Delta\tilde{\mathbf{x}} \quad (5.28)$$

$$\Delta\tilde{\mathbf{x}} = \hat{\mathbf{C}}_{sy} \Delta\mathbf{x} \quad (5.29)$$

where,  $\hat{\mathbf{C}}_{sy} = \begin{bmatrix} \mathbf{C}_{sy}^T & \mathbf{C}_{sr}^T \end{bmatrix}^T$  and matrix  $\mathbf{C}_{sr}$  should be chosen in a way so that  $\hat{\mathbf{C}}_{sy}$  can be invertible. With the new state vector, the expression of the WAC signal vector is obtained as follows.

$$\begin{aligned} \Delta\mathbf{u}_{sw} &= \mathbf{G}_{sw} \Delta\mathbf{y}_s \\ &= \mathbf{G}_{sw} \mathbf{C}_{sy} \Delta\mathbf{x} \\ &= \begin{bmatrix} \mathbf{G}_{sw} & \mathbf{0} \end{bmatrix} \hat{\mathbf{C}}_{sy} \Delta\mathbf{x} \\ &= \begin{bmatrix} \mathbf{G}_{sw} & \mathbf{0} \end{bmatrix} \Delta\tilde{\mathbf{x}} \\ &= \underbrace{\begin{bmatrix} \mathbf{G}_{sw} & \mathbf{0} \end{bmatrix}}_{\tilde{\mathbf{G}}_{sw}} \Delta\tilde{\mathbf{y}}_s. \end{aligned} \quad (5.30)$$

The new output feedback gain matrix  $\tilde{\mathbf{G}}_{sw}$  is subjected to the following structural

constraint.

$$\tilde{\mathbf{G}}_{sw} \circ \tilde{\Theta}_{sw} = \mathbf{0} \quad (5.31)$$

where,

$$\tilde{\Theta}_{sw} = \begin{bmatrix} \Theta_{sw} & \mathbf{U} \end{bmatrix}. \quad (5.32)$$

Here,  $\mathbf{U}$  is a matrix (of appropriate dimensions) of all ones. Finally, the state and performance output equations in terms of the new state vector can be written down as are shown below.

$$\Delta \dot{\tilde{\mathbf{x}}} = \underbrace{\hat{\mathbf{C}}_{sy} \mathbf{A}_s \hat{\mathbf{C}}_{sy}^{-1}}_{\tilde{\mathbf{A}}_s} \Delta \tilde{\mathbf{x}} + \underbrace{\hat{\mathbf{C}}_{sy} \mathbf{B}_{su}}_{\tilde{\mathbf{B}}_{su}} \Delta \mathbf{u}_{sw} + \underbrace{\hat{\mathbf{C}}_{sy} \mathbf{B}_d}_{\tilde{\mathbf{B}}_d} \Delta \mathbf{d} \quad (5.33)$$

$$\Delta \mathbf{z} = \underbrace{\mathbf{C}_{sz} \hat{\mathbf{C}}_{sy}^{-1}}_{\tilde{\mathbf{C}}_{sz}} \Delta \tilde{\mathbf{x}} + \mathbf{D}_{sz} \Delta \mathbf{u}_{sw}. \quad (5.34)$$

Equations (5.28), (5.31), (5.33) and (5.34) are in the appropriate form to apply the ADMM-based algorithm of [30], [1]. It is to be noted that Equation (5.28) is not obtained by transforming (5.9). The particular equation is rather independently specified. The closed loop state equations remain the same for both the original and transformed systems. For the initialization of the optimization calculation, the unconstrained solution of the state feedback matrix for (5.33) is required. The unconstrained solutions of state feedback matrices (symbolized as  $\mathbf{K}_{sw0}^*$  and  $\tilde{\mathbf{K}}_{sw0}^*$ , respectively) for (5.8) and (5.33) are related to each other via the following equation.

$$\tilde{\mathbf{K}}_{sw0}^* = \mathbf{K}_{sw0}^* \hat{\mathbf{C}}_{sy}^{-1}. \quad (5.35)$$

The value of  $\mathbf{K}_{sw0}^*$  is obtained by solving the ARE for the quadruple  $(\mathbf{A}_s, \mathbf{B}_{su}, \mathbf{Q}, \mathbf{R}_s)$  that is defined in (5.8), (5.13) and (5.14).

The methodology proposed above is also applicable to design the output feedback gain matrix with certain non-zero off-diagonal elements. Such a design would be re-

quired if the use of local communication networks is permitted in the supplementary WAC loop. The design of the main WADC is not subjected to any structural constraint for the respective output feedback gain matrix. Therefore, the main WADC can, as usual, be designed through the  $H_\infty$ -norm optimization. However, in this work, the  $H_2$ -norm optimization approach is followed to design both the main and supplementary wide area damping controllers.

## 5.4 Simulation study

The performance of the proposed WAC methodology is validated by carrying out studies over a 68-bus test system. The information about this particular test system can be found in Section 4.4. In this work, the WAC signals are fed to the excitation control systems of generators. All generators are included in the WAC loop. There are techniques available in literature [24], [54] to reduce the scale of the WAC loop. However, for the sake of simplicity and not to lose focus on the main context, not scale reduction is performed in this work. The supplementary WAC signal for a generator is derived from its rotor frequency and active power output. In (5.14) and (5.21),  $\mathbf{R}_s$  and  $\mathbf{R}_m$  are taken to be identity matrices. Matrix  $\mathbf{Q}$  in (5.13) is also taken as a diagonal matrix with the diagonal entry corresponding to an angle or frequency state being set to 100. All other diagonal entries are set to zeros. Matrix  $\mathbf{B}_d$  is taken to be the same as  $\mathbf{B}_{su}$ .

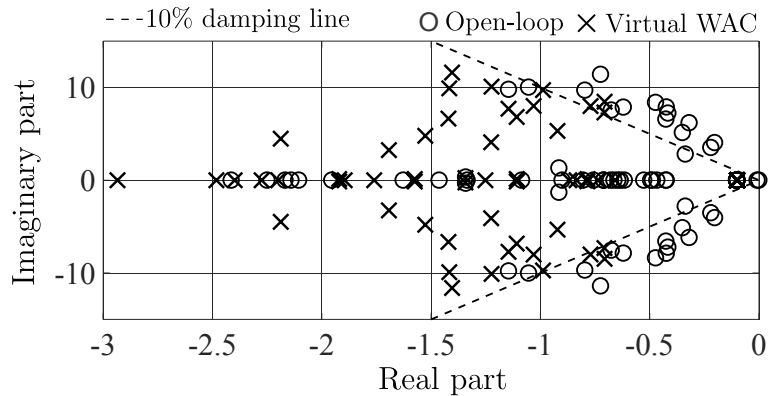


Figure 5.2: Comparison of eigenvalue spectra between open loop and closed loop systems in the case of stand-alone presence of supplementary WADC.

Initially, ordinary simulation studies are carried out to observe if the supplementary WADC alone can damp out inter-area oscillations. The particular situation arises when there is communication failure in the main WAC loop. No time delay is considered in this simulation study since, as mentioned earlier, the implementation of the supplementary wide area damping controller does not require any system-wide communication network. The eigenvalue spectra of the small signal models of open loop and closed loop (with only supplementary WADC) systems are shown in Fig. 5.2. It is observable that the supplementary wide area damping controller retains the ability to perceptibly shift the eigenvalues towards the left side of the imaginary axis. In the presence of the supplementary WADC, only a few eigenvalues lie behind the 10% damping line.

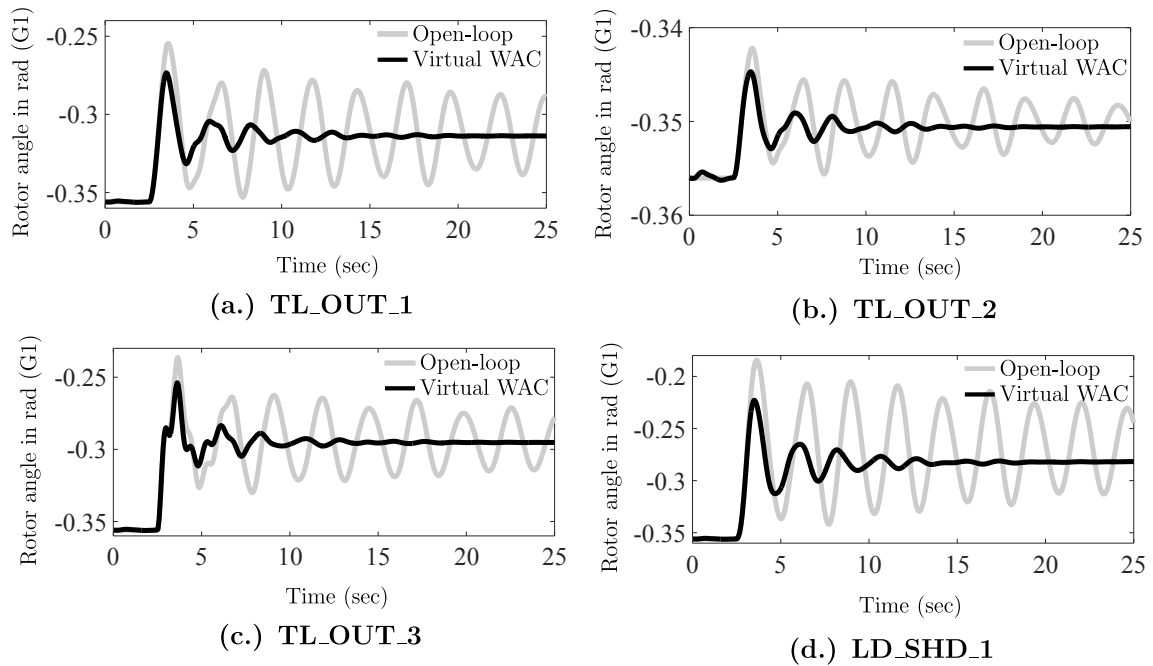


Figure 5.3: Generator 1 rotor angle dynamics for open loop and closed loop systems in the case of stand-alone presence of supplementary WADC. a) TL\_OUT\_1, b) TL\_OUT\_2, c) TL\_OUT\_3, d) LD\_SHD\_1.

The time domain simulations are carried out by considering the same disturbances that are described in Table 4.3 in Section 4.4. The corresponding dynamic responses of the rotor angle of Generator 1 are plotted in Fig. 5.3. Here, the rotor angle is referred to the center-of-inertia of the system. From the plots shown in Fig. 5.3,

it can be seen that there is persistent low frequency oscillation in the rotor angle before the deployment of any wide area damping controller. The deployment of the supplementary WADC helps in damping out the rotor angle oscillation to a great extent even though the main WAC loop is absent. The settling times of all the generator angles, for the closed loop system, are presented in Table 5.1. Here, the settling times are calculated with respect to the 2% tolerance band.

Table 5.1: Generator angle settling times for the closed loop system with only supplementary WADC

Generator id.	Settling time in sec (2% tolerance band)			
	TL_OUT_1	TL_OUT_2	TL_OUT_3	LD_SHD_1
G1	17.3188	16.9575	16.6133	17.0282
G2	15.3999	17.0424	17.2226	17.0150
G3	15.4440	17.0432	17.2196	17.0208
G4	18.2711	17.7621	18.1064	17.0897
G5	18.2671	17.7311	17.3046	17.0662
G6	18.2521	17.7198	17.2868	16.2318
G7	18.2598	17.7391	18.0804	17.1977
G8	17.3298	17.0227	15.3410	17.0433
G9	17.2746	16.1024	18.0854	17.0467
G10	14.8209	14.5727	14.8869	15.6004
G11	15.8610	16.2276	14.9844	16.2974
G12	17.8858	17.0190	17.8191	17.4068
G13	17.4832	17.0813	17.3615	17.0615
G14	18.0157	17.4914	17.0096	17.7232
G15	17.8252	16.3678	17.7727	16.3253
G16	18.5973	17.9236	16.5656	17.4810

Simulation results are also obtained to observe the ideal (i.e., when there is no time delay in the signal flow) performance of the conventional wide area damping controller in the stand-alone mode. The conventional WADC is implemented based upon the state feedback. The state feedback can be modeled as unconstrained output feedback by treating the observable states as system outputs. The dynamic simulation results of the respective closed loop system is produced in Fig. 5.4. The corresponding generator angle settling times are reported in Table 5.2. As expected, the conventional WADC exhibits much higher damping effect compared to the supplementary WADC if there is no time delay in the data communication. However, practically, the time

delay is unavoidable. Thus, the conventional WADC does not really perform in the way as it is ideally expected to perform. This is shown in experimental results.

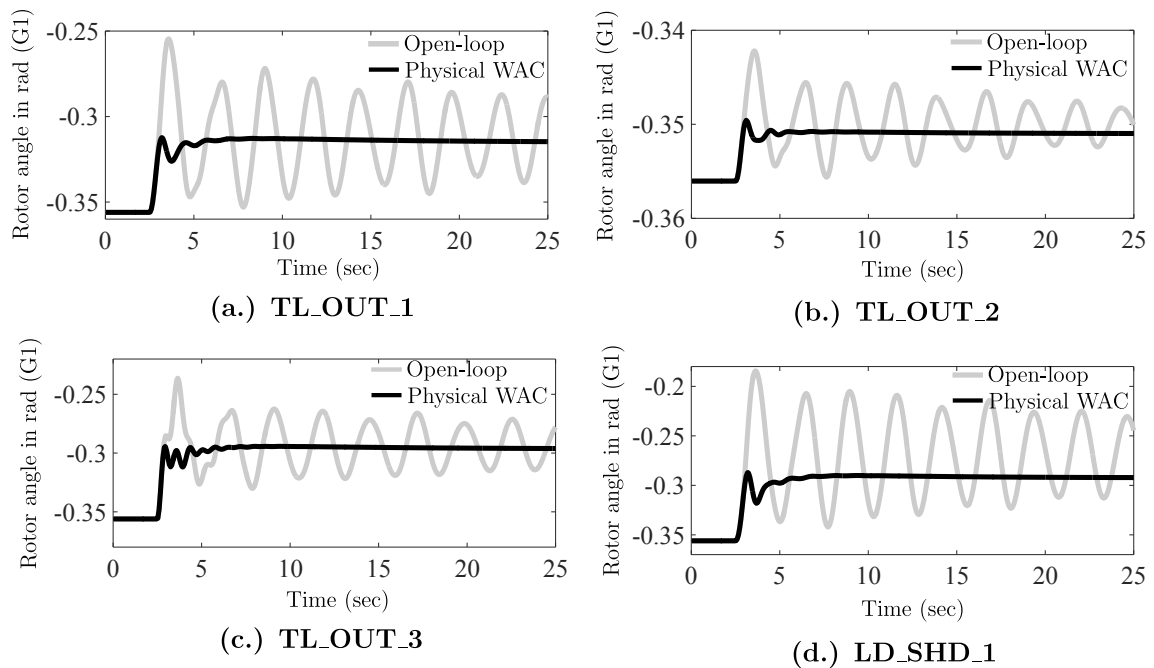


Figure 5.4: Generator 1 rotor angle dynamics for open loop and closed loop systems in the case of stand-alone presence of conventional WADC with no communication delay. a) TL\_OUT\_1, b) TL\_OUT\_2, c) TL\_OUT\_3, d) LD\_SHD\_1.

## 5.5 Experimental results

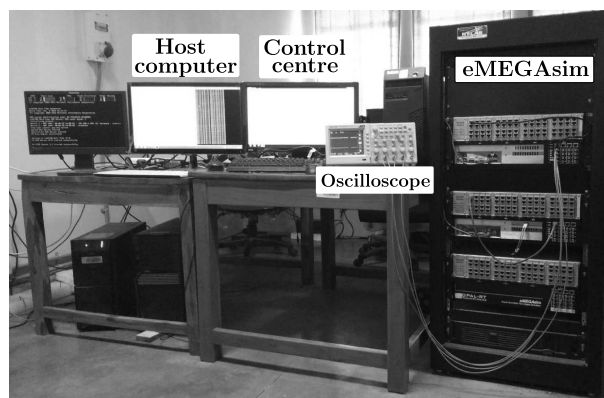


Figure 5.5: Real-time experimentation set up.



Table 5.2: Generator angle settling times for the closed loop system with only conventional WADC

Generator id.	Settling time in sec (2% tolerance band)			
	TL_OUT_1	TL_OUT_2	TL_OUT_3	LD_SHD_1
G1	5.3758	6.7664	6.4210	6.6776
G2	7.2537	5.5312	6.8228	7.0966
G3	7.1956	5.5868	6.8400	6.7463
G4	6.6873	6.8985	6.9058	6.7962
G5	6.7147	6.9018	6.9045	6.8048
G6	6.6685	6.8675	6.8834	6.6457
G7	6.6731	6.8777	6.8885	6.5642
G8	6.6240	6.8662	6.5790	6.7530
G9	5.8710	6.9007	6.8966	7.8787
G10	7.0921	6.0914	7.0221	6.3750
G11	6.2034	4.8362	5.5688	7.7038
G12	8.2851	7.4253	8.1534	8.3536
G13	8.6239	8.1384	8.7197	8.2053
G14	8.0475	8.7381	8.0455	8.9548
G15	6.8244	7.6836	7.6893	7.4561
G16	8.7851	8.0276	7.9591	8.8044

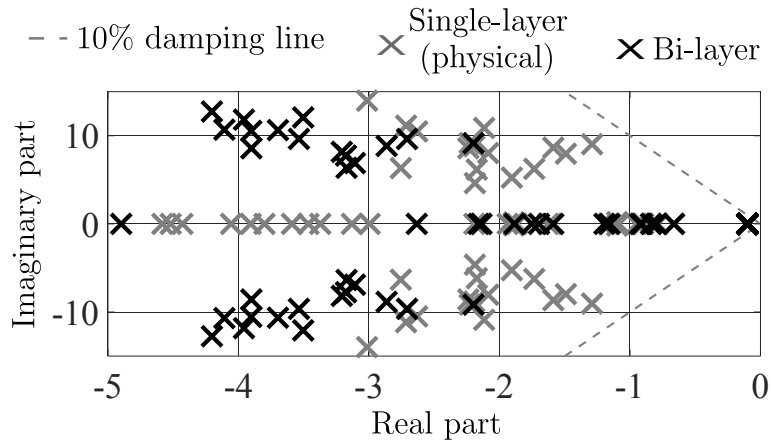


Figure 5.6: Comparison of eigenvalue spectra between the traditional mono-layer and proposed bi-layer WAC systems.

In order to compare the performances of the conventional single-layer and the proposed bi-layer WAC systems, an RT experimentation is carried out by introducing some time delay in the main WAC loop. The experimental set up considered is shown in Fig. 5.5. It consists of the eMEGAsim real time simulator (OPAL-RT, Model no-OP5600), one host computer and another computer that performs the control center

functionality. The eMEGAsim real time simulator and the desktop PCs communicate with one other via an Ethernet switch over a UDP network. The eMEGAsim simulator is used to execute the dynamics of the core power system and the supplementary wide area damping controller. The PMUs are also implemented in the real-time simulator by using the recursive discrete Fourier transform formulation [9] with 100 samples per cycle. The power system dynamics and phasor calculations are run in different cores. The time-stamping of a measurement set is made according to the simulation time. The simulation of the power system model runs with a step size of  $166.667 \mu\text{s}$ . The role of the host computer is to develop the model to be run in the eMEGAsim real-time simulator. The state estimator and the state feedback controller of the main WAC loop are implemented in the computer designated as the control center. The total time required to complete both state estimation and WAC signal generation is found to be around  $2.5 \text{ ms}$ . Therefore, it is ensured that all the computations related to state estimation and WAC signal generation get completed within two sampling instants. The test system, parameter and scenario descriptions remain the same as in the simulation study.

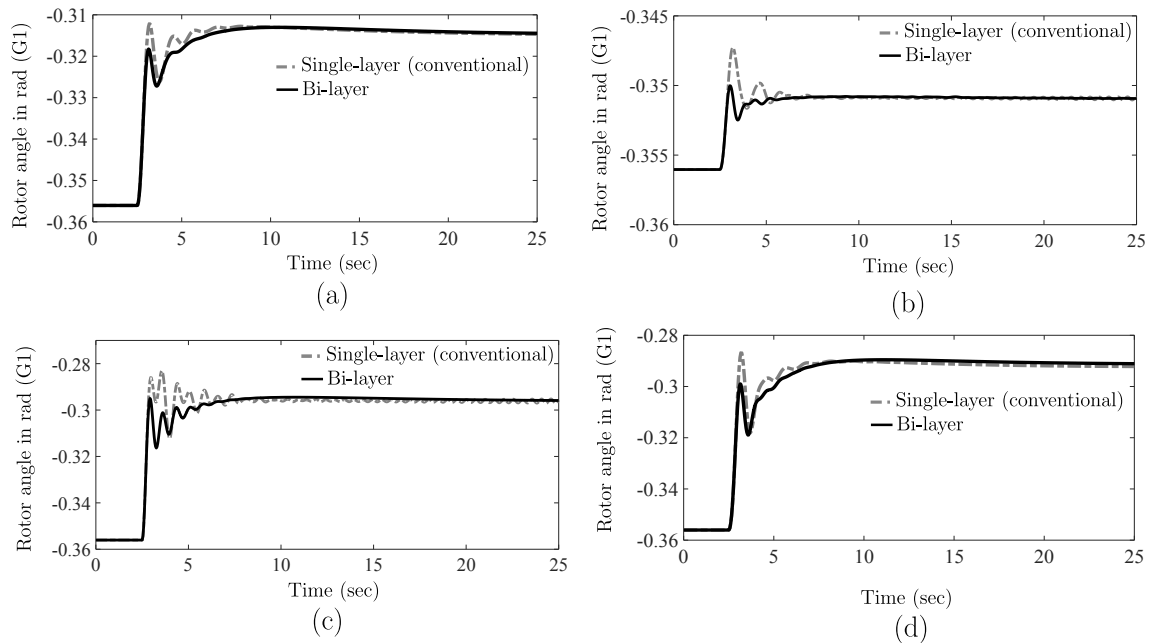


Figure 5.7: Generator 1 rotor angle dynamics for traditional mono-layer and proposed bi-layer WAC systems. a) TL\_OUT\_1, b) TL\_OUT\_2, c) TL\_OUT\_3, d) LD\_SHD\_1.

In the simulation study, it was assumed that the measurements of system quantities are continuously available. In reality, only discrete measurements are available since PMUs can report data only at a finite rate. The reporting rate that is considered in this work is 60 samples/sec, which is consistent with the standard IEEE C37.118.1-2011 [68] for the 60 Hz system. The state estimation and WAC signal generation are re-executed only when a new set (i.e., with a new time stamp) of data is received. The WAC signal received by a generator is latched until a new WAC signal arrives. The real-time experimentation setup used in this work is similar to that in [47] except for the followings.

1. Instead of using external PMUs, those are implemented in the real-time simulator itself.
2. The damping signals from the main WAC loop are sent to the generators via a communication network instead of using hardware ports. The communication between the real-time simulator and the control center is managed via the python application program interface.

The experimental setup employed is simpler, but maintains all the essential practical aspects of the WAC system.

The experiment is carried out by considering an average time delay of 150 ms in the main WAC loop. The original time delay in the main WAC loop implemented is found to be around only 10 ms. In order to further increase the time delay, transportation delay blocks of 140 ms additional delay are placed before the communication network socket in the real-time simulation. The WADC of the main WAC loop is designed with due consideration for the respective time delay.

The comparison of the eigenvalue spectra between the conventional single-layer and the proposed bi-layer WAC systems is shown in Fig 5.6. The results of the time-domain simulations are collected in an oscilloscope through the analog output ports. Each quantity is scaled up or down within the range from -10 to 10 before sending it to an analog output port. For the purpose of better comparison between single-layer (conventional) and bi-layer WAC systems, measurements collected in the oscilloscope

Table 5.3: Generator angle settling times for the bi-layer WAC system

Generator id.	Settling time in sec (2% tolerance band)			
	TL_OUT_1	TL_OUT_2	TL_OUT_3	LD_SHD_1
G1	6.4581	5.6580	6.3390	6.5831
G2	6.2100	5.3744	6.8226	6.6928
G3	6.2098	5.4833	6.8533	6.7907
G4	6.2306	6.9440	7.4482	6.9399
G5	6.3226	6.9694	7.4989	6.9021
G6	6.2283	6.7594	6.9726	5.5933
G7	6.2181	6.8377	7.0285	5.6102
G8	5.5225	6.7871	6.5767	6.8890
G9	5.3311	7.3955	7.4979	7.7370
G10	6.3799	5.4373	6.0235	6.3565
G11	7.7665	5.4178	5.2710	7.6573
G12	6.6527	5.6470	5.5649	7.3553
G13	7.4399	6.0537	6.0886	7.1381
G14	7.7245	7.5739	7.0768	7.3242
G15	7.5771	7.0102	7.2899	7.8116
G16	7.6414	7.1289	7.4518	7.6688

are reproduced in the form of MATLAB plots. The corresponding dynamic simulation results are produced in Fig 5.7. The performance of the conventional WADC is significantly deteriorated because of the delay in the data communication. Even after the deployment of the particular wide area damping controller, persistent oscillation in the rotor angle is observed. On the other hand, the combination of the conventional and supplementary WADCs could damp out the rotor angle oscillation very fast. The rotor angle settling times for different generators under the bi-layer wide area control are reported in Table 5.3. The settling times shown in Tables 5.2 and 5.3 are comparable. Eventually, settling times are somewhat improved in Table 5.3 for certain generators. This, in turn, shows the capability of the supplementary WADC to improve the performance of the WAC system in a practical situation when the communication delay is large in the main WAC loop. Even in the absence of any communication delay in the main WAC loop, the WAC system performance can be improved by adding the supplementary WAC loop.

## 5.6 Summary

The issue of having a practical realization of the supplementary controller for the bi-layer WAC architecture is resolved in this work. The supplementary WAC loop is designed through structurally-constrained  $H_2$ -norm optimization maintaining a block-diagonal structure of the respective feedback gain matrix. The supplementary WADC is, essentially, realized as a set of local controllers although all those local controllers are designed in a coordinated manner through a system level study recognizing the interactions of different state dynamics. A suitable transformation technique is derived to convert the aforementioned  $H_2$ -norm optimization problem into a standard form that is required by the available  $H_2$ -norm optimization solver. The canonical transformation of the  $H_2$ -norm optimization problem derived in this chapter is eventually applicable under any structural constraint on the feedback gain matrix. It is revealed from the case study that the supplementary controller with the aforementioned block-diagonal structure is capable enough to damp out inter-area oscillations alone in the case the main WAC loop is lost because of any communication failure. The satisfactory performance of the lonely supplementary WADC also proves that it is possible to implement the WAC action even if there is no appropriate communication infrastructure in place. In addition, deployment of the proposed supplementary controller can be useful to improve the WAC action in the case the main WAC loop is significantly affected by the communication delay. The degradation of the conventional WAC loop performance because of the communication delay is observed through RT experimentations. The supplementary WADC is found to retain the ability to substantially counterbalance the time delay effect in the conventional WAC loop.

# Chapter 6

## Conclusion and future work

The power system is subjected to different kind of oscillations, mainly, those are classified into two categories: local and inter-area mode oscillations. The local mode oscillations are damped out by using PSSs. However, in order to damp out inter-area oscillations, the wide area controller is required. Therefore, the wide area controller is designed to damp out inter-area oscillations. The design of wide area controller involves the following steps:

1. The small-signal modeling of the entire power system is accomplished to know about different modes of oscillations existing in the power system.
2. Design the PSSs to damp out local mode oscillations.
3. Next step is to damp out inter-area oscillations. That is the wide area controller design is necessary.
4. Get the inputs to the control center from remote locations through PMUs.
5. Calculate the feedback gain matrix that is used in the wide area controller design.
6. The outputs of the wide area controller are given to the controllable devices.

## 6.1 Overall summary

In this work, the wide area controller is implemented in two ways: state feedback and output feedback control. The equivalent state feedback controller is implemented by using output feedback controller gain matrix. The inputs to the wide area controller in both techniques are taken from different PMUs those are installed at different locations, in other words, limited measurements. On the other hand, the outputs of the wide area controller are given to the controllable devices. The controllable devices considered in this work are the generator's excitation systems. The  $H_2$ -norm optimization technique is used in this work to design the wide area controller. The structural constraints are imposed in the  $H_2$ -norm optimization technique to achieve the required feedback gain matrix structure based on the problem formulation. Especially, the contributions of this thesis are divided into three works:

1. WAC design with limited measurements and with unknown load composition.
2. Reduced-scale architecture of the wide area control system.
3. Practical supplementary controller design

## 6.2 WAC Design with limited Measurements and with unknown load composition

Because of the unobservability of the entire power system, it is obligatory to design the wide area controller with available limited measurements. Moreover, in practice, the load composition at each and every bus will vary from time to time. Thus, this particular work addresses resolving these two problems. The structurally constrained  $H_2$ -norm optimization technique is employed to resolve the first problem. The unknown load composition problem is solved by considering CP load alone present at all load buses. Since CP load requires more amount of damping. The performance of the wide area controller with limited state inputs and with unknown load composition is verified through a case study on the New England 39-bus system. It is revealed

from the case study that the wide area controller with limited state input can also sufficiently damp out the inter-area oscillations. In addition, independent of the load present in the system, it is enough to design a controller by assuming that all the loads are static and are of CP type.

### 6.3 Reduced-scale architecture of the wide area control system

The concept of mode-path susceptibility matrix is proposed in this work to identify the dominant source and sink points. After that, the wide area controller is designed by considering the only dominant source and sink points to damp out inter-area oscillations. The structurally constrained  $H_2$ -norm optimization technique is used to design the controller. The 68-bus test system is used to verify the effectiveness of the proposed RSWAC. In addition, the proposed RSWAC is compared with the existing RSWAC [24]. From the case study results, it is observed that the proposed controller displays very good performance over the existing one. Moreover, the effectiveness of the proposed RSWAC performance is tested in real-time by carrying out RT experimentation for different operating conditions.

### 6.4 Practical supplementary controller design

In this work, the practical realization of the supplementary controller for the bi-layer WAC architecture is resolved. The bi-layer WAC architecture is a cluster of two loops, namely, main WAC loop and supplementary WAC loop. The main WAC loop uses the remote measurements and generates the WAC output signals. In contrast, the supplementary WAC loop uses the local measurements and generates the WAC output signals. In the case of any communication network failure, that is the main WAC loop is absent, the supplementary WAC loop always present, since it uses local input signals, and it damps out the oscillations satisfactorily. Therefore, the deployment of the proposed supplementary controller can be useful to improve the WAC action in



the case the main WAC loop is significantly affected by the communication delay. The degradation of the main WAC loop performance because of the communication delay is observed through RT experimentations. The supplementary controller is found to retain the ability to substantially counterbalance the time delay effect in the main WAC loop.

## 6.5 Future scopes of work

The work presented in this thesis demonstrates the enhancement in a wide area control system to damp out low frequency oscillations in the power grid. However, the work can be further extended in many ways, and few methods are discussed below.

### 6.5.1 Fault tolerant wide area control

The wide area control system requires a good and fast communication network to receive the data from remote locations and to send the damping signals to the controllable devices. However, in reality, it is not possible. The communication network failure may be happened at any instant due to whatever may be the reason. In such situations, the wide area controller can not able to give good damping performance. Therefore, it is necessary to design a wide area control system in such a way that it has to give good damping performance at any instant independent of communication network problems. It is also known as fault tolerant wide area control system.

### 6.5.2 Structurally constrained $H_\infty$ -norm optimized WAC design

In this thesis, as mentioned earlier, the structurally constrained  $H_2$ -norm optimization technique is implemented to design the wide area controller to overcome the limited measurements issue. This concept is further extended to the design of a reduced-scale wide area control system without compromising its damping performance. Therefore,

the same concept that is structural constraints can be imposed in the design of  $H_\infty$ -norm to achieve robust control over the power system in many aspects.

### **6.5.3 WAC design for a large power system**

The power system is a large network which requires more time and more storage of data for the execution. Moreover, the wide area control loop requires additional time because of more number of input signals and the number of output damping signals. By taking these considerations into the design, it is needful to design a computationally efficient wide area control system for a large power system to have fine control over the system.

# Bibliography

- [1] F. Drfler, M. R. Jovanovi, M. Chertkov, and F. Bullo. Sparsity-Promoting Optimal Wide-Area Control of Power Networks. *IEEE Transactions on Power Systems* 29, (2014) 2281–2291.
- [2] P. Kundur, J. Paserba, V. Ajjarapu, G. Andersson, A. Bose, C. Canizares, N. Hatziargyriou, D. Hill, A. Stankovic, C. Taylor, T. V. Cutsem, and V. Vittal. Definition and classification of power system stability IEEE/CIGRE joint task force on stability terms and definitions. *IEEE Transactions on Power Systems* 19, (2004) 1387–1401.
- [3] P. Kundur. Power System Stability and Control. New York: McGraw-Hill, 1994.
- [4] K. R. Padiyar. Power System Dynamics - Stability and Control. BS Publications, Hyderabad, India, 2002.
- [5] B. C. Pal and B. Chaudhuri. Robust Control in Power Systems. New York, U.S.A.: Springer, 2005.
- [6] B. C. Pal. Robust Damping Control of Inter-area Oscillations in Power System with Super-conducting Magnetic Energy Storage Devices. Ph.D. thesis, Department of Electrical and Electronics Engineering, Imperial College of Science Technology and Medicine 1999.
- [7] J. Paserba. Analysis and control of power system oscillation. CIGRE Special Publication 38.01.07, Technical Brochure 111, 1996.

- [8] C. W. Taylor, D. C. Erickson, K. E. Martin, R. E. Wilson, and V. Venkatasubramanian. WACS-Wide-Area Stability and Voltage Control System: R and D and Online Demonstration. *Proceedings of the IEEE* 93, (2005) 892–906.
- [9] A. G. Phadke and J. S. Thorp. Synchronized Phasor Measurements and Their Applications. New York: Springer, 2008.
- [10] M. Kanabar, M. G. Adamiak, and J. Rodrigues. Optimizing Wide Area Measurement System architectures with advancements in Phasor Data Concentrators (PDCs). In 2013 IEEE Power Energy Society General Meeting. 2013 1–5.
- [11] V. Centeno, J. de la Ree, A. G. Phadke, G. Michel, R. J. Murphy, and R. O. Burnett. Adaptive out-of-step relaying using phasor measurement techniques. *IEEE Computer Applications in Power* 6, (1993) 12–17.
- [12] K. E. Holbert, G. I. Heydt, and H. Ni. Use of Satellite Technologies for Power System Measurements, Command, and Control. *Proceedings of the IEEE* 93, (2005) 947–955.
- [13] V. Backmutsky and V. Zmudikov. Accurate frequency estimation in power systems by DSP. In Eighteenth Convention of Electrical and Electronics Engineers in Israel. 1995 5.2.4/1–5.2.4/5.
- [14] J. Ren and M. Kezunovic. Real-Time Power System Frequency and Phasors Estimation Using Recursive Wavelet Transform. *IEEE Transactions on Power Delivery* 26, (2011) 1392–1402.
- [15] M. M. Begovic, P. M. Djuric, S. Dunlap, and A. G. Phadke. Frequency tracking in power networks in the presence of harmonics. *IEEE Transactions on Power Delivery* 8, (1993) 480–486.
- [16] A. K. Pradhan, A. Routray, and A. Basak. Power system frequency estimation using least mean square technique. *IEEE Transactions on Power Delivery* 20, (2005) 1812–1816.

- [17] P. K. Dash, A. K. Pradhan, and G. Panda. Frequency estimation of distorted power system signals using extended complex Kalman filter. *IEEE Transactions on Power Delivery* 14, (1999) 761–766.
- [18] V. V. Terzija, M. B. Djuric, and B. D. Kovacevic. Voltage phasor and local system frequency estimation using Newton type algorithm. *IEEE Transactions on Power Delivery* 9, (1994) 1368–1374.
- [19] A. Sridharan and V. Sarkar. A comparative study on phasor and frequency measurement techniques in power systems. In 2016 National Power Systems Conference (NPSC). 2016 1–6.
- [20] T. Lobos and J. Rezmer. Real-time determination of power system frequency. *IEEE Transactions on Instrumentation and Measurement* 46, (1997) 877–881.
- [21] Y. Xia, Y. He, K. Wang, W. Pei, Z. Blazic, and D. P. Mandic. A Complex Least Squares Enhanced Smart DFT Technique for Power System Frequency Estimation. *IEEE Transactions on Power Delivery* 32, (2017) 1270–1278.
- [22] J.-Z. Yang and C.-W. Liu. A precise calculation of power system frequency and phasor. *IEEE Transactions on Power Delivery* 15, (2000) 494–499.
- [23] A. Almutairi. Enhancement of Power System Stability Using Wide Area Measurement System Based Damping Controller. Ph.D. thesis, Faculty of Engineering and Physical Sciences, The University of Manchester 2010.
- [24] Y. Zhang and A. Bose. Design of Wide-Area Damping Controllers for Interarea Oscillations. *IEEE Transactions on Power Systems* 23, (2008) 1136–1143.
- [25] H. Nguyen-Duc, L. Dessaint, A. F. Okou, and I. Kamwa. Selection of input/output signals for wide area control loops. In IEEE PES General Meeting. 2010 1–7.
- [26] A. Heniche and I. Kamwa. Assessment of Two Methods to Select Wide-Area Signals for Power System Damping Control. *IEEE Transactions on Power Systems* 23, (2008) 572–581.

- [27] D. E. Kirk and J. S. Demetry. *Optimal Control Theory: An Introduction*. Englewood Cliffs, NJ: PrenticeHall, 1971.
- [28] S. Skogestad and I. Postlethwaite. *Multivariable Feedback Control*. New York: Wiley, 2001.
- [29] D. Dotta, A. S. e Silva, and I. C. Decker. Wide-Area Measurements-Based Two-Level Control Design Considering Signal Transmission Delay. *IEEE Transactions on Power Systems* 24, (2009) 208–216.
- [30] F. Lin, M. Fardad, and M. R. Jovanovi. Design of Optimal Sparse Feedback Gains via the Alternating Direction Method of Multipliers. *IEEE Transactions on Automatic Control* 58, (2013) 2426–2431.
- [31] C. Stachniss. Robot Mapping - Extended Kalman Filter. <http://ais.informatik.uni-freiburg.de/teaching/ws12/mapping/pdf/slam03-ekf.pdf>.
- [32] D. Simon. *Optimal State estimation; Kalman,  $H_\infty$ , and Nonlinear Approaches*. New Jersey: John Wiley & Sons, 2006.
- [33] J. K. Uhlmann. Simultaneous map building and localization for real-time applications. Ph.D. thesis, Transfer thesis, University of Oxford 1994.
- [34] C. Stachniss. Robot Mapping - Unscented Kalman Filter. <http://ais.informatik.uni-freiburg.de/teaching/ws12/mapping/pdf/slam05-ukf.pdf>.
- [35] I. Kamwa, R. Grondin, and Y. Hebert. Wide-area measurement based stabilizing control of large power systems-a decentralized/hierarchical approach. *IEEE Transactions on Power Systems* 16, (2001) 136–153.
- [36] W. Yao, L. Jiang, Q. H. Wu, J. Y. Wen, and S. J. Cheng. Delay-Dependent Stability Analysis of the Power System With a Wide-Area Damping Controller Embedded. *IEEE Transactions on Power Systems* 26, (2011) 233–240.

- [37] H. Wu, K. S. Tsakalis, and G. T. Heydt. Evaluation of time delay effects to wide-area power system stabilizer design. *IEEE Transactions on Power Systems* 19, (2004) 1935–1941.
- [38] S. Zhang and V. Vittal. Design of Wide-Area Power System Damping Controllers Resilient to Communication Failures. *IEEE Transactions on Power Systems* 28, (2013) 4292–4300.
- [39] R. Majumder, B. Chaudhuri, and B. C. Pal. Implementation and test results of a wide-area measurement-based controller for damping interarea oscillations considering signal-transmission delay. *IET Generation, Transmission Distribution* 1, (2007) 1–7.
- [40] S. Wang, X. Meng, and T. Chen. Wide-Area Control of Power Systems Through Delayed Network Communication. *IEEE Transactions on Control Systems Technology* 20, (2012) 495–503.
- [41] A. C. Zolotas, B. Chaudhuri, I. M. Jaimoukha, and P. Korba. A Study on LQG/LTR Control for Damping Inter-Area Oscillations in Power Systems. *IEEE Transactions on Control Systems Technology* 15, (2007) 151–160.
- [42] E. Ghahremani and I. Kamwa. Dynamic State Estimation in Power System by Applying the Extended Kalman Filter With Unknown Inputs to Phasor Measurements. *IEEE Transactions on Power Systems* 26, (2011) 2556–2566.
- [43] E. Ghahremani and I. Kamwa. Online State Estimation of a Synchronous Generator Using Unscented Kalman Filter From Phasor Measurements Units. *IEEE Transactions on Energy Conversion* 26, (2011) 1099–1108.
- [44] A. K. Singh and B. C. Pal. Decentralized Dynamic State Estimation in Power Systems Using Unscented Transformation. *IEEE Transactions on Power Systems* 29, (2014) 794–804.

- [45] E. Ghahremani and I. Kamwa. Local and Wide-Area PMU-Based Decentralized Dynamic State Estimation in Multi-Machine Power Systems. *IEEE Transactions on Power Systems* 31, (2016) 547–562.
- [46] B. Chaudhuri, R. Majumder, and B. C. Pal. Wide-area measurement-based stabilizing control of power system considering signal transmission delay. *IEEE Transactions on Power Systems* 19, (2004) 1971–1979.
- [47] B. P. Padhy, S. C. Srivastava, and N. K. Verma. A Wide-Area Damping Controller Considering Network Input and Output Delays and Packet Drop. *IEEE Transactions on Power Systems* 32, (2017) 166–176.
- [48] L. Xueyan and Y. Zheng. Comparison of time delay processing methods in control system. In 2015 4th International Conference on Computer Science and Network Technology (ICCSNT), volume 01. 2015 1502–1505.
- [49] J. H. Chow, J. J. Sanchez-Gasca, H. Ren, and S. Wang. Power system damping controller design-using multiple input signals. *IEEE Control Systems Magazine* 20, (2000) 82–90.
- [50] P. Sauer and M. A. Pai. *Power System Dynamics and Stability*. Englewood Cliffs, NJ: PrenticeHall, 1998.
- [51] T. V. Cutsem and C. Vournas. *Voltage Stability of Electric Power Systems*. Power Electronics and Power Systems Series, Springer US, 1998.
- [52] S. P. J. N. Yang and H. Huang. An adaptive extended Kalman filter for structural damage identification II: unknown inputs. *The Journal of the International Association for Structural Control and Monitoring* 14, (2007) 497–521.
- [53] M. A. Pai. *Energy Function Analysis for Power System Stability*. Boston: Kluwer Academic Publishers, 1989.
- [54] W. Yao, L. Jiang, J. Wen, Q. H. Wu, and S. Cheng. Wide-Area Damping Controller of FACTS Devices for Inter-Area Oscillations Considering Communication Time Delays. *IEEE Transactions on Power Systems* 29, (2014) 318–329.



- [55] M. Qiu, W. Gao, M. Chen, J. Niu, and L. Zhang. Energy Efficient Security Algorithm for Power Grid Wide Area Monitoring System. *IEEE Transactions on Smart Grid* 2, (2011) 715–723.
- [56] N. R. Naguru, G. V. N. YatendraBabu, and V. Sarkar. Design and performance analysis of wide area controller in the presence of multiple load types. In 2016 National Power Systems Conference (NPSC). 2016 1–6.
- [57] F. Lin, M. Fardad, and M. R. Jovanovic. Augmented Lagrangian Approach to Design of Structured Optimal State Feedback Gains. *IEEE Transactions on Automatic Control* 56, (2011) 2923–2929.
- [58] N. R. Naguru and V. Sarkar. Optimal wide area control of a power system with limited measurements. In 2015 IEEE International Conference on Signal Processing, Informatics, Communication and Energy Systems (SPICES). 2015 1–5.
- [59] K. Zhou and J. C. Doyle. *Essentials of Robust Control*. Prentice Hall, 1998.
- [60] M. Beiraghi and A. M. Ranjbar. Adaptive Delay Compensator for the Robust Wide-Area Damping Controller Design. *IEEE Transactions on Power Systems* 31, (2016) 4966–4976.
- [61] How to compute  $H_2$  and  $H_\infty$ -norms. [http://www.control.tfe.umu.se/Courses/Optimal\\_Control\\_for\\_Linear\\_Systems\\_2010/lectures/Lecture\\_03\\_OCLS.pdf](http://www.control.tfe.umu.se/Courses/Optimal_Control_for_Linear_Systems_2010/lectures/Lecture_03_OCLS.pdf).
- [62] J. C. Geromel. *Methods and Techniques for Decentralized Control Systems: Analysis and Design*. Milano, Italy: Ed. Clup, 1987.
- [63] G. Rogers. *Power System Oscillations*. Norwell, MA, USA: Kluwer, 2000.
- [64] R. A. Jabr, B. C. Pal, N. Martins, and J. C. R. Ferraz. Robust and coordinated tuning of power system stabiliser gains using sequential linear programming. *IET Generation, Transmission Distribution* 4, (2010) 893–904.

- [65] G. K. Dill and A. S. e Silva. Robust Design of Power System Controllers Based on Optimization of Pseudospectral Functions. *IEEE Transactions on Power Systems* 28, (2013) 1756–1765.
- [66] F. R. S. Sevilla, I. Jaimoukha, B. Chaudhuri, and P. Korba. Fault-tolerant wide-area control for power oscillation damping. In 2012 IEEE Power and Energy Society General Meeting. 2012 1–8.
- [67] X. Wu, F. Drfler, and M. R. Jovanovi. Input-Output Analysis and Decentralized Optimal Control of Inter-Area Oscillations in Power Systems. *IEEE Transactions on Power Systems* 31, (2016) 2434–2444.
- [68] IEEE Standard for Synchrophasor Measurements for Power Systems. *IEEE Std C37.118.1-2011 (Revision of IEEE Std C37.118-2005)* 1–61.
- [69] W. Yao, L. Jiang, J. Wen, Q. Wu, and S. Cheng. Wide-Area Damping Controller for Power System Interarea Oscillations: A Networked Predictive Control Approach. *IEEE Transactions on Control Systems Technology* 23, (2015) 27–36.
- [70] N. R. Chaudhuri, B. Chaudhuri, S. Ray, and R. Majumder. Wide-area phasor power oscillation damping controller: A new approach to handling time-varying signal latency. *IET Generation, Transmission Distribution* 4, (2010) 620–630.
- [71] S. Zhang and V. Vittal. Design of Wide-Area Power System Damping Controllers Resilient to Communication Failures. *IEEE Transactions on Power Systems* 28, (2013) 4292–4300.

## List of Publications

### Journals

1. **Nagasekhara Reddy Naguru**, and Vaskar Sarkar, “Practical Supplementary Controller Design for the Bi-layer WAC Architecture through Structurally Constrained  $H_2$ -norm Optimization,” *IET Gener., Trans. Distrib.*, DOI: [10.1049/iet-gtd.2018.5442](https://doi.org/10.1049/iet-gtd.2018.5442) — Accepted.
2. **Nagasekhara Reddy Naguru**, G V N Yatendra Babu, and Vaskar Sarkar, “Efficient Construction of a Limited Scale WAC Loop by means of Gain Normalized Mode Attenuation Sensitivity Analysis,” — Under Preparation.

### Conferences

1. **Nagasekhara Reddy Naguru**, G V N Yatendra Babu, and Vaskar Sarkar, “Design and performance analysis of wide area controller in the presence of multiple load types,” in *Proc. IEEE 19<sup>th</sup> Nat. Power Syst. Conf.*, India, Dec. 2016, pp. 1-6. DOI: [10.1109/NPSC.2016.7858834](https://doi.org/10.1109/NPSC.2016.7858834).
2. **Nagasekhara Reddy Naguru** and Vaskar Sarkar, “Optimal wide area control of a power system with limited measurements,” in *Proc. IEEE Int. Conf. Signal Process., Informatics, Commun., and Energy Syst.*, India, Feb. 2015, pp. 1-5. DOI: [10.1109/SPICES.2015.7091476](https://doi.org/10.1109/SPICES.2015.7091476).
3. **Nagasekhara Reddy Naguru**, G V N Yatendra Babu, and Vaskar Sarkar, “A comparative study on LQR and  $H_\infty$  control for damping oscillations in power system network considering different operating points,” in *Proc. IEEE Int. Conf. Smart Electric Grid*, India, Sep. 2014, pp. 1-6. DOI: [10.1109/ISEG.2014.7005614](https://doi.org/10.1109/ISEG.2014.7005614).